Investigation of the Behaviour of Laterally Loaded Monopiles in Cohesionless Soil

Kristian Lange Rasmussen
Torben Kirk Wolf
Mette Hansen
MSc Aalborg University
Master's Thesis
08.06.12

AALBORG UNIVERSITY
STUDENT REPORT

The Faculty of Engineering and Science
School of Engineering and Science
Sohngårdsholmsvej 57
9000 Aalborg
Telefon: 9940 8530
http://civil.aau.dk

Title:
Investigation of the Behaviour of Laterally Loaded Monopiles in Cohesionless Soil

Written by:
Mette Hansen
Torben Kirk Wolf
Kristian Lange Rasmussen

Graduate Students
School of Engineering and Science,
Aalborg University, Denmark

Supervisors:
Professor Lars Bo Ibsen
PhD Fellow Hanne Ravn Roesen

Project Period: 2012.02.01 - 2012.06.11

Completed: 2012.06.11

Copies printed: 6

Number of pages: 64

Number of pages (appendix) 25

Mette Hansen | Torben Kirk Wolf | Kristian Lange Rasmussen

Preface

This Master's thesis "Investigation of the Behaviour of Laterally Loaded Monopiles in Cohesionless Soil" is conducted during the Spring of 2012 at the M.Sc. in Structural and Civil Engineering under The Faculty of Engineering and Science at Aalborg University, Denmark.

The thesis consists of three papers and related appendices. A list of references is situated after each paper/appendix. The appendices are numbered by letters. Figures, tables and equations are presented with consecutive numbers in each paper/appendix. The three papers are printed with individual page numbering. Cited references are marked with author specifications and year of publication.

A pdf-script of the thesis and the used computational programs are included on the enclosed CD. Furthermore a set of output data files from a FE model is included at:
https://dl.dropbox.com/u/11984410/Plaxis_data_files.rar

The data files will only be available at this link in the period 2012.06.11 - 2012.06.30.

The study has been supervised by Professor Lars Bo Ibsen and PhD Fellow Hanne Ravn Roesen who are thanked for their assistance during the study. Assistant Engineers Kurt S. Sørensen, Jan Laursen, Kim Borup and Lasse B. Mikkelsen are thanked for their assistance during the testing in the laboratory.

Summary in English

In recent years efforts have been made to increase the production of renewable energy such as wind energy. The industry increases rapidly and wind turbines continue to grow in both size and numbers. In addition new building sites are incorporated as large areas are required in order to build the wind farms. This means that offshore wind farms are being built increasingly farther from the coast and in deeper waters. The turbines are often placed at water depths of 15 - 30 m. The most common offshore foundation for wind turbines are monopiles. These monopiles often have an embedded length of 20 - 30 m and a diameter of 4 - 6 m.

When designing monopiles in regard of lateral loading, current design guidances, i.e. DNV (2010) and API (2007), use the method of p-y curves. The p-y curves are based on a few static and cyclic tests on a few flexible, slender piles, as described in (Cox et al., 1974).The p-y curves are formulated depending on very few properties of the sand and the pile, respectively. For the sand, the angle of internal friction, the relative density, and the specific weight is considered. The dimensions of the pile are considered in terms of length and diameter. However, the general behaviour of the pile is assumed that of slender piles. The monopiles today have a slenderness ratio < 10 and so, this will give the piles a more rigid response which is not accounted for in the current design guidances. Another subject where the design guides are not up to date, is their limited implementation of issues regarding long-term cyclic, lateral loading. This effect may change the stiffness of the soil-pile system and cause a tilting rotation of the wind turbine.

In recent years 3D finite element analysis has become a tool in the investigation of complex geotechnical situations, such as the laterally loaded monopile. In this paper a 3D FEA is conducted as basis for an evaluation of the p-y curves of the design guides. It is found that the applied material models have a significant influence on the stiffness of the obtained p-y curves. p-y curves are obtained by evaluation of soil response during a prescribed displacement and applied load respectively. The responses are not in clear agreement. The p-y curves evaluated by means of FEA are compared to the conventional p-y curve formulation which provides a much stiffer response.

In order to evaluate the effect of cyclic lateral loading a small-scale test of a pile placed in saturated sand is conducted. The pile is 100 mm wide and has a slenderness ratio of 6. The cyclic load affecting the pile is found from the lateral bearing capacity which is defined at a rotation of 3°. The cyclic load is determined as 35 % of this load. Force and displacement is measured as the pile is loaded to evaluate the rotation of the pile. The cyclic test shows decreasing displacement increments with increasing number of load cycles, but a stabilised situation does not occur.

A literature study on state of the art knowledge within the field of cyclic loading is conducted. Theories on degradation of the stiffness of the soil-pile system by Long and Vanneste (1994) and Lin and Liao (1999) are presented as well as recent experimental work on cyclically loaded piles by Peng et al. (2006), Peralta and Achmus (2010), LeBlanc et al. (2010) and Roesen et al. (2011). The measured test results are compared with the theoretical formulations as well as other cyclic load tests. Long and Vanneste (1994) and Lin and Liao (1999) suggest formulations that compared to the measured results give simple estimates on the accumulated rotation of the pile. The measured result agree with recent experimental work that rotation of the pile will keep increasing with increasing number of load cycles. However, in contrast to the measured results, Roesen et al. (2011) finds that the system stabilises. After 15000 load cycles no further increase in rotation occurs.

Summary in Danish (Sammendrag)

I de senere år er det forsøgt at øge produktionen af vedvarende energi såsom vindenergi. Industrien udvider sig hurtigt, og vindmøllerne fortsætter med at vokse i både størrelse og antal. Hertil kommer at nye områder indarbejdes, eftersom store arealer er nødvendige for at bygge vindmølleparker. Det betyder, at offshore vindmølleparker i stigende grad bliver bygget længere væk fra kysten og på dybere vand. Møllerne er ofte placeret på vanddybder på 15 - 30 m. Det mest almindelige offshore fundament for vindmøller er monopæle. Disse monopæle har ofte en længde på 20 til 30 m og en diameter på 4 - 6 m.

Ved udformningen af monopæle i forbindelse med horisontal belastning bruger nuværende designvejledninger, dvs. DNV (2010) og API (2007), p-y kurvemetoden. p-y kurverne er baseret på nogle få statiske og cykliske forsøg på få fleksible, slanke pæle som beskrevet i (Cox et al., 1974). p-y kurverne er formuleret for meget få egenskaber af hhv. sand og pæl. For sandet er den indre friktionsvinkel, lejringstætheden og rumvægten i betragtning. Dimensionerne af pælen betragtes med hensyn til længde og diameter. Dog antages pælens generelle virkemåde at være som for en slank pæl. Monopæle har i dag et slankhedsforhold < 10, hvilket vil give et mere stift respons, som ikke medregnes i de nuværende designvejledninger. Et andet emne, hvor designvejledningerne ikke er opdaterede, er deres begrænsede implementering af langtids-, cyklisk, horisontal belastning. Virkningen herfra kan ændre stivheden af jord-pæl-systemet og forårsage en rotation af vindmøllen.

I de seneste år er 3D finite element analyse blevet et redskab i undersøgelsen af komplekse geotekniske situationer, såsom horisontalt belastede monopæle. I denne afhandling gennemføres en 3D FEA som grundlag for en evaluering af designvejledningernes p-$y$kurver. Det konstateres, at de anvendte materialemodeller har en betydelig indflydelse på stivheden af de beregnede p-y kurver. p-y kurverne opnås ved en evaluering af jordens respons under hhv. tvungen flytning og en påført belastning. Responset er ikke entydig. p-y kurverne evalueret vha. FEA sammenlignes med den konventionelle p-y kurve formulering, der udviser et meget stivere respons.

For at evaluere virkningen af cyklisk horisontal belastning udføres et skaleret forsøg på en pæl placeret i mættet sand. Pælen er 100 mm bred og har et slankhedsforhold på 6. Den cykliske belastning, som påvirker pælen, er fundet fra den horisontale bæreevne, der er defineret ved en rotation på 3°. Den cykliske belastning beregnes som 35 % af denne belastning. Kraft og flytning måles som pælen belastes for at evaluere rotation af pælen. Den cykliske test viser, at flytningsinkrementer mindskes med stigende antal belastningscyklusser, men en stabiliseret situation opnås ikke.

Der er lavet et litteraturstudie om den nyeste viden inden for cyklisk belastning. Teorier om degradering af stivhed af jord-pæl-systemet præsenteres af Long and Vanneste (1994) og Lin and Liao (1999) præsenteres, såvel som nyere eksperimentelt arbejde på cyklisk belastede pæle af Peng et al. (2006), Peralta and Achmus (2010), LeBlanc et al. (2010) og Roesen et al. (2011). De målte testresultater er sammenlignet med de teoretiske formuleringer såvel som andre cykliske belastningsforsøg. Long and Vanneste (1994) og Lin and Liao (1999) har foreslået formuleringer, der i forhold til de målte resultater giver simple estimater på den akkumulerede rotation af pælen. De målte resultater passer med nyere eksperimentelt arbejde, hvor rotation af pælen vil øges med stigende antal belastningscyklusser. Dog nævner Roesen et al. (2011), i modsætning til de målte resultater, at systemet stabiliserer sig. Efter 15000 belastningsperioder opnås ingen yderligere stigning i rotation.

Contents

Chapter 1

Introduction

In recent years efforts have been made to introduce renewable energy as an important source of supply to the global energy consumption. One of these renewable energy sources is wind energy. As of 2011 the total worldwide capacity of wind turbines covers 3 % of the total energy demand (WWEA, 2012). In order to extract more energy from the wind offshore solutions have been introduced. By building offshore the environment is less exposed and therefore larger farms can be built.

Politically, Denmark has established itself as a frontrunner in the development of wind energy. The world's first offshore wind farm was installed in Denmark north of Lolland in 1991. Since then, the wind farms at Horns Rev 1 in 2002 and Horns Rev 2 in 2009 were respectively the world's largest wind farms when introduced (Energy, 2012a). The wind farms were the result of a demand from the Danish Energy Association that a number of demonstration farms were to be built by the Danish energy companies (Energy, 2012b). In 1996 a goal was set that by the year 2005 the installed wind energy should be 1500 MW and by 2030 it should be 5550 MW corresponding to 50 % of the expected consumption. The first goal was reached in 1999, six years before planned. The political effort is ongoing and in March of 2012 a new goal was established: 95 % of the Danish Parliament agreed that 50 % of the electricity consumption will be supplied by wind power in 2020. As of 2010 the supply from wind power was 28 % of the total energy consumption. (Energistyrelsen, 2012)

The investment in offshore wind energy solutions has also become an international subject. The European offshore wind energy sector has expanded consistently in recent years, cf. Figure 1.1.

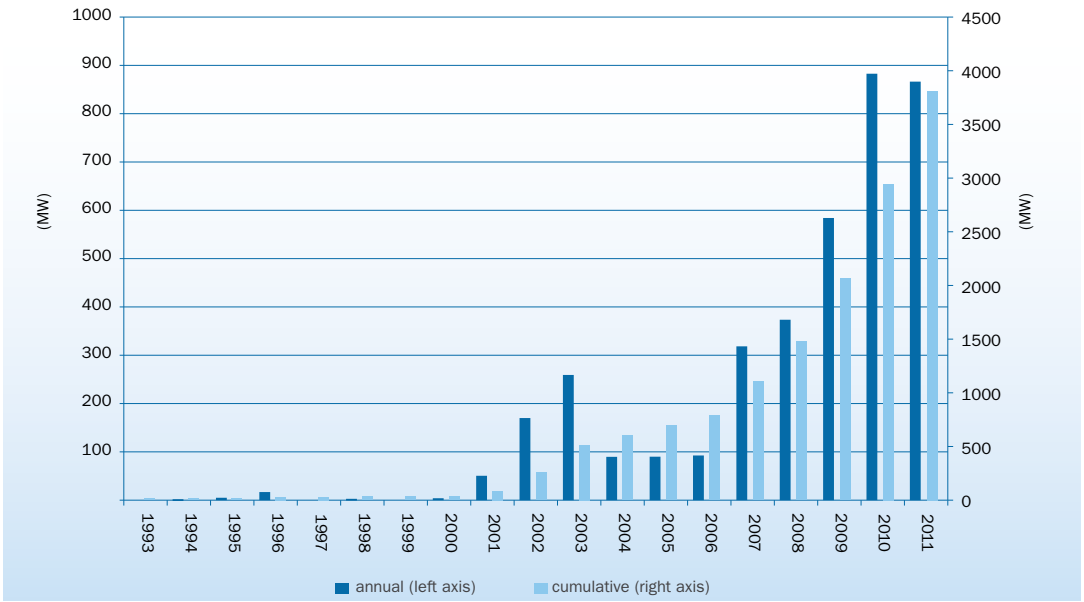

Figure 1.1: Cumulative and annual European offshore wind installations (MW). (EWEA, 2012)

The need for more efficient wind farms yields the development and installation of bigger wind turbines. The average effect of wind turbines in Europe has increased from 2 MW in 2000 to 3.5 MW in 2011 and turbines currently under construction almost reach 4 MW in average. The majority of announced wind turbine models exceed 5 MW in capacity. In addition new building sites are incorporated as large areas are required to build the wind farms. This means that offshore wind farms are being built increasingly farther from the coast and in deeper waters, (EWEA, 2012).

When building in deeper waters the impacts from waves, winds and currents on the wind turbine increase. The combination of bigger turbines and deeper waters lead to increasing demands on the foundation structure. As a result the scales of the structures become larger than the framework within which the employed design calculation methods have been developed. This may lead to either conservative or dangerous solutions. A dangerous solution is obviously not an option. However, as the cost of the foundation of wind turbines in deeper waters can compose a significant amount of the total turbine cost it is of interest to avoid conservative solutions. With the expansion of the wind turbine industry it has become a significant goal to re-evaluate and improve design solutions in order to obtain both cost effective and safe wind turbine foundation structures.

1.1 Foundation Concepts

To date the foundation of offshore wind turbines are deployed by means of the following conventional foundation types: Gravity based foundations, monopiles, tripods/jacket structures and the newer suction bucket, cf. Figure 1.2. On experimental basis is the floating foundation concept. Of these concepts the most common solution is the monopile. According to EWEA (2012) monopiles hold a 60 % share of the foundations currently under construction.

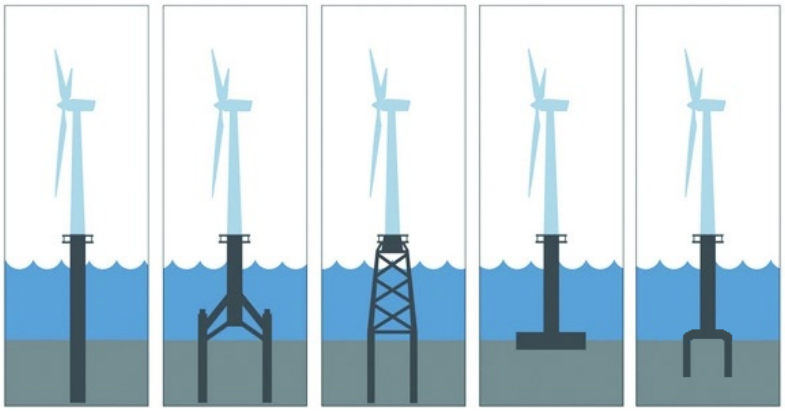

Figure 1.2: The conventional foundation designs for wind turbine structures. From left to right: Monopile, tripod, jacket, gravity based, suction bucket. (The Engineer, 2012) (edited)

The foundation of offshore wind structures must transfer any load from the tower structure into the soil. The load consists of vertical, horizontal, and moment forces. In the following a brief description of the foundation types and their bearing behaviour is presented.

The tripod/jacket foundation is adopted from the older oil and gas industry. Both are steel frame structures anchored to the seabed typically by means of piles. The three or four legs are either vertical or they can be inclined in order to reduce the resulting reaction forces. The structural advantage of jacket constructions is the spread-out steel frame that enables slender constructions less exposed to loads. The foundation also becomes less dependent on the bearing capacity of the upper soil layers, which means that the jacket foundation is suited where weak soil layers are experienced. However, the complex load distribution of the steel frame is also difficult to estimate, and the construction itself is expensive.

The gravity based foundation is a caisson structure that utilises its own weight and width to withstand impacts. It is made of either reinforced concrete, steel, or a composite structure. The caisson is often built as a frame in which ballasting materials, such as gravel or sand, are filled

to increase stability. In this way the foundation can be built on land and floated to the site. In addition, skirts are required to diminish the effects of scour on the bearing capacity. The load transfer is carried as normal and shear forces between the base of the foundation and the seabed. This imposes a certain demand to the bearing capacity of the upper soil layer.

The suction bucket is a new type of foundation that has yet to be installed in commercial wind turbine solutions. Only prototypes or model test foundations have been established for wind turbines. It consists of an open ended steel cylinder closed at the top. This enables an installation by means of applying a vacuum in the hollow room inside the cylinder, hence the name suction bucket. The installation procedure can be reversed if removal is needed. The bearing behaviour of the bucket is similar to that of gravity based and pile foundations depending on the choice of skirt length and diameter.

The monopile foundation consists of a single steel pipe structure drilled, grouted or driven into the soil. The monopile succeeds in its simplicity but heavy installation equipment is needed. The vertical bearing capacity is established along the shaft of the pile and at the pile toe. Horizontal forces and overturning moment are transferred as bedding against the soil which means that the upper soil layer often is important in the establishment of bearing capacity. As mentioned the monopile foundation is the most widely used foundation type for offshore wind turbines. The resistance against lateral loads will be the focus in the following.

1.2 Current Design Guidance for Laterally Loaded Piles

The basis for dimensioning laterally loaded piles is full-scale tests described by Cox et al. (1974). These tests are used to formulate p-y curves that describe the relation between stresses in the soil and the coherent displacements when a pile is subjected to lateral load. The current design regulations, i.e. Det Norske Veritas (DNV, 2010) and American Petroleum Institute (API, 2007), recommend the use of modified p-y curves formulated by O'Niell and Murchison (1983). DNV (2010) and API (2007) incorporate the Winkler model approach with decoupled springs along the pile and the non-linear p-y curves describing the spring stiffness, cf. Figure 1.3.

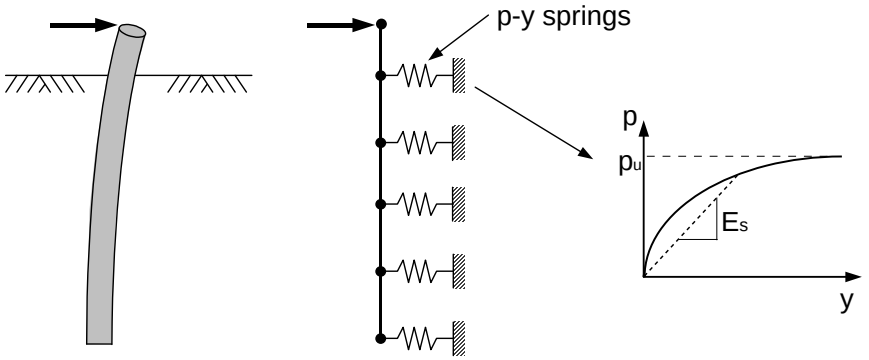

Figure 1.3: Principle for describing soil behaviour with p-y curves. (API, 2000)

The tests only include a few static and cyclic loadings of flexible piles. The slenderness ratio of these piles are $L/D = 34.4$, where L is embedded length of the pile and D is the diameter. The p-y curve formulation for a pile in sand is given by Equation (1.1), (DNV, 2010).

$$p = A\,p_u \tanh\left(\frac{k\,z}{A\,p_u}\,y\right) \tag{1.1}$$

where

p	Soil resistance at a given depth [kN/m]
p_u	Ultimate lateral capacity [kN/m]
A	Coefficient accounting for static or cyclic loading [-]
k	Initial modulus of subgrade reaction [-]
z	Depth below soil surface [m]
y	Pile deflection at a given depth [m]

The soil resistance, p, in Equation (1.1) is dependent on the ultimate lateral capacity, p_u, the initial modulus of subgrade reaction, k, and the coefficient accounting for static or cyclic loading, A. p_u and k are determined based on the friction angle and the relative density of the soil. Hence, no pile properties are incorporated in the determination of these coefficients. Note that the depth below soil surface, z, is also denoted by x in the literature.

The foundations for offshore wind turbines are large diameter monopiles that have slenderness ratio $L/D < 10$ making them behave rigid, cf. Figure 1.4. This makes them out of the range of the method suggested in the current design guidance. The difference in behaviour of flexible and rigid piles can have influence on the soil behaviour, and ultimately the resistance of the pile against loading.

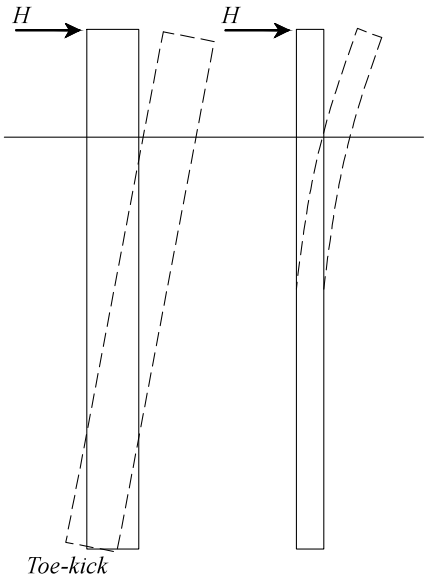

Figure 1.4: Principle for the behaviour of a rigid and a flexible pile.

Not only the ultimate lateral capacity is of great importance when designing wind turbines. The requirements of the rotation of the pile and thereby the stiffness of the soil/pile system are very strict as this will affect the serviceability of the wind turbine. Inflicted by millions of small load cycles due to waves and wind the stiffness of the soil/pile system will by affected. This long-term loading is an issue on which the knowledge is limited. The cyclic tests are of a pile subjected to not more than 100 load cycles. The coefficient accounting for static or cyclic loading, A, in Equation (1.1) was not determined for these long-term loading cycles. The accumulation of displacement can be influenced by factors such as load characteristic, size and number of load cycles, and the relative density of the sand.

1.3 Aim of Thesis

The design of laterally loaded monopiles can be divided into a number of criteria that need be obeyed. In the ultimate limit state (ULS) two requirements must be fulfilled: (1) The design lateral resistance over the length of the pile must exceed the applied characteristic load. (2) The lateral displacement at the pile head shall not exceed some specified limit calculated for the design lateral load and characteristic soil resistance. In the serviceability limit state (SLS) the permanent

deformations of the monopile must not exceed the given deformation tolerances stated in the design guidance. The deformation tolerance is usually given as a maximum allowable rotation of the pile head. (DNV, 2010)

This thesis investigates two issues regarding the lateral loading of piles; both for which the design guidances provide methods that are limited in terms of background research.

The first issue is the application of 3D finite element analysis as a tool for evaluating the lateral response of a monopile foundation in sand subjected to static loading. 3D finite element analysis is a relatively new tool in the design of engineering structures. A case study of a full scale wind turbine is conducted in the program *Plaxis 3D 2011*.

Different approaches to the computation of the *p-y* curves are described. An actual load case and a displacement approach are utilised, and by extracting relevant data from the FE calculations *p-y* curves are computed. These *p-y* curves are evaluated against each other and the established formulations of *p-y* curves from e.g. API (2007).

The second issue is the evaluation of a pile in cohesionless soil subjected to long-term cyclic lateral loading. The aim is to evaluate the effect of long-term cyclic lateral loading of a rigid pile, which corresponds to the environmental loads on a wind turbine. The latest knowledge on the subject of cyclic loading is obtained by a literature study. Theories on degradation of the stiffness of the soil/pile system are introduced as well as the latest experimental work.

The theoretical expressions are compared with measured data from a cyclic test. The test is of a pipe pile with a slenderness ratio of 6 placed in dense sand. The outer diameter of the pile is 100 mm and the embedded length is 600 mm. The pile is subjected to lateral load and the displacement is measured to determine the rotation of the pile. The test results are evaluated with comparison of previous findings.

The thesis encompasses three articles: The first article describes the handling of the FE program *Plaxis 3D 2011* and how *p-y* curves are extracted from the program. The second article is a literature study on soil response for cyclically loaded piles. The third article contains the results of test data and the comparison with theoretical and experimental work.

Chapter 2

Assessment of p-y Curves from Numerical Methods for a Non-Slender Monopile in Cohesionless Soil

Assessment of *p-y* Curves from Numerical Methods for a Non-Slender Monopile in Cohesionless Soil

Mette Hansen, Kristian Lange Rasmussen, Torben Kirk Wolf

Department of Civil Engineering, Aalborg University, Denmark

June 11, 2012

Abstract

In current design the monopile is a widely used solution as the foundation of offshore wind turbines. Winds and waves subject the monopile to considerable lateral loads. The behaviour of monopiles under lateral loading is not fully understood and the current design guidances apply the *p-y* curve method in a Winkler model approach. The *p-y* was originally developed for jag-piles used in the oil and gas industry which are much more slender than the monopile foundation. In recent years the 3D finite element analysis has become a tool in the investigation of complex geotechnical situations, such as the laterally loaded monopile. In this paper a 3D FEA is conducted as basis of a *p-y* evaluation. It is found that the applied material models have a significant influence on the stiffness of the evaluated *p-y* curves. *p-y* curves are obtained near the rotation point by evaluation of soil response during a prescribed displacement but the response is not in clear agreement with the response during an applied load. The *p-y* curves evaluated by means of FEA are compared to the conventional *p-y* curve formulation which provides a much stiffer response.

1 Introduction

The design of laterally loaded monopiles in current design regulations such as Det Norske Veritas (DNV, 2010) or American Petroleum Institute (API, 2007) is done by means of the *p-y* curve method. The pile and soil are modelled as a series of springs that imitate the soil-structure interaction which is conducted in a Winkler model approach. The spring stiffness is represented by the *p-y* curves which take into account the non-linear relationship between soil resistance and lateral deflection of the pile. The *p-y* curve theory was initially developed for the oil and gas industry and is based on test results from slender, flexible piles. They were not developed for piles with diameters of 4 to 6 m which are often used for the foundation of wind turbines today. No approved method exists for the design of large diameter piles and so the *p-y* curve method is still the applied method today.

1.1 Previous Studies

In the *p-y* curve method a number of parameters are not clarified when considering large diameter piles. Some of these limitations have been elaborated in a literature study by Sørensen et al. (2012). Several studies have been made to investigate the behaviour of large diameter piles under lateral loading. Sørensen et al. (2009) conducted a FE analysis supported by a series of scaled tests and found that the initial stiffness of the *p-y* curve increases with pile diameter. This is supported by Moreno et al. (2011) who made similar studies. Hald et al. (2009) studied a full-scale monopile, 4 m in diameter, at Horns Rev and concluded that the *p-y* curves underestimate the soil strength at the top of the pile. It was found that the measured response at the top of the pile was 30-50 % smaller than that predicted by the *p-y* curves. McGann et al. (2011) found that the initial stiffness of the *p-y* curves and the ultimate lateral resistance at depths is overestimated compared to FE models.

In order to consider the actual three dimensional interaction between pile and soil a 3D finite element analysis can be performed. The FEA considers factors such as shear forces, soil-pile interaction, layered soil, coefficient of lateral earth pressure, and soil dilatancy. Most studies have been made by means of the Mohr-Coulomb model (MC), but Moreno et al. (2011) found that the Hardening Soil model (HS) is more suited when comparing the results

with small scale tests in a pressure tank. The Hardening Soil model employs an elasto-plastic behaviour and considers the stress dependent stiffness of the soil and the effects of isotropic hardening. They found that the more extensive Hardening Soil Small Strains model is only slightly more accurate than the Hardening Soil model when considering laterally loaded piles. Considering the extra computational effort they did not recommend the Hardening Soil Small Strains model.

By extracting the pile-soil response in the generated model improved p-y curves can be formulated. A method proposed by Fan and Long (2005) is used for extracting soil resistance from stresses in the pile-soil interface elements. Their paper is however not descriptive regarding the evaluation of the stresses.

1.2 Subjects of Interest

In the literature numerous finite element analyses have been performed in order to create more reliable p-y curves. However, there is a lack of knowledge regarding the effects of extraction methods from the FEM models. The necessary assumptions are therefore elaborated in this paper. A number of issues regarding the stress extraction are addressed: Numerical errors, irregular meshes, choice of stress points, and the pile point of rotation. The computed p-y curves are evaluated regarding the extraction methods. The curves are furthermore compared to the conventional p-y curve methods described in the API.

2 Case Study of Barrow Wind Farm Monopile

The study is carried out as a case study of a monopile foundation of a wind turbine located at Barrow Offshore Wind Farm. The pile properties are estimated according to the foundation design report for the chosen wind turbine at the Barrow Offshore Wind Farm. The pile is a hollow steel cylinder with an embedded length of 29.4 m and an outer diameter of 4.75 m with a wall thickness of 0.1 m. This correspond to a slenderness ratio, L/D, of approximately 6.

A single load case from the extreme load analysis in the design report is chosen corresponding to maximum overturning moment at seabed. A horizontal force of 4656 kN and an overturning moment of 105656 kNm is applied. Torsional moment and bending moment around the x axis are not considered in this paper.

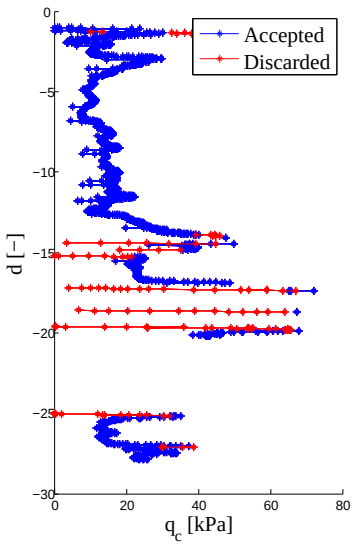

Figure 1: Accepted and discarded data points for the q_c measurements.

2.1 Site Conditions

The soil parameters are estimated on basis of the boring profile and cone penetration test (CPT) conducted at the location of the pile. The pile is chosen on the argument that only sand is present in the soil layers. Both the Mohr-Coulomb parameters and the Hardening Soil parameters can be estimated entirely on basis of the CPT.

The results from the CPT test show significant irregularities. The measurements have been stopped several times during the testing. This may be for numerous reasons. The tip resistance, q_c, may be too high due to occurrence of rocks or very dense layers. Furthermore the testing may have been stopped, so a soil test can be extracted. After each break in measurements, the cone must penetrate slightly into the soil, before the actual resistance of the soil is measured. Therefore the initial measurements after each break must be discarded, as they do not represent the response of the soil. Occasionally the q_c measurements experience peaks that do not represent the soil, without the testing being stopped. This may be due to occurrence of stones etc. These peaks must also be discarded. The accepted and discarded data points of the tip resistance of the CPT, q_c, can be seen in Figure 1.

The soil and strength parameters are determined using the proposed methods of Jamiolkowski et al. (2004) and Bolton (1986), in Equations (1), (2), and (3). However, the coefficient of at rest lateral earth pressure, K_0,

Table 1: Predetermined parameters for the sand.

φ'_{crit} [°]	$\Delta\varphi_1$ [°]	Q_{min} [-]
33	2	10

is unknown. Therefore, an iterative procedure over Equations (1) through (4) is executed. By implementing Equation (4) it is assumed that the soil is normally consolidated. Equation (2) has been adjusted by Ibsen (2012).

$$D_r = \frac{1}{2.96} \ln\left(\frac{\frac{q_c}{P_a}}{24.94}\left(\frac{\sigma'_{v0}\frac{1+2\,K_0}{3}}{P_a}\right)^{0.46}\right) \quad (1)$$

$$\varphi'_{tr} = \varphi'_{crit} + 3^\circ\, I_R - 3^\circ\, D_r - \Delta\varphi_1 \quad (2)$$

$$I_R = D_r\left(Q_{min} - \ln\frac{p'}{1\text{kPa}}\right) - 1 \quad (3)$$

$$K_0 = 1 - \sin\varphi'_{tr} \quad (4)$$

where P_a is the atmospheric pressure, $\Delta\varphi_1$ is a strength reduction due to silt content, I_R is the relative dilatancy index, φ'_{crit} is the critical angle of internal friction, and Q_{min} is a parameter adjusting for mineral strength. For a complete list of symbols, see the list in the end of the article. The value of φ'_{crit} is determined as recommended by Bolton (1986). The value of $\Delta\varphi_1$ corresponds to a silt content of 5-10 percent. Q_{min} is set to the value for quartz. A cap of 4 on the I_R values has been applied as recommended by Bolton (1986). The parameters, which need to be determined before the iteration, are listed in Table 1.

The relative densities evaluated and the mean values for each layer are shown in Figure 2. It is assumed that the mean values evaluated over the occasionally limited data within a layer represent the behaviour of the entire layer. All the remaining properties are inherently behaving in the same manner. The evaluated soil and strength parameters are listed in Table 2.

The constrained modulus used in the Hardening Soil material model is calculated using Kulhawy and Mayne (2012), cf. Equation (5). The remaining two moduli are calculated using Equations (6) and (7). It should be noted that poisson's ratio, ν, in (6) should be set to 0.3.

$$E_{oed} = q_c\, 10^{1.09-0.0075\,D_r} \quad (5)$$

$$E_{50} = \frac{(1-2\,\nu)\,(1+\nu)}{(1-\nu)}\,E_{oed} \quad (6)$$

$$E_{ur} = 3\,E_{50} \quad (7)$$

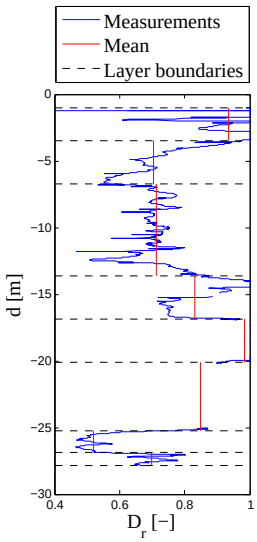

Figure 2: Evaluated D_r and corresponding mean values at each layer.

Table 2: Strength and unit weight parameters evaluated on basis of CPT test. Effective cohesion, c', is zero for all layers.

Soil Layer	K_0 [-]	γ [kN/m^3]	φ'_{tr} [°]	ψ [°]
1	0.32	19	42	12
2	0.34	19	41	12
3	0.31	19	43	12
4	0.31	21	43	12
5	0.32	21	42	12
6	0.32	21	42	12
7	0.32	19	42	11
8	0.31	19	43	12

The fit of Equation (5) to the test data in (Kulhawy and Mayne, 2012) is not convincing, as seen in Figure 3. Therefore the evaluated stiffnesses may lead to a response in the FEM model that differs from reality.

The moduli will normally vary over the depth, following the shape of a power function, as given in (Brinkgreve et al., 2012), Equations (8), (9) and (10).

$$E_{oed} = E^{ref}_{oed}\left(\frac{c\,\cos\varphi - \frac{\sigma'_3}{K^{nc}_0}\,\sin\varphi}{c\,\cos\varphi + p^{ref}\,\sin\varphi}\right)^m \quad (8)$$

$$E_{50} = E^{ref}_{50}\left(\frac{c\,\cos\varphi - \sigma'_3\,\sin\varphi}{c\,\cos\varphi + p^{ref}\,\sin\varphi}\right)^m \quad (9)$$

$$E_{ur} = E^{ref}_{ur}\left(\frac{c\,\cos\varphi - \sigma'_3\,\sin\varphi}{c\,\cos\varphi + p^{ref}\,\sin\varphi}\right)^m \quad (10)$$

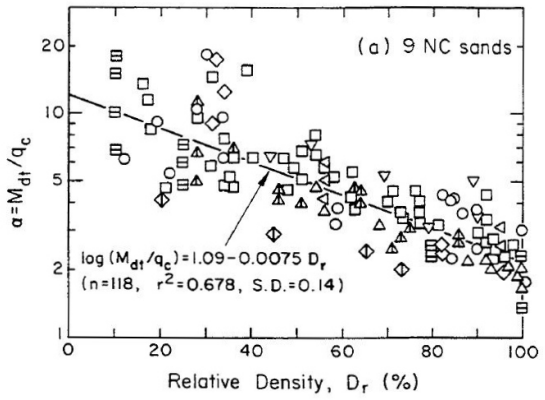

Figure 3: Fit of E_{oed} function to data in mini-CPT tests. (Kulhawy and Mayne, 2012)

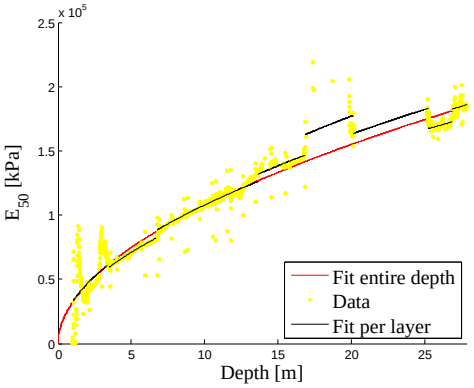

Figure 4: Fitted model and computed values of E_{50}.

In Equation (8) p^{ref} is the primary principal stress, σ_1. In Equations (9) and (10) p^{ref} is the confining pressure. It is assumed that the confining pressure can be set to K_0 σ_{v0} and that $\sigma_1 = \sigma_{v0}$.

According to von Soos (1990) the power m can lie in the range $0.5 < m < 1.0$. This range of m will provide convex curves, giving moduli at gradually stabilizing values. At a given reference pressure, the reference moduli and m can be fitted to the values given by Equations (5), (6), and (7). Such a fit is shown on Figure 4. The reference pressure is set to σ_{v0} at the middle of the layer. The power law fits the data well with a power, m, of 0.5. The values regarding the moduli evaluated from the fit of the models of Equations (8), (9) and (10) are given in Table 3. For the Mohr-Coulomb model, the modulus E' is set to the average value of E_{50} at each layer.

3 Numerical Modelling

The Barrow Wind monopile is modelled by means of the commercial finite element program *Plaxis 3D 2011*. Model parameters are constructed according to the geometry and properties given for the pile. The monopile is modelled as a hollow steel cylinder constructed as structural plate elements with linear stiffness. Plate elements are two-dimensional 6-node triangular elements used to model thin two-dimensional structures. The plates are assigned a thickness in order to model the stiffness of the pile. The soil elements are 3D 10-node tetrahedral elements which corresponds to 6 nodes at each of the sides of the tetrahedron. Interface elements are applied to the plate elements in order to model the soil-structure interaction properly. The interface elements consists of 12 nodes, a pair of 6-node triangular compatible with the 6-noded soil and structural elements. The strength and stiffness of the interface elements can be modified by a reduction factor, R_{inter}, in order to model the transition layer which is usually weaker than the surrounding soil. At the pile toe the interface elements are applied in extension of the plate elements. This is done to provide a flexible response and avoid stress concentrations (Brinkgreve et al., 2012).

Table 3: Constitutive parameters for Hardening Soil and Mohr-Coulomb model evaluated on basis of CPT.

No.	E' [MPa]	E_{50}^{ref} [MPa]	E_{oed}^{ref} [MPa]	E_{ur}^{ref} [MPa]	p^{ref} [kPa]
1	3.5	3.8	2.0	10.2	24.4
2	3.6	4.1	3.0	12.8	80
3	5.7	6.2	4.0	18.0	178
4	7.8	8.2	5.5	24.2	277
5	9.2	9.5	6.4	28.7	342
6	8.6	8.8	5.9	26.5	424
7	8.8	8.9	6.1	26.7	491
8	10.4	10.6	7.1	31.9	516

The boundary conditions are modelled so that no boundary effects are experienced when the analysis is run. The failure mechanism must be able to run at a distance to the boundaries. By conducting preliminary tests it is ensured that the failure zone does not reach the boundaries of the numerical model. The soil layers found in the boring profile are extended horizontally across the model. The soil can be divided into clusters to achieve a finer mesh near the pile. The sides of the model are restrained horizontally in their out-of-plane direction. The

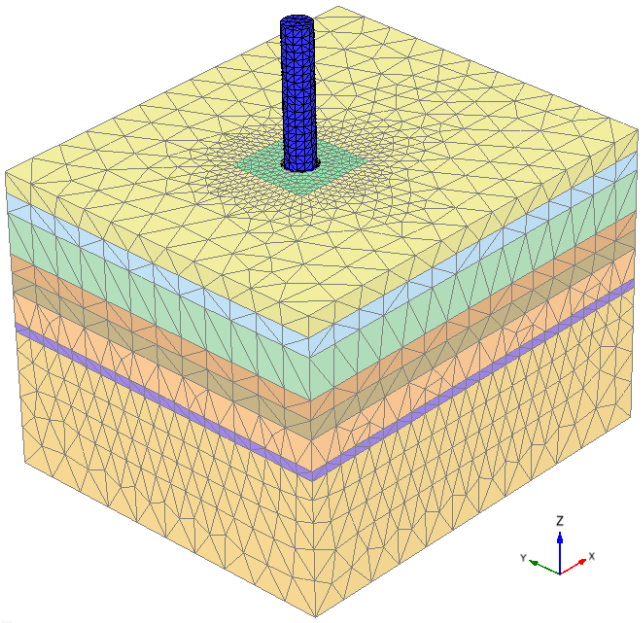

Figure 5: The three-dimensional meshed model in *Plaxis 3D 2011*.

bottom surface is restrained in all directions. These are the standard boundaries in *Plaxis 3D 2011* and they are applied automatically when defining the model boundaries.

Bending moment loads cannot be applied directly in *Plaxis 3D 2011*. To comply with this limitation the pile head is extended above the soil surface so that the applied lateral load yields a moment force at the seabed according to the specified load case. A plate is added at the pile head in order to distribute the added load evenly onto the pile head. The load is applied at the centre of the top plate. The pile above seabed should have no structural influence on the embedded pile. To avoid second order effects from the pile above seabed it is assigned a high stiffness and very small unit weight. The resulting numerical model can be seen on Figure 5.

3.1 Method of Response Extraction from *Plaxis 3D 2011*

The calculation in *Plaxis 3D 2011* is controlled by means of phases. For each phase an output data file is written which contains results from the calculations. In order to obtain results that show the load-response development a number of successive phases, each with increasing load amplitude, are defined with the final phase being the extreme load case. For each phase stresses are extracted. The soil resistance, p, is taken as the x-component of the total stress acting at the circumference of the pile during loading. Each loading phase is followed by a plastic phase in which the load is removed and the average nodal plastic displacement in the pile structural elements at the given depth is taken as the pile deformation response, y. These phases define the plastic response of the soil by which the deformation is extracted.

3.1.1 Integration Method

Very few control parameters are available when meshing in *Plaxis 3D 2011*. The fineness can be controlled by introducing volumes with increased fineness, but the overall output is not controllable by the user. This means that the mesh output is rather random of nature and no symmetry can be introduced when evaluating stresses. When integrating stresses across the pile circumference one stress point may represent a larger element than the next. This would require extensive analyses of each nodal point for every evaluation of pile-soil response. A simple approach is to divide the pile into a number of slices for each depth of p-y curve evaluation. The height of the slice corresponds to the distance between each p-y curve. A slice of a stress evaluation can be seen in Figure 6. The slices are evenly distributed along the entire circumference and the arc length of each slice is relative to the number of slices introduced. Within each slice the traction is taken as the average traction of all present nodes. The angle, θ, by which the average traction is evaluated is the angular orientation of the slice in relation to the pile centre and the load direction, cf. Figure 7.

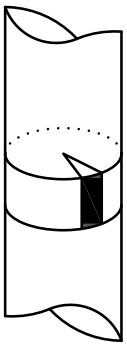

Figure 6: A pile slice at a given depth of stress evaluation.

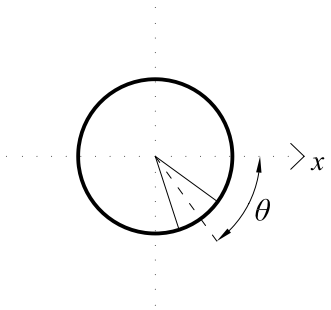

Figure 7: The angle, θ, by which traction is evaluated for a pile slice related to load direction.

The number of slices is chosen by considering the number of stress points for the given mesh. For the mesh fineness applied in this analysis the interface consists of a total of 3600 stress points from which stresses are extracted. A certain number of stress points within each slice must be available for the average to be considered representative. In this way the effects of stress oscillations, as depicted in Figure 8, can be reduced. This leads to restrictions regarding the maximum number of slices and p-y curves in proportion to the fineness of the mesh. The number of p-y curves is set to 20 which provides an average of 180 stress points per curve. A division into 16 slices is chosen which then provides an average number of stress points per slice of 11.25. This is considered as a reasonable representation of the average stress within each slice.

3.1.2 Extraction from Interface

Stresses in interface elements consist of effective normal stress, σ'_N, and shear stresses, τ_1 and τ_2. σ'_N is the effective normal stress acting normal to the interface surface. τ_1 is the shear stress acting along the circumference of the pile. τ_2 is the shear stress acting vertically along the length of the pile and is therefore not considered.

Plaxis 3D 2011 has difficulties simulating the cylindrical pile with the triangular elements. The corners of the structure elements peak out because they cannot enclose a perfectly circular shape. When the numerical analysis is run the effect of this can be seen as zones or stripes of stress concentrations scattered across the surface of the pile. The patterns are related to the stress points of the elements and are correlated with the element contours of the mesh. The stress concentrations increase when the mesh is coarsened as fewer elements around the pile circumference leads to increased angles between the surfaces. An example of the interface stress oscillations for a typical mesh fineness can be seen in Figure 8.

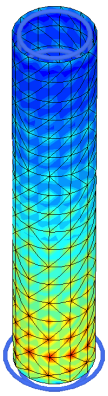

Figure 8: Pile interface normal stress oscillations (red spots).

It must be assured that these stress concentrations do not influence the result of the average pile-soil response without having to refine the mesh extensively. The lateral pile-soil response can be extracted from the model by evaluating stresses in either plate, interface or soil elements. Either method should give similar results given that the equilibrium between pile and soil must be fulfilled.

3.1.3 Extraction from Plates

Stresses in plate elements in *Plaxis 3D 2011* cannot be extracted directly as the structural response is evaluated as forces at the plate element integration points that are extrapolated to the element nodes (Brinkgreve et al., 2012). Stress evaluation of the plate elements would require establishment of the differential equations of shell elements by means of a finite difference method and is therefore not considered in this paper.

3.1.4 Extraction from Soil

Stresses in soil elements are evaluated by considering the effective Cartesian stresses acting in the direction of the considered displacement, x. The considered stresses are the normal stress acting in x-direction, σ'_{xx}, and the shear stress acting on the y-plane in x-direction, σ'_{yx}. The shear stress acting on the z plane in x-direction, σ'_{zx} acts on the vertical plane z and is therefore not considered.

The x-component stress at a point in the soil can be represented by the traction vector, T_x, at the pile surface expressed in Equation (11), (Fan and Long, 2005).

$$T_x = \sigma'_{xx}\, n_x + \sigma'_{xy}\, n_y + \sigma'_{xz}\, n_z \qquad (11)$$

where σ'_{xx}, σ'_{xy}, and σ'_{xz} are Cartesian stresses (note that $\sigma'_{xy} = \sigma'_{yx}$ and $\sigma'_{xz} = \sigma'_{zx}$) and n_x, n_y, and n_z are components of unit normal along the x-, y-, and z-directions. These are given in Equations (12), (13), and (14) respectively.

$$n_x = \cos\theta_x \qquad (12)$$

$$n_y = \cos\theta_y \qquad (13)$$

$$n_z = \cos\theta_z \qquad (14)$$

where θ is the angular orientation of the stress point in relation to the pile centre. The total soil response, p_x, per unit length of pile, which corresponds to the subgrade reaction, is found by integrating the soil resistance over the pile circumference at given depth during loading.

When extracting stresses from the surrounding soil elements, the stresses cannot be evaluated at the exact circumference of the pile. In order to obtain an adequate amount of stress points within each integration area (see Figure 6) stress points at a certain distance from the pile must be implemented. This issue is illustrated in Figure 9. Being that the stress points are further from the pile, forces are distributed to a larger area. This means that stresses become lower. The response obtained from the soil elements are therefore expected to be slightly lower than those obtained from the interface.

3.1.5 Comparison of Extraction Methods

Figure 10 shows the calculated soil resistances from interface elements for a depth of 3.9 m at load step 500 kN in the MC model analysis. The out-of-plane normal stress, σ_N, in Figure 10a shows a small stress at the back side of the

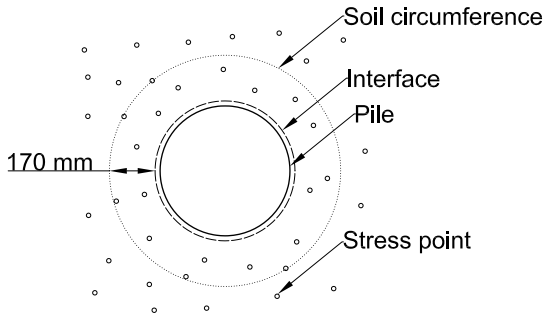

Figure 9: Required circumference for obtaining sufficient stress points in soil.

pile and the largest stresses at the front side corresponding the active and passive pressure respectively. The x component of the out-of-plane stress, $\sigma_{N,x}$, in Figure 10b, shows that the contributions from the sides of the pile reduce to near zero values. Similarly in Figure 10c, the radial shear stress, τ_r, is largest on the side of the pile and are near zero on the front and back of the pile. As a result the x component of the radial shear stress, $\tau_{r,x}$, in Figure 10d is close to τ_r. The soil resistances for all slices are integrated over the pile circumference yielding the subgrade reaction for the given depth. An example of the subgrade reactions evaluated by means of interface and soil elements respectively can be seen in Figure 11. There is some difference between the two curves of the subgrade reactions originating from the fact that the stresses in the soil elements are evaluated at a distance from the pile. At the bottom of the pile some deviation is observed which is related to the complex behaviour of the soil in this area.

On basis of Figure 11 the soil resistance evaluated from interface elements are preferred

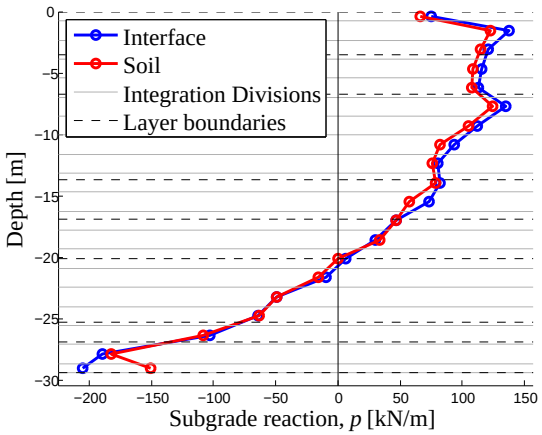

Figure 11: Subgrade reactions along depth of pile evaluated from interface and soil elements, respectively, load step 500 kN.

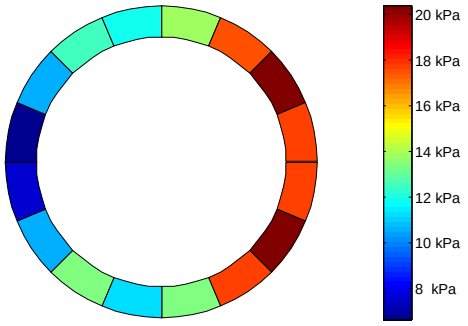

(a) Out-of-plane normal stress, σ_N

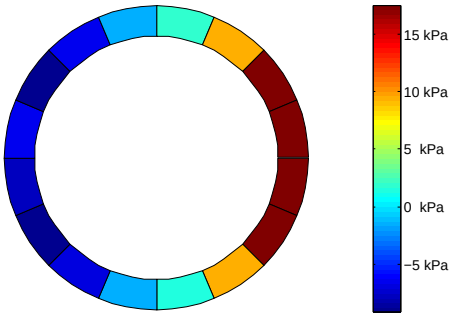

(b) x component, $\sigma_{N,x}$

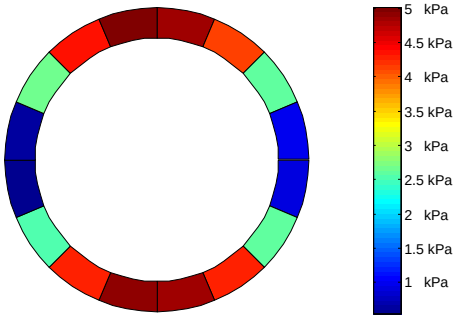

(c) Radial shear streess, τ_r

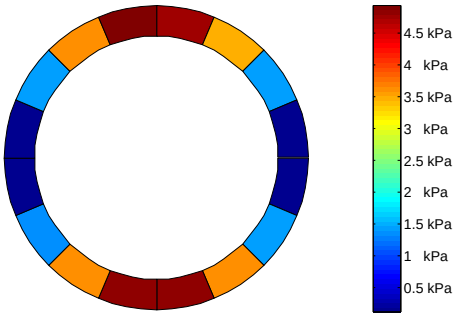

(d) x component, $\tau_{r,x}$

Figure 10: Interface response for MC model at depth 3.9 m, load step 500 kN. Right-hand side is active side of pile.

over soil resistance evaluated from soil elements. The corresponding pile deflection at load step 500 kN and a fitted linear line are seen in Figure 12. It is seen that the pile behaves almost rigid as depicted with a point of rotation and a slight curve compared to the fitted line.

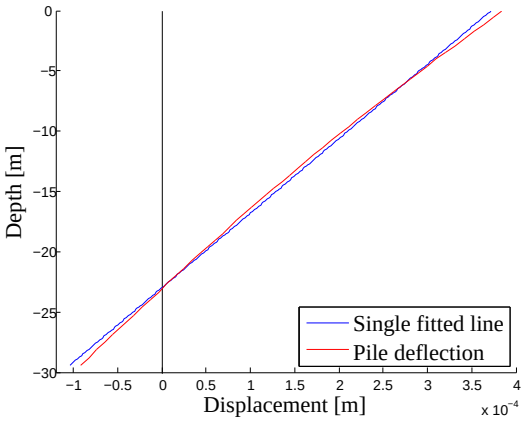

Figure 12: Pile deflection at load step 500 kN

3.2 Pile Excitation by Forced Displacement

Non-slender piles during lateral loading exhibit rigid behaviour and rotate around a point of zero deflection forming a soil wedge as depicted in the possible failure mode in Figure 13. An issue when constructing p-y curves by means of finite element modelling is the evaluation of soil response in proximity to the pile rotation point.

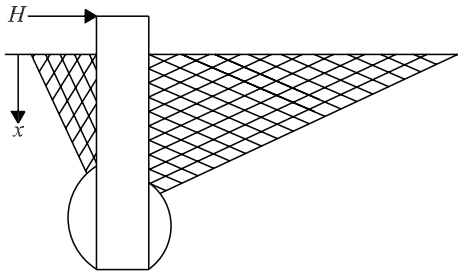

Figure 13: Possible failure mode for a smooth surfaced, non-slender pile at shallow depth (Sørensen et al., 2012).

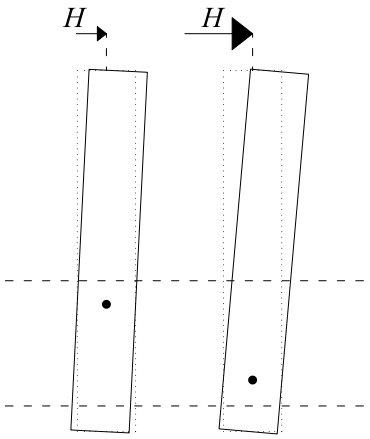

Figure 14: Schematic of the range of possible rotation points for different load amplitudes.

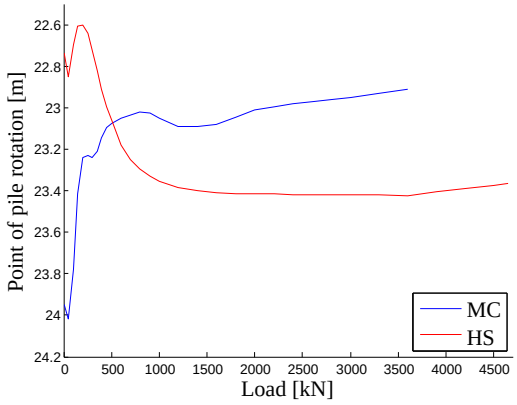

Figure 15: Point of pile rotation for the MC model and HS model respectively.

In the finite element model this results in the soil response being irregular near the point of rotation. The location of this point changes when applying different load amplitudes as exemplified in Figure 14. The variating location of the point of pile rotation for the load case for both the MC model and the HS model is shown in Figure 15.

Around the point of pile rotation the subgrade reactions are close to zero, cf. Figure 11. At depth near the point of rotation, displacements and subgrade reactions representing the entirety of a p-y curve cannot be achieved. Due to this, the p-y curves are difficult to extract when applying a horizontal load. In order to cope with this issue an appropriate forced displacement may be applied to the pile in order to simulate the necessary pile excitation.

A forced displacement is applied to the entire pile surface in the direction of load. The measured response is taken as the p-y behaviour, where p is the resulting subgrade

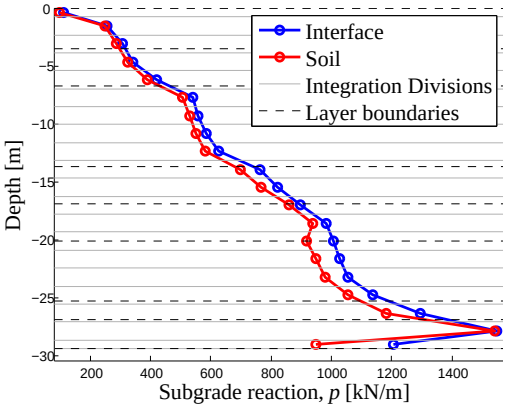

Figure 16: Subgrade reaction at forced displacement, y = 0.05 m.

reaction during the forced displacement and y is found as the plastic displacement after the forced displacement is removed. The resulting subgrade reactions along the pile length for a given forced displacement can be seen in Figure 16. It is observed from Figure 16 that the subgrade reaction increases with depth and that it does not reach zero at any point. Similar to the observation during loading in Figure 11 deviations are visible near the pile bottom.

In Figure 17 the extracted p-y curves from the forced displacement are depicted together with curves extracted from the load case for three different depths, i.e. 1.5 m, 7.7 m, and 29 m, respectively. The p-y curve at a depth of 1.5 m shown in Figure 17a displays a much stiffer response for the load case. At depth 7.7 m, Figure 17b, the responses are almost identical. At depth 29 m in Figure 17c a negative response is observed for the load case which is related to the toe kick. For the load case it is also noticed that the amount of deflection, y, is much less than that depicted for a depth of 1.5 m in Figure 17a. Not shown here, the p-y curves close to the pile rotation point for the load case show even smaller deflection and an unreliable response. It is not possible to make reliable conclusions regarding the response for the load case in this area. Thus, the choice of excitation method for p-y curve evaluation should be the forced displacement when near the point of pile rotation. Near the top and bottom of the pile the load case is applicable and should be the choice as it represents the actual failure mechanism.

3.3 Comparison of Material Models

Another observation in Figure 17 is the near vertical initial response of the p-y curves. This is

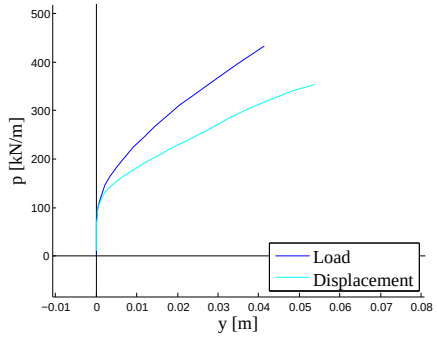

(a) $x = 1.5$ m

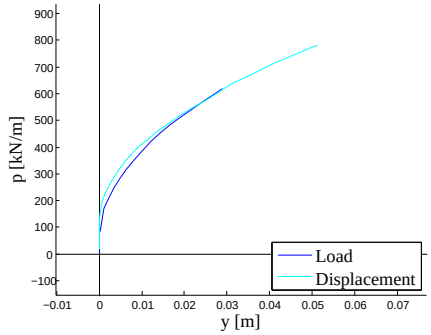

(b) $x = 7.7$ m

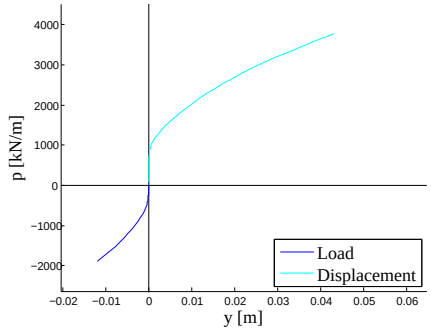

(c) $x = 29$ m

Figure 17: p-y curves determined by means of the MC model for load and forced displacement respectively.

observed at all depths for the p-y curves computed for the MC analysis. The observation is related to the elastic perfectly plastic behaviour of the MC model. At excitations up to a certain threshold the pile exhibits almost zero plastic deformation. Based on this observation the p-y behaviour of the MC model is considered unreliable. Analysis results with inclusion of a HS model in the analysis results at a depth of 7.7 m is shown on Figure 18. The pile exhibits immediate plastic response which corresponds to the hyperbolic stress-strain relation in the stiffness behaviour of the HS model. This results in a response less stiff than obtained by the MC model.

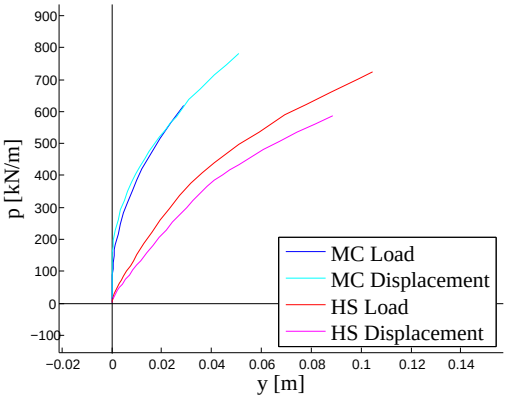

Figure 18: p-y curves determined by means of the MC model and HS model respectively.

3.4 Comparison of Soil Response with API Method

The p-y curves obtained from the finite element model are set against the curves obtained by the traditional method of (API, 2007). This juxtaposition for a shallow depth can be seen on Figure 19. Here the Mohr-Coulomb curves seem to fit well with the API curve. However, the issue regarding the infinite initial modulus of the MC-curve is present. The HS curves show a respond that is significantly less stiff than the API curves. This suggests that API (2007) overestimates the initial subgrade modulus, E^*_{py}, at shallow depth.

At greater depths this difference becomes more substantial. At approximately half the pile depth, the methods disagree considerably. This is seen on Figure 20. This pattern indicates that the assumed linear increase of initial subgrade modulus in API (2007) greatly overestimates the stiffness of the response.

However, caution should be taken, when comparing the obtained results with (API,

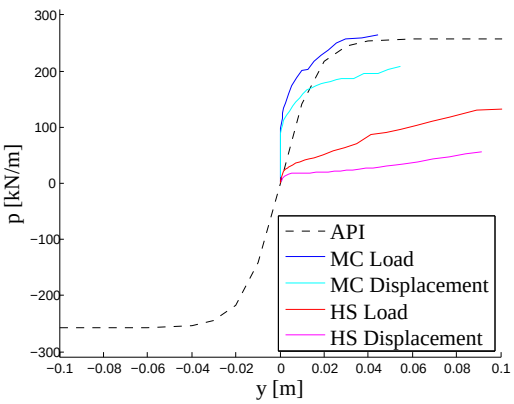

Figure 19: $p - y$ curves at d = 0.4 m.

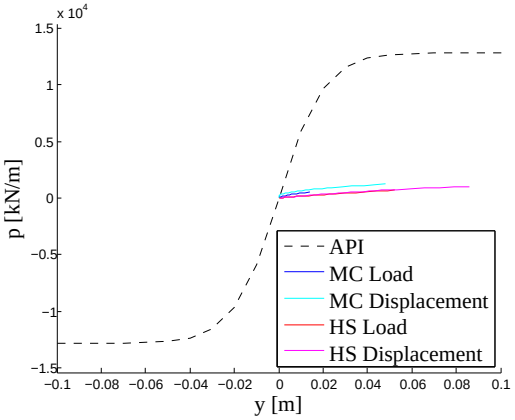

Figure 20: $p - y$ curves at d = 15.5 m.

2007). The finite element model has not been validated. As no test results for the simulated pile are available, the output of the model cannot be deemed verified. The extraction method need validation as well. The obtained p-y curves must be incorporated in a Winkler model, and the response must be held up against the response given directly from the FEM model. The exact values from the model cannot be deemed fully reliable. Nevertheless, the general shapes of the curves, and the behaviour over the depth of the pile are believed to be representative of the true behaviour.

4 Conclusion

In this paper a numerical analysis of a laterally loaded monopile in sand is conducted. The analysis is conducted by means of the finite element program *Plaxis 3D 2011*. A case study of a full-scale wind turbine is provided as the subject for research. A method for extracting p-y curves by evaluating stress points is presented. Two different excitations, applied load and forced displacement, are utilised in order to evaluate p-y curves. p-y curves are evaluated by means of two material models in the numerical analysis: The Mohr-Coulomb model and the Hardening Soil model. Finally, the extracted p-y curves are compared to the p-y curves formulated in the API. The general conclusions are:

- Stress oscillations in the interface elements in *Plaxis 3D 2011* are observed. They are related to the modelling of curved structures in the finite element formulation. The method for extracting p-y curves considers the average stresses in order to cope with this.

- The slices conducted in the method for extracting p-y curves produce stress results that fit reasonably with the expected traction on the pile surface.

- The p-y curves evaluated from forced displacement provide the best basis for extraction of p-y curves along the entire length of the pile.

- Near the top and bottom of the pile, using applied load as excitation method must be recommended, due to the misleading failure mode of a forced displacement in these areas.

- The deflection of the pile consists of rigid body motion during loading. A slight curvature is noticed.

- The Mohr-Coulomb model shows no plastic deformation in a considerable range of loading due to its bilinear stress-strain curve. The Hardening Soil model provides immediate response which results in less stiff p-y curves.

- The conventional p-y curves formulated in API shows a much stiffer response at depth than either of the applied material models and excitation methods. This may be related to the linearly increasing initial subgrade modulus, E^*_{py}.

List of Symbols

p	Subgrade reaction
y	Lateral pile deflection
L	Pile length
D	Pile diameter
H	Load
q_c	Tip resistance
φ'_{tr}	Friction angle
φ'_{crit}	Critical friction angle
$\Delta\phi_1$	Silt, strength reduction
I_R	Relative density index
Q_{min}	Mineral strength adjustment
p'	Effective overburden pressure
P_a	Atmospheric pressure
D_r	Relative density
ψ	Dilation angle
γ	Unit weight
K_0	Earth pressure coefficient at rest
E_{50}	Secant modulus at 50 % strength
E_{oed}	Oedometer modulus
E_{ur}	Unload-reload modulus
E'	Effective modulus
m	Power of stress dependent stiffness
p_{ref}	Reference pressure
ν	Poisson's ratio
T	Traction
n	Component of unit normal
θ	Angular orientation
σ	Stress
τ	Shear stress
R_{inter}	Interface reduction factor
θ	Angle
E^*_{py}	Initial stiffness of p-y curve

References

API, **2007**. American Petroleum Institute API. *Recommended Practice for Planning, Designing and Constructing Fixed Offshore Plat-forms-Working Stress Design, RP 2A-WSD*, 2007.

Bolton, **1986**. M. D. Bolton. *The strength and dilitancy of sands*. Géotechnique 36 no. 1, pages 65–78, 1986.

Brinkgreve, Engin, and Swolfs, **2012**. R. B. J. Brinkgreve, E. Engin, and W. M. Swolfs. *Plaxis 3D 2011 Manual*, 2012.

DNV, **2010**. Det Norske Veritas DNV. *Offshore standard DNV-OS-J101: Design of offshore wind turbine structures. Technical report DNV-OS-J101*, 2010.

Fan and Long, **2005**. Chia-Cheng Fan and James H. Long. *Assessment of existing methods for predicting soil response of laterally loaded piles in sand*, 2005.

Hald, Mørch, Jensen, Bakmar, and Ahle, **2009**. Tue Hald, Christian Mørch, Leo Jensen, Christian LeBlanc Bakmar, and Kim Ahle. *Revisiting monopile design using p-y curves - Results from full scale measurements on Horns Rev*, 2009.

Ibsen, **2012**. Lars Bo Ibsen. *Ph.D 3 - Modeling Real Soils*, 2012.

Jamiolkowski, Lo Presti, and Manassero, **2004**. M. Jamiolkowski, D. C. F. Lo Presti, and M. Manassero. *Evaluation of Relative Density and Shear Strength of Sands from CPT and DMTl*, 2004.

Kulhawy and Mayne, **2012**. F. H. Kulhawy and P. W. Mayne. *Manual on Estimating Soil Properties for Foundation Design*, 2012.

McGann, Arduino, and Mackenzie-Helnwein, **2011**. Christopher R. McGann, Pedro Arduino, and Peter Mackenzie-Helnwein. *Applicability of Conventional p-y Relations to the Analysis of Piles in Laterally Spreading Soil*, 2011.

Moreno, Mikalauskas, and Diaz, **2011**. Alejandro Borobia Moreno, Linas Mikalauskas, and Jose Luis Troya Diaz. *Experimental and Numerical Evaluation of the behaviour of laterally-loaded non-slender piles*, 2011.

Sørensen, Brødbæk, Møller, Augustesen, and Ibsen, **2009**. Søren Peder Hyldal Sørensen, Kristian Thoustrup Brødbæk,

Martin Møller, Anders Hust Augustesen, and Lars Bo Ibsen. *Evaluation of Load-Displacement Relationships for Non-slender Monopiles in Sand*, 2009.

Sørensen, Brødbøk, Møller, and Augustesen, **2012**. Søren Peder Hyldal Sørensen, Kristian Thoustrup Brødbøk, Martin Møller, and Anders Hust Augustesen. *Review of laterally loaded monopiles employed as the foundation for offshore wind turbines*, 2012.

Soos, **1990**. P. von Soos. *Grundbautaschenbuch Part 4*. 1. edition, 1990.

Chapter 3

A Literature Study on the Effects of Cyclic Lateral Loading of Monopiles in Cohesionless Soil

A Literature Study on the Effects of Cyclic Lateral Loading of Monopiles in Cohesionless Soils

Mette Hansen, Kristian Lange Rasmussen, Torben Kirk Wolf

Department of Civil Engineering, Aalborg University, Denmark

June 11, 2012

Abstract

Today, monopiles are the most typical foundation for offshore wind turbines. During their lifetime large diameter, stiff piles are subjected to millions of small cyclic loads due to environmental forces. The long-term cyclic loading can change the granular structure of the soil surrounding the pile. This may change the stiffness of the soil-pile system and create an accumulated rotation of the pile. The behaviour of the soil-pile system is very complex and the influence of soil parameters, number of load cycles, and size, amplitude and characteristic of the load are examined, as they all contribute to the rotation an the change in stiffness. The scope of this article is to outline current design methods and the state of the art knowledge within the subject of long-term cyclic, lateral loading of piles.

1 Introduction

Today's focus on renewable energy sources as a replacement for fossil fuels and gasses has made the offshore wind industry expand rapidly. Large farms with wind turbines still increasing in size are installed in rough environment and are subjected to lateral loads from wind, waves and current. Monopile foundations are the most common foundation of offshore wind turbines. Currently, these steel cylinders have reached a diameter of 4 - 6 m and have a slenderness ratio, $L/D < 10$, where L denotes the length of the pile and D is the diameter.

A wind turbine will, during its lifetime, be subjected to large loads caused by storms which describe the ultimate limit state (ULS). However, also smaller long-term cyclic loads will affect the serviceability limit state (SLS) and fatigue limit state (FLS). These cyclic loads will rock the pile and restructure the soil grains surrounding the pile. This may change the stiffness of the combined pile-soil system and induce accumulated rotation of the tower due to this change. Change in the stiffness of the pile-soil system changes the frequency of this system which then can interfere with the excitation frequencies. The excitation frequencies are the frequencies of the rotor and the blades, approximately 0.3 Hz and 1.0 Hz, respectively. The natural frequency of the tower is normally designed to be in-between to avoid resonance (LeBlanc et al., 2010a). The design criteria is often very strict due to operating behaviour and often the accumulated permanent rotation of the tower must not exceed 0.5°. As the rotation is an important factor in the design criteria it is important to investigate the effect of long-term cyclic loading on the pile-soil system. In the present standards, i.e. DNV (2010) and API (2007) cyclic loading is not given much attention. These standards use p-y curves based on few full-scale experiments for laterally loaded slender piles and use a simple reduction factor to reduce the ultimate soil resistance for cyclic loading. The effect of long-term cyclic loading of monopiles placed in cohesionless soil is possible to be a critical design factor and the effect of change in load characteristic, soil parameters, number of load cycles have not been properly examined.

A new potentially critical load case, long-term cyclic loading, is possibly the main design criteria and the effect of change in the above mentioned factors should be analysed. Therefore, the concept of degradation due to cyclic loading is of interest. Methods for determining degradation of p-y curves have been presented by Long and Vanneste (1994) and Lin and Liao (1999) based on full-scale tests. Other authors have tried to determine the cyclic load effect

by other theories; Testing of soil, small-scale testing and numerical modelling. Niemunis et al. (2005) have suggested a model to predict accumulated deformations based on laboratory tests on sand. Triaxial tests in combination with theoretical and numerical models have been used by Hinz et al. (2006) and Achmus et al. (2009) to determine the relation between cyclic loading and deflection. Small-scale experiments are conducted by Peng et al. (2006), Peralta and Achmus (2010), LeBlanc et al. (2010a) and LeBlanc et al. (2010b) using theories on degradation and concept of superposition to evaluate cyclic loading effect on displacement and change in soil stiffness.

The scope of this article is to outline the current design methods, the state of the art knowledge on the topic and need for further investigations.

2 Behaviour of Cohesionless Soil under Long-Term Cyclic Loading

Subjected to cyclic loading cohesionless soil can experience accumulation of excess pore water pressure. The build-up of this will reduce the effective stresses causing cyclic liquefaction or cyclic mobility, cf. Figure 1.

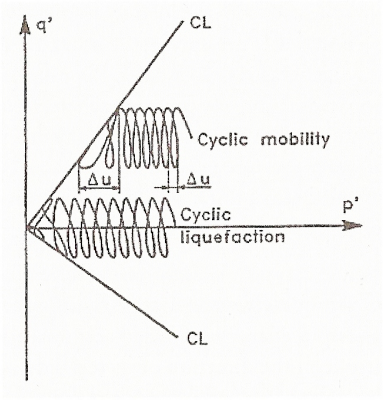

Figure 1: Definition of cyclic liquefaction and cyclic mobility. (Ibsen, 1994)

The build-up of excess pore water pressure is a system behaviour related to drainage conditions and therefore more relevant for shallow foundations. For cohesionless soils of very loose densities a contracting behaviour can be observed. However, the monopile is a deep foundation normally placed in rather dense sands, which makes the concept of cyclic liquefaction less relevant (Lesny, 2010). During the lifetime of an offshore wind turbine waves and wind will cause millions of small cyclic lateral loads. Subjected to those, cohesionless soil will deform both elastic and plastic. Theories on determining the accumulated plastic deformation due to relatively low long-term cyclic loading takes its origin in shakedown theory. Shakedown theory is originally developed for elastic-perfectly plastic materials. However, the theory is used to some extend in soil mechanics, even though behaviour of soils are more complicated. Shakedown has different deformation outcomes related to the type of force applied. For the given problem of long-term cyclic lateral loading elastic and plastic behaviour occurs initially. The shakedown is the development of accumulated plastic strains where the plastic strain increments will decrease with number of cycles and the material will stabilise with eventually only elastic deformation occurring, cf. Figure 2.

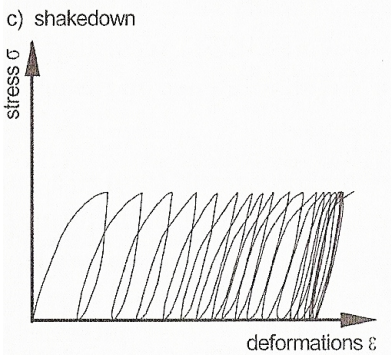

Figure 2: Principle of shakedown due to cyclic loading. (Lesny, 2010)

However, when applying the shakedown theory to soil mechanics in cohesionless soils the theory fits only partially. Cohesionless soil keeps deforming even after long time repetitive loading and does not reach perfect elasticity, but will keep deforming (Goldscheider, 1977). The constant development of strains can increase the accumulated strains of the structure to a point where it becomes unserviceable. Goldscheider (1977) investigated plastic shakedown in sand. After a larger number of cycles the plastic displacement increments will have become almost insignificant. He suggested the allowable total displacement was based on the number of cycles for the lifetime of the wind turbine with an additional small, negligible displacement, Figure 3.

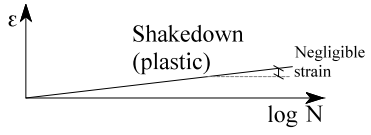

Figure 3: Principle of plastic shakedown. After Peralta (2010)

3 Current Design Regulations

Reese et al. (1974) and O'Neill and Murchison (1983) have formulated the theory on p-y curves for sand to describe the relationship between soil resistance created in the non-uniform stress field surrounding the pile and the lateral displacement of the pile under lateral load, cf. Figure 4. The bending of the pile is described by the fourth-order differential equation for beam bending (DNV, 2010)

$$E_p\, I_p \frac{\mathrm{d}^4 y}{\mathrm{d}z^4} + Q_A \frac{\mathrm{d}^2 y}{\mathrm{d}z^2} - p(y) = 0, \quad z \in [0; L] \quad (1)$$

where E_p and I_p are the elasticity modulus and the second moment of area of the pile, respectively. Q_A is the axial load from the turbine tower. The p-y curves are modelled using the Winkler approach with decoupled springs along the pile, each supporting a pile division. For each spring a non-linear p-y curve is created. These curves are adopted and used in current methods for designing laterally loaded piles in the standard codes DNV (2010) and API (2007). The methods are highly empirical as they are fitted by only a few full-scale experiments described by Cox et al. (1974). The experiments encompass both static and cyclic test with up to 100 load cycles. These experiments are conducted on piles in sand with a diameter of 0.61 m and with slenderness ratio about 30. Other tests have been conducted validating the p-y curves but all tests are conducted using slender piles. The basis for the p-y curves differs significantly from the piles used as monopiles today as the difference in slenderness ratio is pronounced and the amount of load cycles in the tests are limited.

The procedure for creating the p-y curves for cyclic lateral load on monopiles in sand by DNV (2010) is

$$p = A\, p_u \tanh\left(\frac{k\, z}{A\, p_u}\, y\right) \quad (2)$$

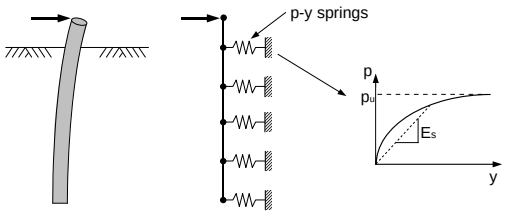

Figure 4: Principle for describing soil behaviour with p-y curves. (API, 2000)

where the p-y relationship is determined from the static ultimate load, p_u. k is the initial modulus of subgrade reaction, z is the distance from soil surface and $A = 0.9$ for cyclic loading. The p-y curves are formulated depending on very few properties of the sand and the pile respectively. For the sand, the angle of internal friction, the relative density, and the specific weight are considered. The dimensions of the pile are considered in terms of length and diameter. However, the general behaviour of the pile is assumed that of slender piles. The monopiles today have a slenderness ratio < 10 and so, this will give the piles a more rigid response which is not accounted for in the current design guidances, i.e. DNV (2010) and API (2007). The difference in behaviour of flexible and rigid piles has great influence on the soil behaviour and the development of a "toe-kick" is significant for rigid piles, cf. Figure 5.

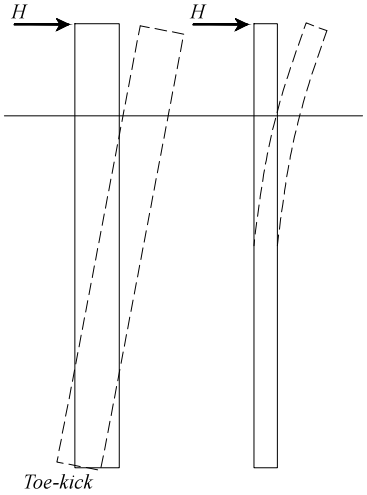

Figure 5: Principle for the behaviour of a rigid and a flexible pile.

Accumulation of displacement and change in stiffness of the soil-pile system are possible over time due to cyclic loading. The relation between the cyclic loading in coherence with number of load cycles and the load amplitude is not considered in the design standards.

4 Methodology for Long-Term Cyclic Loading

In order to incorporate the effect of long-term cyclic loading of a pile, the concept of degradation is adopted by means of different methods. A degradation index is presented by Idriss et al. (1978) as Equation (3) to describe the change in stiffness and shape of the hysteresis loop as a

function of the number of cycles.

$$\delta = \frac{E_{sN}}{E_{s1}} = N^{-a} \tag{3}$$

where E_{sN} and E_{s1} are the secant moduli of N and 1 cycles, respectively, and a is the gradient of the regression line for a logarithmic scale, cf. Figure 6 and 7.

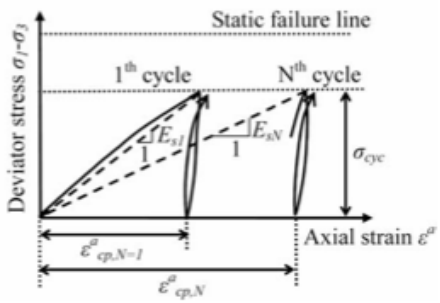

Figure 6: Degradation of stiffness after number of cycles. (Achmus et al., 2009)

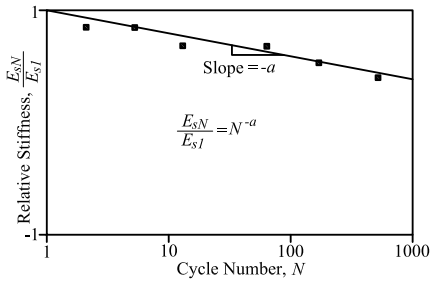

Figure 7: Degradation of stiffness after number of cycles. K is the subgrade modulus. After (Briaud and Little, 1988)

This degradation factor has become a generally adopted concept in determining cyclic load effects, leading to explicit methods for determining the stress-strain relations for cyclic loading. The concept was continued by Briaud and Little (1988) who proposed a power function for degrading the soil resistance as a function of the number of load cycles. With origin in this formulation and the static p-y curves Long and Vanneste (1994) analysed results from 34 full-scale laterally loaded pile tests to investigate which model parameters influenced the behaviour of the pile when repetitively loaded. The 34 tests varied in many aspects from each other: pile type and installation method, length and diameter of the pile, soil density, number of cycles, and load characteristic. The slenderness ratio spanned from 3 to 84 covering both very rigid and flexible piles placed in different cohesionless soils varying from loose to dense compaction. The piles were loaded differently; one- and two-way loaded, subjected from 5 to 500 load cycles. A degradation factor, m, was determined, influenced by the cyclic load ratio, F_L, The installation method, F_I, and the soil density, F_D.

$$m = 0.17\, F_L\, F_I\, F_D \tag{4}$$

Long and Vanneste (1994) specified expressions for calculating soil resistance, p, and displacement, y, as a function of load cycles when using static nonlinear p-y curves. The soil resistance was decreased while pile deflection was increased with increasing number of load cycles, cf Equation (5) and (6).

$$p_N = p_1\, N^{(\alpha-1)m} \tag{5}$$

$$y_N = y_1\, N^{\alpha\, m} \tag{6}$$

where the subnotation $_N$ denoted N cycles and $_1$ denoted the first cycle. The factor α controlled the relative contribution of soil resistance and deflection and was applied so change in p-y relation with depth could be incorporated. The value of the factor varied from 0 to 1. However, changing the α factor provided no improvement in results, so a constant value of $\alpha = 0.6$ was applied, making the method independent of depth.

Lin and Liao (1999) also developed an expression for a degradation parameter, t, to account for different model properties with the purpose of calculating the accumulation of pile displacements. This was derived from analysis of 26 full-scale lateral load tests with pile slenderness ratios from 4 to 84, subjected to a maximum of 100 load cycles. They derived the same factors of influence: Cyclic load ratio, ϕ, installation method, ξ, and soil density, β. In addition, the degradation factor was dependent on pile-soil relative stiffness ratio expressed by a depth coefficient, L/T.

$$t = \eta \frac{L}{T}\, \phi\, \xi\, \beta \tag{7}$$

where the coefficient η changes with the model parameters such as soil density, load characteristic and method of installation. To determine the accumulated displacement the relationship between strain, ε, and displacement, y, proposed by Kagawa and Kraft (1980) was used

$$\varepsilon = \frac{y}{2.5\, D} \tag{8}$$

where D is the diameter of the pile. Kagawa and Kraft (1980) investigated displacement due to lateral load and found that a large part of the accumulated strain happened within a radius of 2.5 m diameters of the pile. Lin and Liao (1999)

use the strain ratio, R_s, expressed by a logarithmic function, to determine strains as a function of load cycles

$$R_s = \frac{\varepsilon_N}{\varepsilon_1} = 1 + t\ln(N) \quad (9)$$

where ε_N is the strain accumulation after N cycles and ε_1 iss the strain after the first cycle. Additionally, Lin and Liao (1999) investigate the combination of variable load amplitudes. Here, a principle of strain superposition similar to Miner's rule is used (Miner, 1945). An adapted version is proposed by Stewart (1986) to superpose strains in triaxial tests. This theory yields that a specific amount of strain can be developed for various numbers of load cycles at different load levels, cf. Figure 8. Thus, for cohesionless soils it is assumed that at some point the maximum strain will have accumulated independently of the size of the cyclic load; the number of cycles will differ instead. With origin in Equation (9) the amount of strain for a number of cycles at a given load level, N_a, can be found and from this, an equivalent number of cycles for a smaller load level, N_b^*, is determined.

$$N_b^* = \exp\left(\frac{1}{t_b}\left(\frac{\varepsilon_{1a}}{\varepsilon_{1b}}\left(1 + t_a\ln(N_a)\right) - 1\right)\right) \quad (10)$$

where t and ε_1 are the degradation factor and strain for the first load cycles for the respective load cases. a and b denote two different load levels. For varying load amplitudes the total amount of strain can be determined.

$$\varepsilon_{N(a+b)} = \varepsilon_{1b}\ [1 + t_b\ln(N_b^* + N_b)] \quad (11)$$

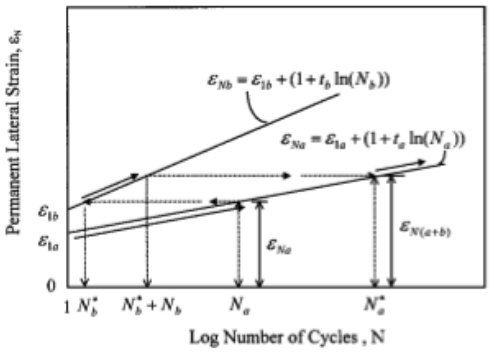

Figure 8: Method used in pile permanent displacement calculations for mixed loads. (Stewart, 1986)

Lin and Liao (1999) used 20 tests to develop the degradation factor, t. Measured and calculated displacements were then found for six additional tests with change in load levels and load characteristics for each ten cycles. In Figure 9 results from Lin and Liao (1999) are presented. As comparison, results from using the method by Long and Vanneste (1994) are presented for one load level along with the measured result by Briaud and Little (1988). For the first three load levels (up to 30 cycles) the calculated and measured displacements are much alike. However, at the fourth load level the calculations overrate the displacement.

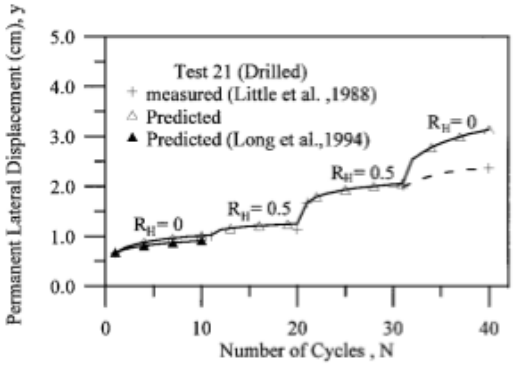

Figure 9: Permanent lateral displacement for number of cycles of test pile. After (Lin and Liao, 1999).

Both Long and Vanneste (1994) and Lin and Liao (1999) have presented simple methods for estimating displacements for piles. The disadvantage of using these explicit methods is their use of an empirical foundation: Their methods are based on experiments conducted on slender piles cyclically loaded to a maximum of 500 cycles. When using these explicit methods for larger numbers of cycles, variation in characteristic and model dimensions should be investigated. Solving implicitly using the finite element method, strains are determined for every load cycle in the load history. This can accumulate computational error when calculating strains for thousands of cycles and the process is time consuming. The studies already done on the effect of cyclic behaviour show that it is a very complex problem. The soil/pile system is affected by material properties of both soil and pile, geometry of the pile and the multifaceted loading. There is a need for experimental work that can validate and improve the theoretical basis so it fits today's problem of cyclic long-term loading of monopiles.

5 Experimental Studies of Cyclic Loading

The formulations by Long and Vanneste (1994) and Lin and Liao (1999) are based on full-scale tests. The formulas are based on empirical data with only a low number of load cycles. Further experiments are needed as a basis for determining the effect of long-term lateral loading. The full-scale test is the primary and best basis to

support the theory but it is very expensive and time consuming. A small-scale test is therefore often used in several experiments to obtain data from long-term cyclic loading which then is converted to fit real conditions. Some of the newer research on cyclic loading is presented in the following.

When working with cyclic lateral loading the load characteristics are defined by the ratios ζ_b and ζ_c (LeBlanc et al., 2010a). ζ_b describes the ratio between the maximum cyclic moment, M_{max}, and the maximum static moment capacity, M_S. ζ_c describes the ratio between maximum and minimum moment, M_{min}, of a load cycle.

$$\zeta_b = \frac{M_{max}}{M_S} \, , \, \zeta_c = \frac{M_{min}}{M_{max}} \tag{12}$$

Peng et al. (2006) investigated different loading devices for small-scale testing and invented a device themselves where the effect of long-term cyclic loading was examined. Most of their focus was on the actual testing device but some test results were presented. They investigated two-way loading of a 44.5 mm wide pile with a slenderness ratio of 9. The pile was placed in dry sand with a relative density of 71.7 %. The applied loading was in the ranges ζ_b = 0.2 to 0.6 and ζ_c = (-1) to (-0.6) creating load amplitude both in and out of balance. 10000 load cycles were conducted for each test and within that range Peng et al. (2006) concluded that the accumulated pile displacement would keep increasing and that displacements were largest for unbalanced loading.

A development in the concept of degradation was made by Achmus et al. (2009) who researched the degradation of stiffness in cohesionless soils as a consequence of cyclic loading. Based on triaxial tests and FEM, design charts for determining deflection along a pile as function of the number of cycles were developed. The degradation was expressed by means of the ratio of the secant elastic modulus, cf. Figure 6. The secant modulus, E_s, is elastic and dependent on the stress conditions along the pile.

$$E_s = k \, \sigma_{at} \left(\frac{\sigma_m}{\sigma_{at}} \right)^{\lambda} \tag{13}$$

where k and λ are material parameters and σ_{at} and σ_m are atmospheric pressure and mean principal stress. The accumulation of strains and thereby the plastic strain ratio is estimated by the semi-empirical approach presented by Huurman (1996).

$$\frac{E_{sN}}{E_{s1}} \cong \frac{\varepsilon_{cp,1}}{\varepsilon_{cp,N}} = N^{-b_1 (X)^{b_2}} \tag{14}$$

where ε_{cp} is the plastic axial strain. The ratio of secant stiffness and the ratio of the plastic axial strain are determined between the N^{th} and the first cycle. b_1 and b_2 are material parameters and X is the cyclic stress ratio which defines the relation between major principal stresses for cyclic stress state and static failure state. In triaxial tests the initial stress state is isotropic with constant confining pressure during cyclic loading. For real in situ conditions the stresses are anisotropic so to overcome these differences a characteristic cyclic stress ratio, X_c, is defined.

$$X_c = \frac{X^1 - X^0}{1 - X^0} \tag{15}$$

where indices 1 and 0 define states of loading and unloading. The outcome of the study is design charts recommended by Achmus et al. (2009) for preliminary design giving the deflection as function of number of load cycles, cf. Figure 10. The charts provide deflection curves for up to 10000 cycles. However, the study lacks the support of full- or small-scale tests.

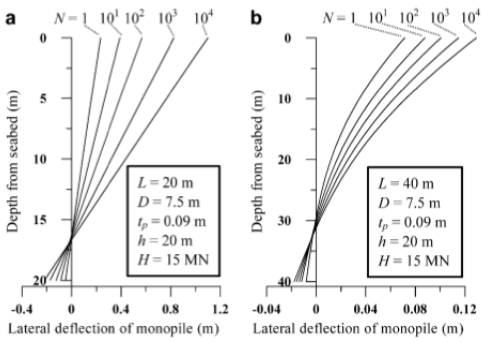

Figure 10: Deflection-Number of cycles curve. (Achmus et al., 2009)

Peralta and Achmus (2010) conducted a series of 13 small-scale tests on rigid and flexible piles with 60 mm diameter and slenderness ratio from 3.2 to 8.3. The piles were tested in medium dense to dense sand with relative densities, D_r, from 0.40 to 0.60. They were subjected to one-way loading of varying load size, ζ_b, for 10000 load cycles and the displacement of the pile was found.

The accumulated displacements obtained from the experiments were compared with results obtained from the power and logarithmic functions by Long and Vanneste (1994) and

Lin and Liao (1999) expressed in Equation (6) and (9), respectively. It was found that the results from flexible piles fitted the logarithmic function best while the power function fitted the results from the rigid piles best.

Small-scale tests were conducted by LeBlanc et al. (2010a) who also put a great amount of work in to the scaling of model and real conditions. They made 21 tests on piles in sand with relative densities, D_r, of 0.04 and 0.38; 6 static and 15 cyclic tests. The pile had a diameter of 80 mm and a slenderness ratio of 4.5. The tests were conducted with variation in ζ_b from 0.2 to 0.53 and ζ_c from -1 to 1 describing both static loading and one- and two-way cyclic loading. The number of load cycles also varied from approximately 8000 to 65000. LeBlanc et al. (2010a) suggest that the best fit of the accumulation of rotation is a power function.

$$\frac{\Delta\theta(N)}{\theta_s} = \frac{\theta_N - \theta_1}{\theta_s} = T_b(\zeta_b, R_d) T_c(\zeta_c) N^{0.31} \quad (16)$$

where θ_N is the rotation at N cycles, θ_1 is the rotation after the first load cycle and θ_s is the rotation in a static test at a load equivalent to the one provided by the maximum cyclic load, cf. Figure 11.

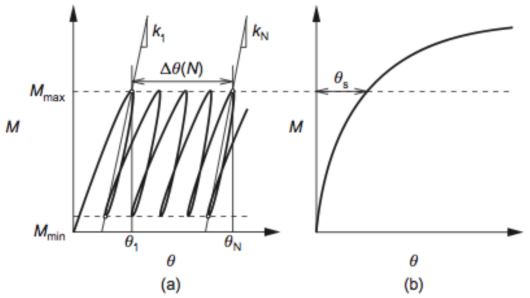

Figure 11: Method for determination of stiffness and accumulated rotation: (a) cyclic test; (b) static test. After (LeBlanc et al., 2010a)

T_b and T_c are dimensionless functions depending on the load characteristics and relative density. For T_b a linear relationship with ζ_b is found depending on D_r, cf. Figure 12. A non-linear relationship between T_c and ζ_c is also found illustrating that the largest accumulation of rotation happens when ζ_c= -0.6 which is a two-way loading.
A study on the change in stiffness of the soil-pile system did not provide as clear results as the rotation accumulation. It cannot be concluded how the stiffness is affected by the relative density. However, similar for all tests is an increase in stiffness with increase in number of load cycles. This increase is contradictory to

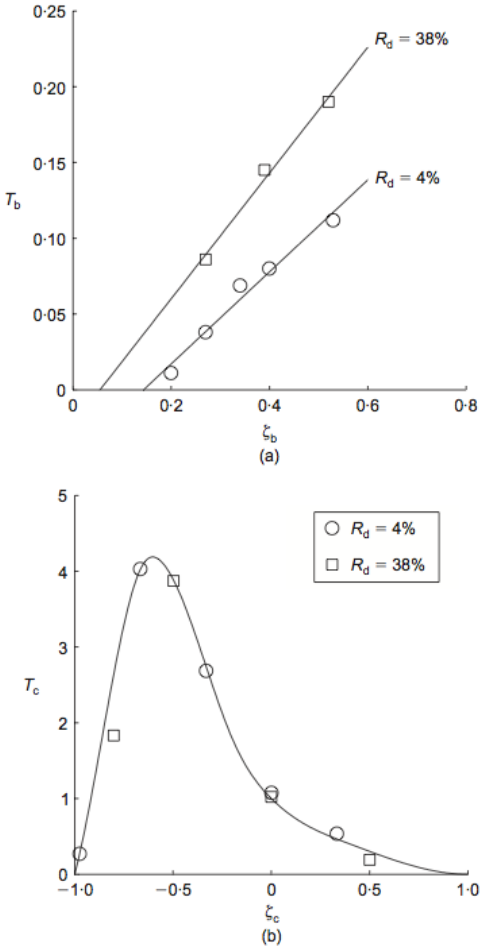

Figure 12: Functions relating (a) T_b and (b) T_c to relative density, D_r, and characteristics of cyclic load in terms of ζ_b and ζ_c. (LeBlanc et al., 2010a)

current methodology which uses degradation of static p-y curves to account for cyclic loading.

Achmus et al. (2011) presented a FE-model based on strain degradation to verify the results obtained by LeBlanc et al. (2010a) and found good agreement between the simulations and the test results.

Based on the method by LeBlanc et al. (2010a) and a super positioning concept similar to Miner's rule, LeBlanc et al. (2010b) created design charts for determining the accumulated pile rotation due to random two-way loading. The procedure is based on a limited amount of empirical data from small-scale tests and further research should by carried out to investigate the complicated behaviour of change in parameters.

6 Summary

Currently, the design guidance is limited in knowledge on long-term cyclic loading of laterally loaded piles. They are based on full-scale testing of slender piles subjected to a low number of cycles.

The issue of long-term lateral loading is of complex matters. The physical behaviour of sand subjected to load cycles is a continuous plastic deformation with decreasing deformation increments. This effect of long-term lateral loading has been formulated by Long and Vanneste (1994) and Lin and Liao (1999) as an exponential and a logarithmic expression, respectively, depending on a degradation factor. Both authors find that the degradation factor can be determined based on installation method, soil density and load ratio. In addition Lin and Liao (1999) incorporates a depth coefficient. Still, these theories are based on full-scale testing of no more than 500 load cycles. The small-scale tests on laterally loaded piles focus on a high number of load cycles, i.e. approximately 10000 cycles. Different load scenarios with varying load characteristic and amplitude is tested with the outcome that Peng et al. (2006), Peralta and Achmus (2010) and LeBlanc et al. (2010a) agree that the pile will keep deforming and the exponential expression by Long and Vanneste (1994) fits rigid piles behaviour.

The influence of long-term lateral loading of offshore wind turbines is a multifaceted problem. Though many author have studied the area it is clear that no general approach have been accomplished yet and further studies are needed.

References

Achmus, Kuo, and Abdel-Rahman, **2009**. M. Achmus, Yu-Shu Kuo, and Khalid Abdel-Rahman. *Behaviour of Monopile Foundations under Cyclic Lateral Load*. Computer and Geotechnics, 36(5), 725–735, 2009.

Achmus, Albiker, and Abdel-Rahman, **2011**. M. Achmus, J. Albiker, and Khalid Abdel-Rahman. *Investigations on the Behaviour of Large Diameter Piles under Cyclic Lateral Load*. 2011. ISBN: 978-0-415-58480-7.

API, **2007**. American Petroleum Institute API. *Recommended Practice for Planning, Designing and Constructing Fixed Offshore Plat-forms-Working Stress Design, RP 2A-WSD*, 2007.

API, **2000**. American Petroleum Institute API. *User Manual Program PYGMY.* The University of Western Australia, Department of Civil and Resource Engineering, 2000.

Briaud and Little, **1988**. J. L. Briaud and R. L. Little. *Full Scale Cyclic Lateral Load Tests on six Single Piles in Sand*. Miscellaneous Paper, Geotechnical Division, Texas AandM University, College Station, Texas, USA, GL 88-27, 1988.

Cox, Reese, and Grubbs, **1974**. W. R. Cox, L. Reese, and B. R. Grubbs. *Field Testing of Laterally Loaded Piles in Sand*. Proc. 6th Offshore Technological Conference, Houston, Paper No. 2079, 459–472, 1974.

DNV, **2010**. Det Norske Veritas DNV. *Offshore standard DNV-OS-J101: Design of offshore wind turbine structures. Technical report DNV-OS-J101*, 2010.

Goldscheider, **1977**. M. Goldscheider. *Shakedown and Incremental Collapse of Structures in Dry Sand Bodies*, 1977.

Hinz, Lesny, and Richwien, **2006**. P. Hinz, K. Lesny, and W. Richwien. *Prediction of Monopile Deformation under High Cyclic Lateral Load*. Institute for Soil Mechanics and Foundation Engineering, Germany, 2006.

Huurman, **1996**. M. Huurman. *Development of Traffic Induced Permanent Strain in Concrete Block Pavements*. Heron, 41(1) 2952, 1996.

Ibsen, **1994**. L. B. Ibsen. *The Stable State in Cyclic Loading*. Soil Dynamics and

Earthquake Engineering, Vol. 13, No. 1, 63–72, 1994.

Idriss, Dobry, and Singh, **1978**. I. M. Idriss, R. Dobry, and R. D. Singh. *Nonlinear Behavior of Soft Clays During Cyclic Loading*. Journal of Geotechnical Engineering Division, ASCE, Vol. 104, No. GT12, 1427–1447, 1978.

Kagawa and Kraft, **1980**. T. Kagawa and L. M. Kraft. *Lateral load-deflection relationships of piles subjected to dynamic loadings*. Soils and Foundations, 20(4), 19–34, 1980.

LeBlanc, Houlsby, and Byrne, **2010a**. C. LeBlanc, G. Houlsby, and B. Byrne. *Response of Stiff Piles to Long-term Cyclic Lateral Load*. Géotechnique 60, No. 2, 79–90, 2010a.

LeBlanc, Houlsby, and Byrne, **2010b**. C. LeBlanc, G. Houlsby, and B. Byrne. *Response of Stiff Piles to Long-term Cyclic Lateral Load*. Géotechnique 60, No. 9, 715–721, 2010b.

Lesny, **2010**. Kerstin Lesny. *Foundations of Offshore Wind Turbines - Tools for Planning and Design*. 1. edition, 2010. ISBN:978-3-86797-042-6.

Lin and Liao, **1999**. S. S. Lin and J. C. Liao. *Permanent Strains of Piles in Sand due to Cyclic Lateral Loads*. Journal of Geotechnical and Geoenvironmental Engineering, 125(No. 9), 789–802, 1999.

Long and Vanneste, **1994**. J. Long and G. Vanneste. *Effects of Cyclic Lateral Loads on Piles in Sand*. Journal of Geotechnical and Geoenvironmental Engineering, 120(No. 1), 225–244, 1994.

Miner, **1945**. M. A. Miner. *Cumulative Damage in Fatigue*. Journal of Applied Mechanics, 12, A159–A164, 1945.

Niemunis, Wichtmann, and Triantafyllidis, **2005**. A. Niemunis, T. Wichtmann, and T. Triantafyllidis. *A High-cycle Accumulation Model for Sand*. Computer and Geotechnics, 32(4), 245–263, 2005.

O'Neill and Murchison, **1983**. M. W. O'Neill and J. M. Murchison. *An Evaluation of p-y Relationships in Sands*, 1983.

Peng, Clarke, and Rouainia, **2006**. J. R. Peng, B. G. Clarke, and M. Rouainia. *A Device to Cyclic Lateral Loaded Model Piles*. Geotechnical Testing Journal, 29(4), 1–7, 2006.

Peralta, **2010**. K. P. Peralta. *Investigations on the Behaviour of Large Diameter Piles under Long-term Lateral Cyclic Loading in Cohesionless Soil*, 2010.

Peralta and Achmus, **2010**. K. P. Peralta and M. Achmus. *An Experimental Investigation of Piles in Sand Subjected to Lateral Cyclic Loads*, 2010. ISBN 978-0-415-59288-8.

Reese, Cox, and Koop, **1974**. L.C. Reese, W. R. Cox, and F. D. Koop. *Analysis of Laterally Loaded Piles in Sand*. OTC Huston, (paper no. 2080), 1974.

Stewart, **1986**. H. E. Stewart. *Permanent Strains from Cyclic Variable-Amplitude Loadings*. Journal of Geotechnical Engineering, Vol. 112(No. 6), 646–660, 1986.

Chapter 4

Small-Scale Testing of Cyclic Laterally Loaded Pile in Cohesionless Soil

Small-Scale Testing of Cyclic Laterally Loaded Pile in Cohesionless Soil

Mette Hansen, Kristian Lange Rasmussen, Torben Kirk Wolf

Department of Civil Engineering, Aalborg University, Denmark

June 11, 2012

Abstract

The accumulated rotation due to long-term lateral loading is a current issue of interest as today's design guidance have little knowledge in this area. In this paper a small-scale test of a pile subjected to cyclic, lateral loading is treated in order to investigate the effect of cyclic loading. The pile has a length/diameter ratio, slenderness ratio, of 6 that resembles the ratio of offshore wind turbines today and is placed in saturated sand. Force and displacement during the cyclic loading is recorded to determine the accumulated deformation of the pile. The measured data is compared to theoretical expressions as well as results from other recent small-scale tests.

1 Introduction

The monopile foundation is the most commonly used foundation for wind turbines. These foundations often have a diameter of 4 - 6 m and a slenderness ratio, the ratio between the length and the diameter of the pile, of approximately 5 as the normal embedded length is 20 - 30 m. Long-term lateral loading of piles is an area on which the recent design guidances have little knowledge. It is of current interest since the long-term loading may create rotation (tilt) of the pile by change in the soil-pile system which is critical in the serviceability limit state (SLS).

The issue is rather complex as many parameters seem to influence the behaviour of the soil-pile system. Parameters such as load characteristic, number of load cycles and their amplitudes, and soil parameters are all possible to affect this system. Theory on the subject of cyclically loaded piles in sand have among others been presented by Long and Vanneste (1994) and Lin and Liao (1999) in terms of degradation factors. These are implemented in determining deformation of the pile by means of soil density, installation method of the pile, and load ratio. The theories are simple and give an estimate on deformations based on relatively few full-scale experiments with no more than 500 load cycles. As full-scale testing is comprehensive experimental studies in small-scale testing is pursued. In the following, the more recent work in small-scale testing in sand by Peng et al. (2006), Peralta and Achmus (2010), LeBlanc et al. (2010a) and Roesen et al. (2011b) is outlined.

In order to further investigate the subject of long-term lateral loading a small-scale experiment of a pile placed in saturated soil is conducted. First a monotonic loading is applied to the pile to determine the ultimate capacity. Based on the capacity, a cyclic load is chosen and the pile is subjected to one-way cyclic loading. The test results are compared with the theoretical basis for determining effects of cyclic load.

2 Recent Small-Scale Cyclic Testing

Peng et al. (2006) subjects a 44.5 mm wide pile with a slenderness ratio of 9 to two-way loading. The load scenarios are both balanced and unbalanced. The pile is placed in dry sand with a relative density, $D_r = 0.72$. Based on a few tests subjected to approximately 10000 load cycles they reach the conclusion that the soil-pile system will keep deforming with increase in number of cycles. They also observe that larger deformation is caused by unbalanced loading in comparison with balanced loading.

Peralta and Achmus (2010) investigate one-way loading of piles with a diameter of 60 mm and varying length, describing slenderness ratios from 3.2 to 8.3. The tests are conducted in dry sand with D_r from 0.4 to 0.6. Also Peralta and Achmus (2010) experience a continuous deformation after 10000 load cycles. They fit their results to a power and a logarithmic expression and they conclude that the deformation of the rigid piles fit the power function best and the more slender piles fit the logarithmic function.

LeBlanc et al. (2010a) perform both one- and two-way loading of a 80 mm wide pile with a slenderness ratio of 4.5. The sand has D_r of 0.04 and 0.38. In several of their tests the pile is loaded with 8000 to 9000 cycles, for a few tests approximately 18000 cycles are applied and one test is conducted with 65000 cycles. In agreement with Peng et al. (2006) and Peralta and Achmus (2010) they conclude that the system keeps deforming with increase in number of load cycles. They find that a power function fit their data best.

Roesen et al. (2011b) conduct a cyclic loading test of a 60 mm wide pile with a slenderness ratio of 6. The test is of one-way loading. The pile is placed in saturated sand with relative density between 0.78 to 0.87. Approximately 46000 load cycles is applied. In contrast to the previous tests Roesen et al. (2011b) present results where the accumulation in rotation of the pile stabilises. This happens after approximately 15000 load cycles.

3 Experimental Programme

Before the cyclic load test a monotonic load test is carried out. A monotonic load is applied until a predetermined rotation of the pile is reached. The load at this rotation will by defined as the ultimate lateral capacity. The ultimate limit state (ULS) load is used to determine the cyclic load. The size of the maximum force in a load cycle is determined based on LeBlanc et al. (2010a). The load characterising fatigue limit state (FLS) and the serviceability limit state (SLS) is presented by (LeBlanc et al., 2010a) as 28 to 45% of the ULS, respectively. The cyclic test is carried out as a one-way long-term lateral loading. The test setup is capable of producing more than 40000 load cycles.

3.1 Test Setup

The test setup is developed based on the test setup by LeBlanc et al. (2010a) with some geometric deviations. For cyclic lateral loading the load characteristics are defined by the ratios ζ_b and ζ_c (LeBlanc et al., 2010a). ζ_b describes the ratio between the maximum cyclic moment, M_{max}, and the maximum static moment capacity, M_S. ζ_c describes the ratio between maximum and minimum moment, M_{min}, of a load cycle, cf. Equation (1). A list of symbols is in the back of the article.

$$\zeta_b = \frac{M_{max}}{M_S} \ , \ \zeta_c = \frac{M_{min}}{M_{max}} \tag{1}$$

The tests are conducted in a cylinder shaped, steel container which has an inner diameter of 1980 mm and a depth of 1200 mm, cf. Figure 1. The bottom of the container is equipped with equally distributed pipes and 300 mm gravel, used as draining material, which is covered with a sheet of geotextile. The pipes are perforated making a drainage system to ensure a homogeneous and saturated soil as water level at all times is kept 20 - 40 mm above soil surface.

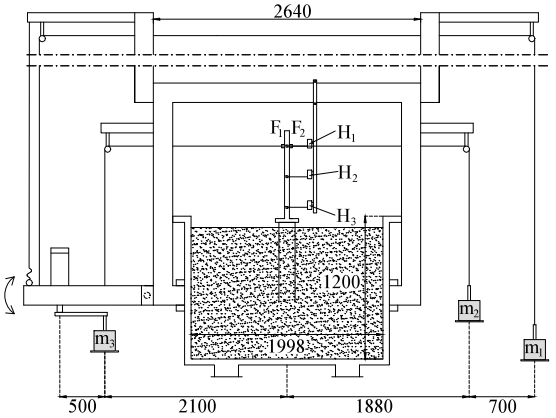

Figure 1: Sketch of the test setup for cyclic loading with dimension in mm. F_1 and F_2 denote the force transducers and H_1, H_2 and H_3 denote the horizontal displacement transducers. m_1, m_2 and m_3 are the weights of mass.

Two different loading systems are used for the static and the cyclic load tests. The static test is conducted, by means of a motor attached to the load frame 600 mm above the soil surface, pulling the pile through a steel wire in a monotonic movement at a speed of 0.02 mm/s. The steel wire is connected to the pile via a load transducer fixated to the pile. For the static test one horizontal and two vertical displacement transducers are attached to the pile to determine the rotation of the pile, as presented by Roesen et al. (2011a). A different setup with three horizontal displacement transducers, H_1, H_2 and H_3 is used for the cyclic test, cf. Figure 1.

The loading system for creating cyclic load is based on the test setup by LeBlanc et al. (2010a) and is a simple mechanical system of weights connected by steel wires to control the loading of the pile. A load frame with pulleys is fixated to the container connecting the masses m_1, m_2 and m_3 via the wires, cf. Figure 1. The wires also connect the masses to a lever on which a motor, providing a rotating behaviour of m_3, is attached. The lever is attached to the load frame by a pivot. Initially, the weight of m_1 is chosen sufficiently to outbalance the weight of this lever, creating an outer system in balance. Masses m_2 and m_3 are each attached to the pile through load transducers with wires at 600 mm above the soil surface and provide the opportunity of different load scenarios as they control the cyclic load characteristic: m_2 controls ζ_b and thereby the average cyclic moment where m_3 controls the cyclic amplitude, expressed by ζ_c. The wire to the outer left is for safety, carrying no weight during the test. The motor produces a sinusoidal long-term cyclic behaviour and to simulate environmental load a rotation frequency of 0.1 Hz is used for the cyclic test (Peng et al., 2006).

The two load transducers attached through wires to m_2 and m_3 measure the actual load that the pile is subjected to. For static loading only one load transducer is used. All measurement equipment is connected to a PC-based data acquisition HBM Spider which transfers measuring data to the computer. Time, forces and horizontal displacements are recorded with a sampling rate of 1 Hz during long-term cyclic loading. During the static tests the sampling rate is 2 Hz.

3.2 Procedure

The pile used in the tests is an aluminium, hollow cylinder with an outer diameter of 100 mm and a slenderness ratio of 6. The pile is installed in the middle of the container with a motor identical to that applying the load under static loading and at the same speed. For the static test a wire is mounted at 600 mm above soil surface. The pile is pulled to a rotation of 3 degrees, then unloaded completely, and reloaded to a rotation higher than 3 degrees. To out-balance the lever in the cyclic test the counterbalance $m_1 = 27$ kg. Once the outer system is in balance the wires are mounted for the cyclic test also in a height of 600 mm above soil surface.

The maximum force during a load cycle is, preferably, 35 % of the ULS load, which is the load resembling FLS. A one-way loading is desired. The combination of the weights is chosen to reach a maximum load of 35 % of the ultimate capacity and a minimum load of 5 - 10 % of the ultimate capacity. To correspond the load a weight of $m_2 = m_3 = 12$ kg is placed on the rig.

Table 1: Material properties of Aalborg University Sand No. 1.

d_s [g/cm^3]	e_{max} [-]	e_{min} [-]	d_{50} [mm]	$U=\frac{d_{60}}{d_{10}}$ [-]
2.64	0.858	0.549	0.14	1.78

3.3 Soil Conditions

The container is filled with 300 mm of gravel and 800 mm of sand. The tests are conducted in fully saturated soil. The sand used in the test setup is Aalborg University Sand No. 1. Material properties can be seen in Table 1. Homogeneity of the soil is important for the interpretation of soil parameters and for comparison of test results. Therefore, the soil is loosened by applying an upward gradient of 0.9 and hereafter the soil is prepared for testing by vibrating it so the sand will compact. Water level will at all times be kept above the soil surface. When vibrating, the water level is approximately 100 mm above the soil surface to ensure no air enters the soil. The gravel in the bottom of the container ensures proper drainage conditions and a homogeneous in-flow.

Prior to the load tests cone penetration tests (CPT) are conducted to evaluate the state of the soil. A mini cone with a diameter of 15 mm is pushed through the sand with a velocity of 5 mm/s. The cone penetrates approximately 360 mm down into the soil. A change in equipment before the cyclic test made it possible to penetrate further, 500 mm. For the static and the cyclic test three CPTs are conducted for each: One in the middle of the container and one to each side in a distance of 500 mm from the middle. An additional CPT test of nine CPTs is conducted to evaluate the variations in homogeneity and the compaction of the sand. All CPTs are made in a straight line parallel to the direction of the force. From the CPTs the cone resistance is obtained, cf. Figure 2. The CPT cone is very sensitive and a proper cone resistance is first obtained when the resistance stabilises. Figure 2 shows a good resemblance among the CPTs and a smooth linear increase except for CPT 1 and CPT 9. CPT 1 shows much higher resistance and both

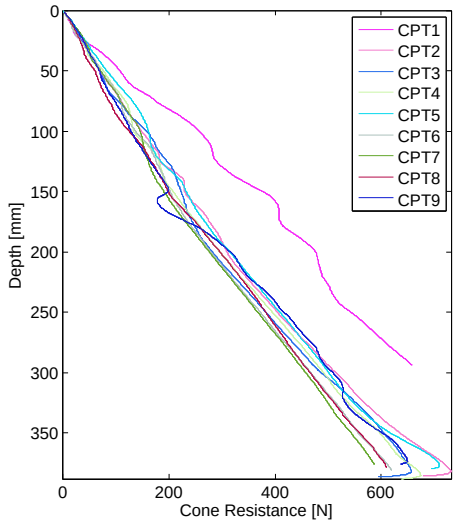

Figure 2: Cone resistance for the nine CPTs taken additionally. The CPTs are taken in order from the passive side to the active side.

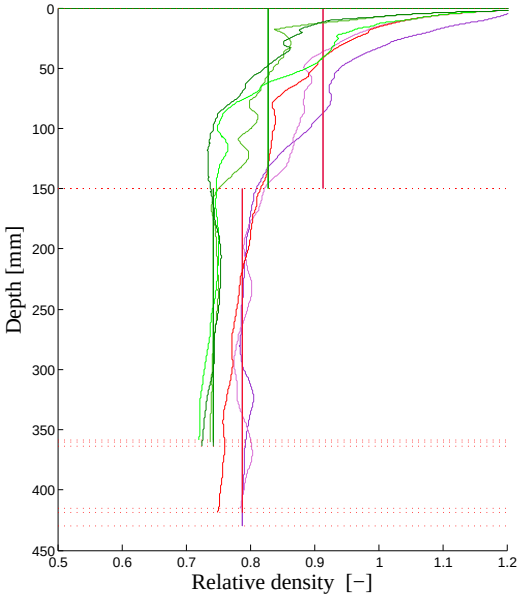

Figure 3: The relative density of the sand for the static test and the cyclic test in green and red shades, respectively.

CPT 1 and CPT 9 are more uneven in their shapes. These two CPTs are made closest to the edge of the container and are clearly affected hereby. The compaction of the sand may be different as the preparation of the sand with the vibration device is difficult along the sides. For CPT 2 to CPT 8 the soil behaves very similar and uniform and are thereby presentable data for determining soil parameters. Also, the resemblance in the cone resistance for those seven CPTs supports using three CPTs to obtain suitable data for the static test and the cyclic test.

The cone resistance is the basis of all further determination of soil parameters. An iterative process proposed in (Ibsen et al., 2009) with Equation (2) to (5) is the first step in finding soil parameters.

$$\gamma = \frac{d_s + e\, S_w}{1 + e}\gamma_w \tag{2}$$

$$\sigma_1' = (\gamma - \gamma_w)\, x \tag{3}$$

$$D_r = c_2 \frac{\sigma_1'^{\,c_3}}{q_c^{c_1}} \tag{4}$$

$$D_r = \frac{e_{max} - e}{e_{max} - e_{min}} \tag{5}$$

where the degree of saturation, $S_w = 1$ and x is the depth. From Equation (2) to (5) the unit weight, γ, the void ratio, e, and thereby the relative density, D_r, are derived. For both the static and the cyclic test the relative densities are shown, cf. Figure 3. q_c is the cone resistance, σ_1' is the vertical effective stress and c_1, c_2 and c_3 are coefficients to determine the relative density from the mini-CPT. The three relative densities obtained from the CPTs taken before the static test are plotted in red shades and the ones made before the cyclic test are shades of green. Near the soil surface very large fluctuations are observed which is a clear sign that the CPT cone has not stabilised. Proper cone resistances are obtained after approximately 150 mm and values obtained above this depth are disregarded. A combined mean relative density for all three CPTs is made for each test. This is done separately for the relative densities above and below 150 mm under soil surface, cf. Figure 3. This clearly illustrates that the values obtained above this limit differ from the more stabilized values below the limit. One mean value is used as representative for the entire soil layer and these are determined on behalf of values obtained from 150 mm below the soil surface and down. The mean relative density for the two tests, μ, are given in Table 2. The standard deviations, σ, are also shown. It should be noted that the standard deviations are not used in any further calculations, as the parameters are not normally distributed.

An interesting observation, cf. Figure 3, is that the relative density seems to decrease slightly with depth. This behaviour is especially pronounced for the CPT made before the cyclic test. Due to overburden pressure the opposite effect would be expected. This decrease may be caused by the sand being a young deposit. Further vibration and thereby a better compaction may create an increasing relative density with soil depth.

Table 2: Mean value, μ, and standard deviation, σ, of soil parameters of Aalborg University No. 1.

Test	Statistical parameter	D_r [-]	e [-]	γ' [kN/m^3]
Static	μ	0.74	0.63	10.3
	σ	0.01	0.00	0.1
Cyclic	μ	0.79	0.61	10.8
	σ	0.02	0.00	0.2

The strength parameters of the sand are calculated using formulas derived in (Ibsen et al., 2009), cf. Equations (6), (7), and (8). These expressions are derived for Aalborg University Sand No. 1 at confining pressures, σ_3', in the range of 5 kPa to 800 kPa. As σ_3' is outside this range over the entire depth of the setup, σ_3' is set to 5 kPa in the derivation of the strength parameters. This is considered a better estimation than using confining pressures outside the range of validity of the formulas. The results are shown in Table 3.

$$\phi_{tr} = 0.152\, D_r + 27.39\, \sigma_3'^{-0.2807} + 23.21 \quad (6)$$

$$\psi_{tr} = 0.195\, D_r + 14.86\, \sigma_3'^{-0.09764} - 9.946 \quad (7)$$

$$c = 0.032\, D_r + 3.52 \quad (8)$$

Table 3: Mean value, μ, and standard deviation, σ, of strength parameters evaluated on basis of CPT test.

Test	Statistical parameter	φ [°]	ψ [°]	c [kPa]
Static	μ	51.9	17.2	5.9
	σ	0.1	0.2	0.0
Cyclic	μ	52.6	18.1	6.0
	σ	0.2	0.3	0.0

4 Testing Results

Initially, the static test is run to determine the ultimate load capacity of the laterally loaded pile. The pile is loaded in a monotonic movement and the force-rotation relationship is shown in Figure 4. At a force of approximately 400 N a break on the curve appears. A reason for the break may be found in the test setup. A small chain connects the wire from the motor to the pile. A slip between two links in this chain may have caused the break. The failure load is defined at a rotation of 3°. Thus, the ultimate capacity is approximate 660 N. The pile is afterwards un- and reloaded. The reloading curve continues to increase in force after having crossed the maximum force of the first load curve.

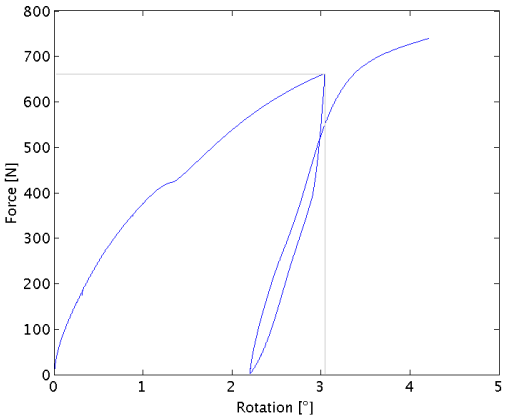

Figure 4: The force-rotation relationship in the static test with failure determined at 3°.

The load applied as m_3 for the cyclic test is determined to 12 kg. Friction in the setup can affect the system. Though, this mass is considered sufficient. Before the test is run the system is in balance. The load transducers are reset and the oscillation in load from the cyclic movement is obtained, cf. Figure 5. The force measured from the sinusoidal loading shows similar, even load cycles for force 1, F_1. A small sinusoidal behaviour is obtained from the load transducer, i.e. force 2, due to friction in the test setup or perhaps due to noise in the measurements. Force 2, F_2, should remain constant during the test. However, the variation is little and will not affect the interpretation, as the resulting force, F, affecting the pile is the difference between F_1 and and F_2, cf. Figure 6. The resulting force varies between

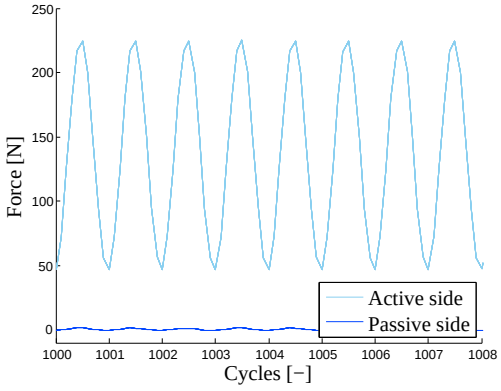

Figure 5: Forces measured under cyclic loading. The active and passive side denote the sides of F_1 and F_2, respectively.

average values of 216 N and 44 N. The force should keep a constant amplitude over time.

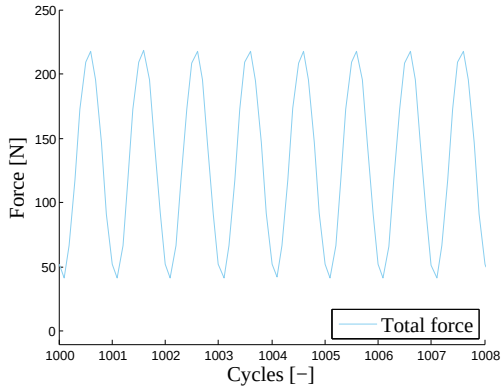

Figure 6: Forces measured under cyclic loading.

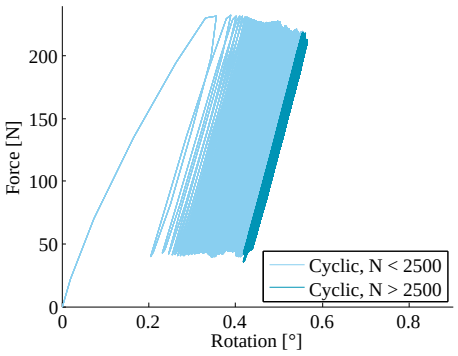

Figure 8: Force/rotation relation at cyclic loading.

However, the maximum force per load cycle slightly decreases over time, cf. Figure 7. The minimum and maximum values of the minimum and maximum forces for the load cycles are given in Table 4. The difference in load may be due to friction in the setup. Figure 8 shows the

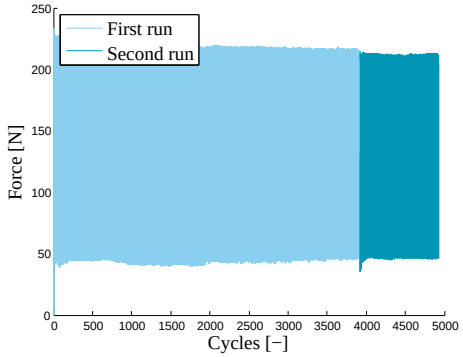

Figure 7: Resulting force from the cyclic loading. The test stops around 3900 cycles and is started again (first and second run).

rotation of the pile affected by load cycles.The response is an increase in stiffness with increasing number of cycles. From the first load cycle a permanent rotation of approximately 0.2° is obtained and the next load cycle only creates an additional permanent rotation of less than 0.03°. Almost half of the rotation is obtained from the first load cycle. In Figure 8 load cycles for $N < 2500$ are light blue and $N > 2500$ are dark blue. The incremental accumulation in rotation decrease with number of cycles. Approximately 5000 load cycles are recorded. A small increase in the load amplitude can be detected after approximately 4000 load cycles, i.e. 0.42° rotation, cf. Figure 8. The cyclic test experienced a mechanical stop and was started again, which caused the irregular behaviour.

The percentage of accumulated rotation after a certain number of load cycles, $\Delta\theta(N)$, is given for the maximum and minimum force in the load cycles. Long and Vanneste (1994) and Lin and Liao (1999) suggest that the rotation of the first load cycle is treated separately. The accumulated rotation after the first rotation is normalised as $\Delta\theta(N) = \theta_N - \theta_1$. Definitions are shown in Figure 9. θ_s is the rotation in a static test at the same load as the corresponding cyclic load. The total

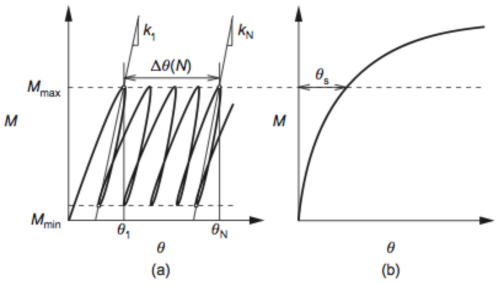

Figure 9: The rotation as function of number of load cycles. (LeBlanc et al., 2010a)

rotation of 100 % is defined after 4919 load cycles, cf. Table 5. The design criteria for

Table 4: Minimum and maximum force in load cycles.

F_{min} [N]	F_{max} [N]
210 - 233	36 - 49

dimensioning laterally loaded piles is related to the permanent accumulated rotation, i.e. the plastic deformations. Previous small-scale testing have determined rotation for the maximum loads, even though this rotation contain both elastic and plastic deformations. However, in agreement with Roesen et al. (2011b) it is assumed that the representative accumulated rotation for describing deformations is given by the minimum load in a load cycle. This load represents the least elastic deformation which is

Table 5: Accumulated rotation for minimum and maximum force in the load cycles.

Load cycle N	$\Delta\theta(N)$ for F_{min} [%]	$\Delta\theta(N)$ for F_{max} [%]
10	33.4	28.6
100	66.0	64.7
1000	84.8	85.7
2000	90.3	91.6
4000	97.3	96.7
4919	100	100

desirable when determining permanent rotation.

The static test and the cyclic test are plotted together in Figure 10. The maximum cyclic force is approximately 33 % of the ULS load. It appears from Figure 10 that the cyclic test has a stiffer response than the static test. When plotting the rotation as a function of number of cycles the initial part of the curve is steep, cf. Figure 11. The curve flattens as the accumulated rotation increments decrease. It is clear that the soil-pile system gets more stable with increase in number of load cycles. However, for the limited data a stabilised situation does not occur and increase in rotation follows with the increase in number of cycles. The rotation will keep increasing with decreasing increments.

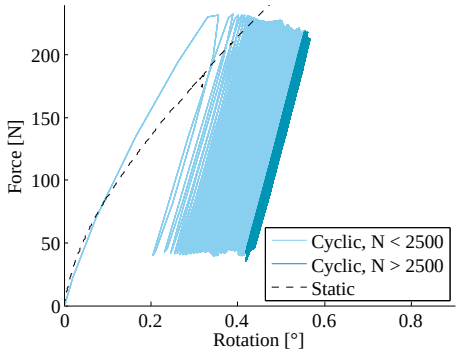

Figure 10: The force-rotation relationship at the static test and the cyclic test.

This tendency is also experienced in other small-scale tests by Peng et al. (2006), Peralta and Achmus (2010) and LeBlanc et al. (2010a), where around 10000 cycles are conducted. However, a small-scale experiment by Roesen et al. (2011b) shows stabilising behaviour. The test runs almost 50000 load cycles and after 15000 cycles no significant rotation is detected. Two simple power and logarithmic expressions are given by Long and Vanneste (1994) and Lin and Liao (1999), respectively, Equation (9) and

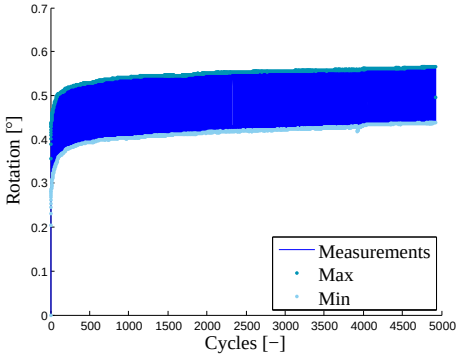

Figure 11: The rotation as function of number of load cycles.

(10). They describe the accumulated rotation of a cyclic loaded pile and are based on tests of laterally loaded piles, cf. Hansen et al. (2012) for further clarification.

$$\frac{y_N}{y_1} = N^{\alpha\, m} \tag{9}$$

$$\frac{\varepsilon_N}{\varepsilon_1} = 1 + t\ln(N) \tag{10}$$

where m and t are degradation factors. The subnotation $_N$ denotes N cycles and $_1$ denotes the first cycle. The factor α controls the relative contribution of soil resistance and deflection and is applied so change in p-y relation with depth can be incorporated. The value of the factor varies from 0 to 1. However, changing the α factor provides no improvement in results, so a constant value of $\alpha = 0.6$ is applied, making the method independent of depth. ε_N is the strain accumulation after N cycles and ε_1 is the strain after the first cycle.

The two expressions are fitted by a degradation factor for a driven pile in sand with $D_r = 0.77$ and a load characteristic corresponding to the small-scale test. These expressions are compared to the normalised maximum and minimum rotation for number of cycles, cf. Figure 12. In Table 6 Pearson's correlation coefficient, R, and the root mean square error, RMSE, are given to describe the correlation between the measured results and the power and logarithmic function by Long and Vanneste (1994) and Lin and Liao (1999), respectively. Looking at Pearsons correlation coefficient, R, the shape of the curves for both expressions fit the data well. However, RSME, give a mean value of how close the data is fitted to the expressions. The logarithmic expression fit the minimum rotation best and the power expression fit the maximum rotation best. Since the minimum rotation is assumed to give the most exact permanent rotation the logarithmic

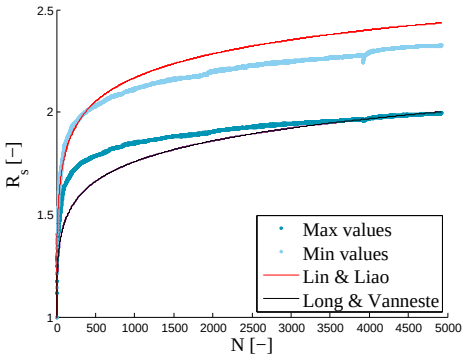

Figure 12: The normalised maximum and minimum rotation compared to logarithmic and exponential functions by Long and Vanneste (1994) and Lin and Liao (1999).

Table 6: Pearsons correlation coefficient, R, and root mean square error between measured data and the functions by * Long and Vanneste (1994) and **Lin and Liao (1999)

		Pow.fit*	Log.fit**
$\theta(\mathrm{N})/\theta_1(\mathrm{min})$	R	0.977	0.990
	RMSE	0.339	0.090
$\theta(\mathrm{N})/\theta_1(\mathrm{max})$	R	0.973	0.989
	RMSE	0.068	0.377

function fits the best. However, it overestimates the rotation after the first 350 cycles. Peralta and Achmus (2010) suggest fitting accumulated rotation to power and logarithmic expressions. Also, LeBlanc et al. (2010a) uses a power function. The measured data is fitted with the functions

$$\frac{\theta_N}{\theta_1} = a\,N^b \tag{11}$$

$$\frac{\theta_N}{\theta_1} = a\,+\,ln(N)^b \tag{12}$$

where a and b are fitting coefficients and the rotation is normalised by the rotation from the first load cycle. LeBlanc et al. (2010a) normalise their data differently by $\Delta\theta(\mathrm{N})/\theta_s$ defined in Figure 9. LeBlanc et al. (2010a) only normalise the maximum accumulated rotations, since the minimum rotation is zero for the static rotation, θ_s, for one-way loading with $\zeta_c = 0$. However, in the conducted small-scale test ζ_c is not zero and thus the minimum rotation is normalised as well.

In Figure 13 and Figure 14 the logarithmic and the power functions are fitted the minimum and maximum accumulated rotation, respectively. The correlation between each function and the measured data is given by Pearson correlation coefficient, R, and RMSE in Table 7 for the minimum and maximum measured rotations. Both functions fit the measured data well with correlation coefficients between 0.959 and 0.988. The RMSE show a slightly smaller mean error for the maximum rotations. However, not one of the functions can be favoured as they are very alike. Normalising the rotation according to LeBlanc et al. (2010a) makes little change. A slightly better fit is obtained by the logarithmic function according to R and RMSE. It most be emphasised that both expressions give good fits.

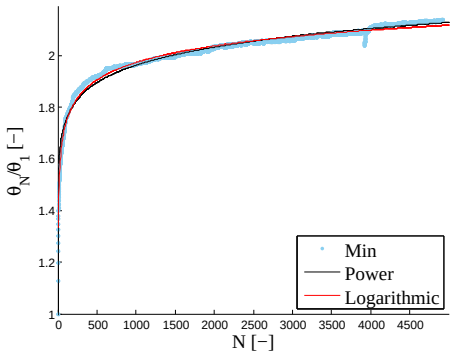

Figure 13: Logarithmic and exponential functions fitted to minimum rotation.

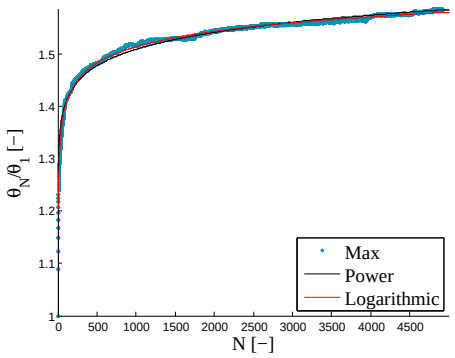

Figure 14: Logarithmic and exponential functions fitted to maximum rotation.

5 Conclusion

To analyse the effect that environmental forces have on offshore wind turbines small-scale testing is conducted. The test is of an aluminium pipe pile with an outer diameter of 100 mm and a length of 600 mm corresponding to a slenderness ratio of 6. The pile is placed in saturated cohesionless soil with a relative density between 70 - 80 %. The relative density of the sand is determined based on CPTs conducted prior to the test. A monotonic test is conducted loading the pile to a 3° rotation and afterwards the pile

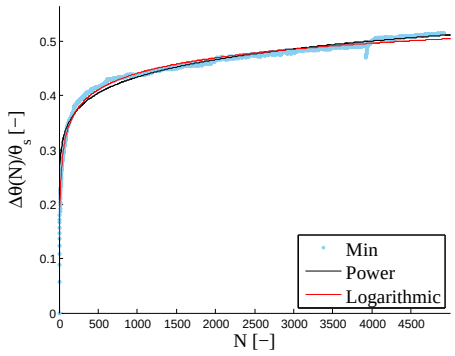

Figure 15: Logarithmic and exponential functions fitted to minimum rotation normalised as LeBlanc et al. (2010a).

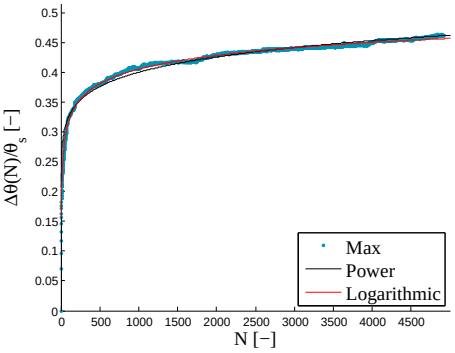

Figure 16: Logarithmic and exponential functions fitted to maximum rotation normalised as LeBlanc et al. (2010a).

is unloaded and then reloaded again. The load is applied by a motor pulling the pile with a speed of 0.02 mm/s. The ultimate capacity is defined at 3° rotation to 660 N. A cyclic load simulating FLS is chosen to approximately 35 % of the ultimate capacity. This load is applied by a rotating arm with a frequency of 0.1 Hz causing a sinusoidal loading of the pile. Applied force and displacement are measured and the rotation is found.

The test results show an accumulated rotation of the pile as it is subjected to the load cycles. The rotation increments decrease with increasing number of load cycles, but no stable situation occurs. Comparing the static and cyclic test the stiffness response is larger for the cyclic test. The stiffer response may be due to different relative densities in the two tests. The frequency of which the load is applied may have an influence as the cyclic load is applied approximately 190 times faster than the cyclic load. The results give an indication of the expected behaviour of long-term loading of piles in sand. However, further investigations

		POW. fit*	Log. fit*
$\frac{\theta(N)}{\theta_1}$(min)	R	0.962	0.981
	RMSE	0.020	0.014
$\frac{\theta(N)}{\theta_1}$(max)	R	0.959	0.988
	RMSE	0.009	0.005
$\frac{\theta(N)}{\theta_s}$(min)	R	0.949	0.982
	RMSE	0.010	0.006
$\frac{\theta(N)}{\theta_s}$(max)	R	0.940	0.989
	RMSE	0.009	0.004

Table 7: Pearsons correlation coefficient, R, and root mean square error, (RMSE), between measured data and the functions suggested by * Peralta and Achmus (2010) and LeBlanc et al. (2010a)

with a larger number of load cycles should be conducted, as 5000 cycles does not describe long-term loading.

Long and Vanneste (1994) and Lin and Liao (1999) suggest degradation of stiffness of the soil-pile system based on large-scale experiments of maximum 500 load cycles. The degradation is influenced by the relative density, the installation method and the load ratio. Lin and Liao (1999) also included a depth coefficient in the degradation. Long and Vanneste (1994) and Lin and Liao (1999) suggest a power and a logarithmic expression, respectively. Both expressions give a simple estimate of the accumulated rotation for the number of cycles applied. However, the methods are not clear on whether the rotation should be found as the maximum or the minimum rotation for a load cycles. It is the authors opinion that the minimum rotation in a load cycle represents the permanent rotation best as the elastic deformation is at its minimum as well.

Recent small-scale testing provides information on rotation of a cyclically loaded pile. Peng et al. (2006), Peralta and Achmus (2010) and LeBlanc et al. (2010a) test different load scenarios with approximately 10000 cycles applied. They all agree with the measured results that rotation will keep increasing with number of load cycles. Peralta and Achmus (2010) and LeBlanc et al. (2010a) suggest fitting of data by a power and logarithmic expression. The measured results can be fitted well by both expressions. Here, it should be kept in mind that the measured results only include less than 5000 cycles. Roesen et al. (2011b) measures cyclic loading of a pile subjected to approximately 46000 cycles. A stabilisation seems to occur around 15000 load cycles.

List of symbols

D_r	Relative density
ζ_b, ζ_b	Ratios for load characteristic
M_{min}, M_{max}, M_S	Minimum, maximum and static moment capacity
F	Measured force
H	Measured horizontal displacement
m_1, m_2, m_3	Masses in cyclic setup
d_s	Specific grain density
e	Void ratio
d_{50}	50%-quantile
U	Uniformity coefficient
γ	Unit weight
S_w	Degree of saturation
σ'_1, σ'_3	Effective vertical, horizontal stress (effective)
μ	Mean value
σ	Standard variation
x	Depth
q_c	Cone resistance
c_1, c_2, c_3	Constants for determining D_r from mini CPT (0.75, 5.14, 0.42)
ϕ_{tr}	Friction angle
ψ	Dilation angle
c	Cohesion
K_0	Earth pressure coefficient at rest
p	Subgrade reaction
y	Displacement
ε	Strain
θ	Rotation angle
N	Number of cycles
α	Depth factor
m, t	Degradation factors
R	Pearson's correlation coefficient
$RMSE$	Root mean square error
a, b	Fitting coefficients

References

Hansen, Rasmussen, Wolf, Ibsen, and Roesen, **2012**. M. Hansen, K. L. Rasmussen, T. K. Wolf, L. B. Ibsen, and H. R. Roesen. *A literature study on the effects of cyclic lateral loading of monopiles in cohesionless soils*. Department of Civil Engineering, Aalborg University, Aalborg, Denmark, 2012.

Ibsen, Hanson, Hjort, and Taarup, **2009**. L. B. Ibsen, M. Hanson, T. Hjort, and M. Taarup. *MC-Parameter Calibration of Baskarp Sand No. 15*, 2009.

LeBlanc, Houlsby, and Byrne, **2010a**. C. LeBlanc, G. Houlsby, and B. Byrne. *Response of Stiff Piles to Long-term Cyclic Lateral Load*. Géotechnique 60, No. 2, 79–90, 2010a.

Lin and Liao, **1999**. S. S. Lin and J. C. Liao. *Permanent Strains of Piles in Sand due to Cyclic Lateral Loads*. Journal of Geotechnical and Geoenvironmental Engineering, 125(No. 9), 789–802, 1999.

Long and Vanneste, **1994**. J. Long and G. Vanneste. *Effects of Cyclic Lateral Loads on Piles in Sand*. Journal of Geotechnical and Geoenvironmental Engineering, 120(No. 1), 225–244, 1994.

Peng, Clarke, and Rouainia, **2006**. J. R. Peng, B. J. Clarke, and M. Rouainia. *A device to Cyclic Lateral Loaded Model Piles*. Geotechnical Testing Journal, Vol. 29(No. 4), 2006.

Peralta and Achmus, **2010**. K. P. Peralta and M. Achmus. *An Experimental Investigation of Piles in Sand Subjected to Lateral Cyclic Loads*, 2010. ISBN 978-0-415-59288-8.

Roesen, Andersen, and Ibsen, **2011a**. H. R. Roesen, L. V. Andersen, and L. B. Ibsen. *Small-Scale Testing Rig for Long-Term Cyclically Loaded Monopiles in Cohesionless Soil*. Department of Civil Engineering, Aalborg University, Aalborg, Denmark, 2011.

Roesen, Andersen, Ibsen, and Foglia, **2011b**. H. R. Roesen, L. V. Andersen, L. B. Ibsen, and A. Foglia. *Experimental Setup for Cyclic Lateral Loading of Monopiles in Sand*. Department of Civil Engineering, Aalborg University, Aalborg, Denmark, 2011.

Chapter 5

Concluding Remarks

The aim of this thesis was to evaluate two issues regarding the design of laterally loaded monopiles in sand which current design guidance does not cover. The first issue is the application of finite element analysis as a tool for evaluating the lateral response of a monopile in sand subjected to static loading. The second issue is the evaluation of piles in sand subjected to long-term cyclic lateral loading. The effect of long-term cyclic lateral loading of a rigid pile is evaluated by means of a small-scale cyclic load test. The evaluation was conducted by means of three approaches:

- **Numerical modelling:** A case study of the response to lateral loading of a full-scale wind turbine foundation was conducted by means of the finite element program *Plaxis 3D 2011*.
- **Literature study:** The current state of knowledge on cyclic, lateral loading of piles was studied.
- **Small-scale cyclic load test:** Small-scale tests were conducted at the Geotechnical Engineering Laboratory at Aalborg University. A static load test was conducted in order to specify the static lateral bearing capacity of the test setup. A test of long-term cyclic, lateral loading of a pile was conducted in order to evaluate the behaviour of a soil/pile system.

In the following sections summaries of the three approaches are presented along with findings. First, the numerical modelling is presented and conclusions are outlined. Second, the literature study and the small-scale cyclic load test are presented.

5.1 Numerical Modelling

The numerical modelling is conducted by means of the finite element program *Plaxis 3D 2011*. A case study of a full-scale wind turbine is provided as the subject for research. Two material models are used for the numerical analysis: The Mohr-Coulomb model and the Hardening Soil model. The soil parameters for both material models are found from a CPTu and a boring profile for the site. In this connection a CPT program has developed to extract these parameters. The pile is modelled as found in the provided turbine foundation design report.

On basis of the conducted numerical analyses stresses and deformations are extracted from *Plaxis 3D 2011* by means of a program which has been developed for this purpose. The program constructs p-y curves on basis of the evaluated stresses and deformations. Stress oscillations in the interface elements in *Plaxis 3D 2011* are observed. They are related to the modelling of curved structures in the finite element formulation. The method for extracting p-y curves considers the average stresses in order to cope with this. The slices conducted in the method for extracting p-y curves produce stress results that fit reasonably with the expected traction on the pile surface.

Two different excitations, load and forced displacement, are applied in order to evaluate p-y curves near the point of pile rotation. The first excitation is an actual load case for maximum bending moment at seabed which is applied in a number of increasing load steps. For each load step a phase is added in which the load is removed. The other excitation is a displacement controlled approach in which a prescribed lateral displacement is applied to the entire pile surface. Equivalent to the load approach, the prescribed displacement is subsequently removed for each step. The p-y curves

evaluated from forced displacement shows much more deflection than those evaluated by means of applied load. The deflection of the pile during applied load consists of rigid body motion. A slight curvature is noticed.

p-y curves are evaluated by means of two material models in the numerical analysis: The Mohr-Coulomb model and the Hardening Soil model. The extracted p-y curves are compared to the p-y curves formulated in the API. The Mohr-Coulomb model shows no plastic deformation in a considerable range of loading due to its bilinear stress-strain curve. The Hardening Soil model provides immediate response which results in less stiff p-y curves. The conventional p-y curves formulated in the API shows a much stiffer response at depth than either of the applied material models and excitation methods. This may be related to the linearly increasing initial stiffness of the p-y curve, E^*_{py}.

5.2 Evaluation of Cyclic Load Testing and Comparison with Current Knowledge on the Subject

The design guidance is limited in knowledge on long-term cyclic loading of laterally loaded piles. They are based on full-scale testing of slender piles subjected to a low number of cycles.

As an addition to previous experimental work, cf. (Roesen et al., 2011), a cyclic load test is performed. The test is of an aluminium pipe pile with an outer diameter of 60 mm and a length of 600 mm corresponding to a slenderness ratio of 6. The pile is placed in a container with saturated cohesionless soil. The sand is compacted to have a relative density between 70 - 80 % similar to real offshore conditions. The relative density of the sand is determined based on CPTs conducted prior to the test. At first, a static test is conducted to find the ultimate lateral capacity. The pile is loaded monotonic to a point of 3° rotation and afterwards an unloading/reloading is carried out. The load is applied by a motor pulling the pile with a speed of 0.02 mm/s. The ultimate capacity is define at 3° rotation to 660 kN. A cyclic load similar to the environmental load affecting a real offshore wind turbine in FLS is chosen to approximately 35 % of the ultimate capacity. This load is applied by a rotating arm with a frequency of 0.1 Hz causing a sinusoidal loading of the pile. Force and displacement are measured of the pile and the rotation is found.

The test results show an accumulated rotation of the pile as it is subjected to the load cycles. An increase in rotation is carried out through the entire test and so, no stable situation occurs. The rotation increments decrease with increasing number of load cycles, though. This makes the increase in accumulated rotation for the last load cycles minimal compared with the accumulated rotation for the first load cycles.

Comparing the static and cyclic test the stiffness response is larger for the cyclic test. The stiffer response can be caused by a difference in relative density between the two tests. Also the frequency of which the load is applied can have influence. The cyclic load is applied approximately 190 times faster than the cyclic load. This can cause the soil to respond differently in the two situation.

The results give an indication of the expected behaviour of long-term loading of piles in sand. However, further investigations with a larger number of load cycles should be conducted, as 5000 cycles does not describe long-term loading from environmental loads on wind turbines in FLS.

The issue of long-term lateral loading is very complex. Large-scale experiments of maximum 500 load cycles are used by Long and Vanneste (1994) and Lin and Liao (1999) to described the effect of long-term lateral loading. They suggest degradation of the stiffness of the soil/pile system. The degradation is influenced by the relative density, the installation method and the load ratio. Lin and Liao (1999) also included a depth coefficient in the degradation. Long and Vanneste (1994) and Lin and Liao (1999) suggest a power and a logarithmic expression, respectively. Comparing the cyclic test results these expressions show that both expressions can give a simple estimate of the accumulated rotation for the number of cycles applied. However, the methods are not clear on whether the rotation should be found as the maximum or the minimum rotation for a load cycles. It is the authors opinion that the minimum rotation in a load cycle represents the permanent rotation best as the elastic deformation is at its minimum as well. Thereby, the logarithmic expression

by Lin and Liao (1999) fit the best.

Recent small-scale testing provides information on rotation of a cyclically loaded pile. Peng et al. (2006), Peralta and Achmus (2010) and LeBlanc et al. (2010) test different load scenarios for a pile placed in sand and approximately 10000 cycles are applied. They all agree with the measured results that rotation will keep increasing with number of load cycles. Peralta and Achmus (2010) and LeBlanc et al. (2010) suggest fitting of data by a power and logarithmic expression. The measured results can be fitted well by both expressions. Here, it should be kept in mind that the measured results only include less than 5000 cycles. Roesen et al. (2011) measures cyclic loading of a pile subjected to approximately 46000 cycles. A stabilisation seems to occur around 15000 load cycles.

5.3 Direction for Further Investigations

5.3.1 Numerical Work

The comparison of conventional p-y formulations to those computed by means of 3D FEM was not verified. The method of p-y curve extraction should in future research be verified against experimental results or existing well-founded case calculation. In this way it is possible to consider the validity of the findings. The application of advanced soil models such as the Hardening Soil model provided a response much different to that of the Mohr-Coulomb model. From the provided analyses this difference seems to be because of the stiffness relations of the models. If the Hardening Soil model proves to be the better approach it should be compared to the API p-y formulation e.g. through profound parametric studies. Also the Hardening Soil small strain model could be included to further investigate the small strain influence on the lateral pile response. It was not possible to model the toe kick satisfactory. This should be addressed in future studies. Modelling of the conducted experimental tests by FEM in order to calibrate existing constitutive models or introduce improved ones. At present the modelling of small-scale tests is not possible to a satisfactory degree. Constitutive models able to model cyclic loading should also be investigated.

5.3.2 Experimental Work

To assess the p-y method for cyclically loaded piles used in current design guidance full-scale testing on offshore wind turbines is needed. As full-scale testing is time consuming and expensive small-scale tests are used to predict and assess the soil/pile interaction during cyclic loading of a pile. The experimental work conducted focus on simulating cyclic loading of offshore wind turbines in cohesionless soil in small-scale. Further analyses should be extended to different soil types as well as layered soil. Also change in compaction which affects the friction angle and elasticity modulus of sand should be investigated. Strain gauges along the pile would benefit to obtaining p-y curve for the small-scale test.

The influence of long-term lateral loading of offshore wind turbines is a multifaceted problem and a rather new issue. The effects of cyclic behaviour can be affected by several factors and further research in this area should include difference in load characteristics as only one one-way loading test is conducted. To simulate real environmental conditions best different combinations in load intensities and varying load amplitudes should be considered. Further investigations of a high number of load cycles are needed to determine if a stabilise situation will occur in time. Additional test of varying pile diameter and with piles in other materials are also important to supply previous work. Another aspect, which Long and Vanneste (1994) and Lin and Liao (1999) also consider, is the pile installation.

Bibliography

API, **2007**. American Petroleum Institute API. *Recommended Practice for Planning, Designing and Constructing Fixed Offshore Plat-forms-Working Stress Design, RP 2A-WSD*, 2007.

API, **2000**. American Petroleum Institute API. *User Manual Program PYGMY.* The University of Western Australia, Department of Civil and Resource Engineering, 2000.

Cox et al., **1974**. William R. Cox et al. *Analysis of Laterally Loaded Piles in Sand.* 12, 1974.

DNV, **2010**. Det Norske Veritas DNV. *Offshore standard DNV-OS-J101: Design of offshore wind turbine structures. Technical report DNV-OS-J101*, 2010.

Energistyrelsen, **2012**. Energistyrelsen. *Energistyrelsen.* URL: `http://www.ens.dk`, 2012.

Energy, **2012a**. DONG Energy. *DONG Energy.* URL: `http://www.dongenergy.com`, 2012.

Energy, **2012b**. DONG Energy. *Horns Rev.* URL: `http://www.hornsrev.dk/default.htm`, 2012.

EWEA, **2012**. The European Wind Energy Association EWEA. *The European Wind Energy Association.* URL: `http://www.ewea.org`, 2012.

Janbu, **1963**. N. Janbu. *Soil compressibility as determined by oedometer and triaxial tets*, 1963.

LeBlanc, Houlsby, and Byrne, **2010**. C LeBlanc, G. T. Houlsby, and B. W. Byrne. *Response of stiff piles in sand to long-term cyclic lateral loading*, 2010.

Lin and Liao, **1999**. S. S. Lin and J. C. Liao. *Permanent Strains of Piles in Sand due to Cyclic Lateral Loads.* Journal of Geotechnical and Geoenvironmental Engineering, 125(No. 9), 789–802, 1999.

Long and Vanneste, **1994**. J. Long and G. Vanneste. *Effects of Cyclic Lateral Loads on Piles in Sand.* Journal of Geotechnical and Geoenvironmental Engineering, 120(No. 1), 225–244, 1994.

O'Niell and Murchison, **1983**. M. W. O'Niell and J. M. Murchison. *An Evaluation of p-y Relationships in Sands*, 1983.

Peng, G., and Rouainia, **2006**. J. R. Peng, Clarke B. G., and M. Rouainia. *A Device to Cyclic Lateral Loaded Model Piles.* Geotechnical Testing Journal, 29(4), 1–7, 2006.

Peralta and Achmus, **2010**. K. P. Peralta and M. Achmus. *An Experimental Investigation of Piles in Sand Subjected to Lateral Cyclic Loads*, 2010. ISBN 978-0-415-59288-8.

Roesen, Andersen, Ibsen, and Foglia, **2011**. H. R. Roesen, L. V. Andersen, L. B. Ibsen, and A. Foglia. *Experimental Setup for Cyclic Lateral Loading of Monopiles in Sand.* Department of Civil Engineering, Aalborg University, Aalborg, Denmark, 2011.

Technology, **2012**. Cooper Technology. *Light Weight Deflectometer.* URL: `http://www.cooper.co.uk/info/index.asp?page=prima_100_lwd_124`, 2012.

The Engineer, **2012**. The Engineer. *Wind Energy gets serial.* URL: `http://www.theengineer.co.uk`, 2012.

WWEA, **2012**. World Wind Energy Association WWEA. *World Wind Energy Association.* URL: `http://www.wwindea.org`, 2012.

Appendix

Appendix A

Log of Laboratory Testing

Table A.1: Log for laboratory work. * Measurement setup 1 uses two vertical and one horizontal displacement measures. ** Measurement setup 2 uses three horizontal displacement measures.

Date	Procedure	Note
Mar. 22.		Container is filled with sand and water.
Apr. 10.	CPT 1 Vibration 1	3 tests. All holes (the grid of holes are separated in two groups - every other hole in one group).
Apr. 11.	CPT 2	3 tests.
Apr. 16.	Static test 1	Measurement setup 1* is used. Error in displacement reading V_2.
Apr. 17.	Vibration 2 CPT 3	All holes. 3 tests. The measurements look good. The cone resistance is irregular.
Apr. 18.	Vibration 3 CPT 4 Vibration 4 CPT 5	All holes 3 tests. The measurements look well. The cone resistance is slightly irregular. Only vibration of half of the holes. 9 tests. Irregular cone resistances. Air bubbles in the sand. Outer tests diverge from the others.
Apr. 20.	Vibration 5 CPT 6	All holes. 9 tests - right to left.
Apr. 25.	Static test 2	Measurement setup 2** is used. Error in displacement readings.
May 4.	Vibration 6 & 7	Vibration is repeated, as gradient was applied after vibration 6.
May 6.	CPT 7	3 tests.
May 6. - 9.		Overflow on load and displacement transducers due to noise.
May 9.	Cyclic test 1 Vibration 8 CPT 8	Test is stopped. Too small material thickness of cantilever beam - failure of setup. All holes. 3 tests.
May 10.	Cyclic test 2	Test runs 12 hours and stops. Restart of test - Recording of measurements stop due to technical problems.
May 22.	Static test 3	Overflow in displacement measurements due to noise.

The container is part of a new test setup. The tests run in the container are the first conducted. The preparation of the soil has been a time consuming process. Several complications induced by test setup, measuring devices and computer programmes have delayed the process. In Table A.1 the log for the laboratory work is shown. Below, specific details in the process are commented.

CPT 1, CPT 2 and Static Test 1

After filling the container with sand three CPT tests are conducted (CPT 1) to view the compaction of the sand without having vibrated. From the first run of CPTs the relative density, $D_r = 0.44$. The sand is vibrated and from the three new CPTs (CPT 2) a D_r= 0.73. CPTs are conducted prior to every test to follow the development in D_r. Static test 1 is conducted after this (Results are presented in 4).

CPT 3 and CPT 4

In Figure A.1 (a) the cone resistance from three tests in CPT 3 are shown. At low depths the curves are almost linear and follow the same tendency. However, difference in resistance is pronounce at lower depths and the resistance fluctuates at high depths. Some fluctuation can be explained by the sand being a young deposit and a better compaction by vibration is needed. $D_r = 0.79$ at CPT 3. The sand is vibrated and CPT 4 show $D_r = 0.82$.

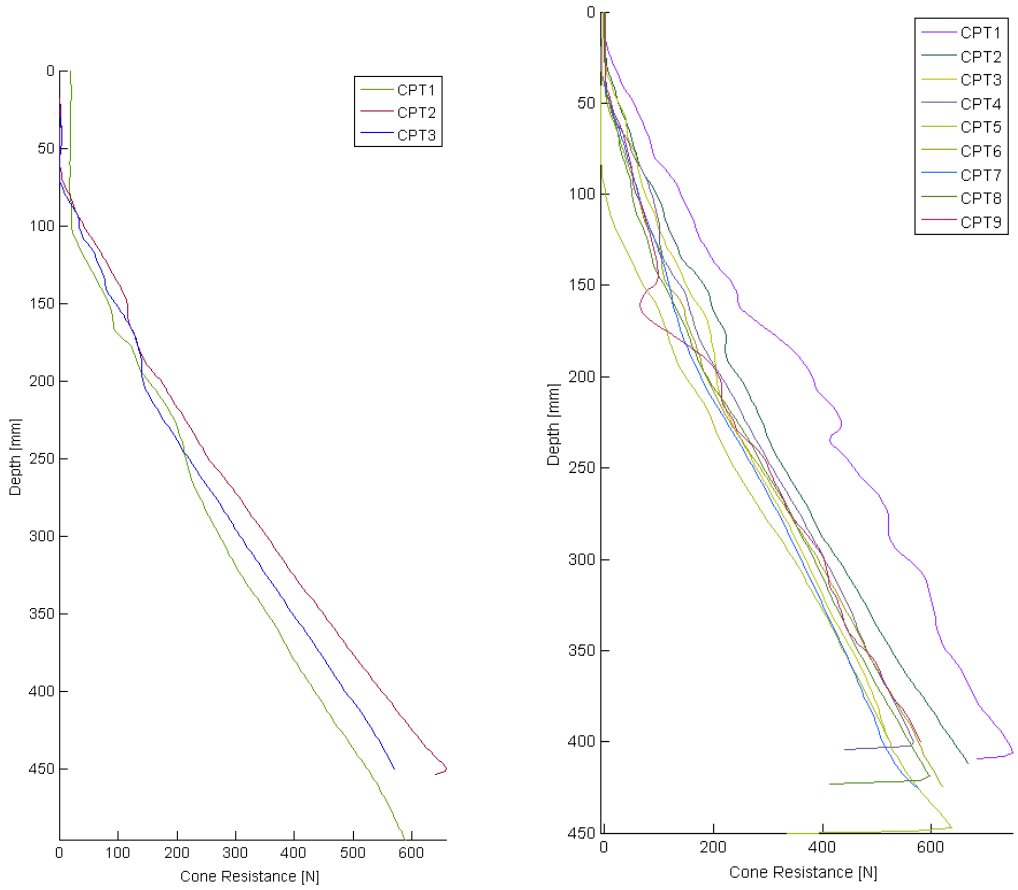

(a) (b)

Figure A.1: Cone resistance for the three tests in CPT 3 and the nine tests in CPT 5.

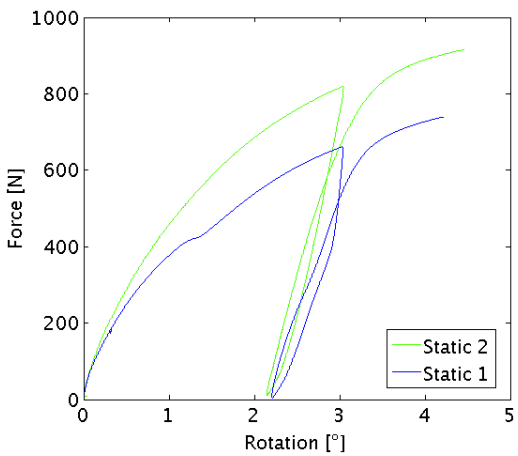

(a) Static test 1 and static test 2.

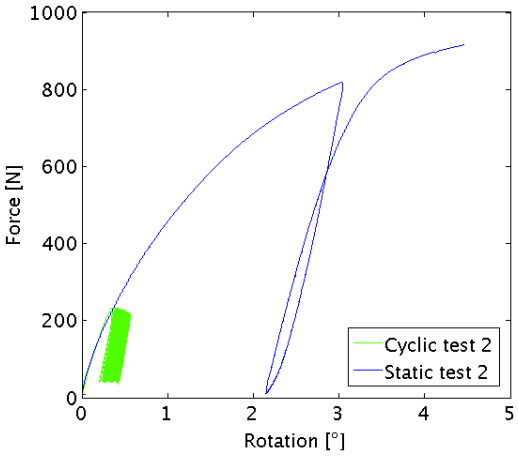

(b) Static test 2 and cyclic test 2.

Figure A.2: Force/rotation relationships.

CPT 5

After the fourth time of vibrating the sand the magnitude of the cone resistance obtained from the different tests are getting closer. The far outer tests are quite irregular, though, and they diverge from the other tests, cf. Figure A.1 (b). During CPT 5 air bubbles were detected as the cone penetrated down through the sand. Only half the holes are used for vibration before CPT 5 which can have caused the air pockets in the sand. From this, it was concluded that for further vibrations, all holes are used. $D_r = 0.80$ for CPT 5.

Static Test 2

The force/displacement from the static test 2 is plotted with static test 1, cf. Figure A.2 (a). The sand have gained larger resistance for a rotation of 3°. The increase in applied force is from 660 N in static test 1 to 820 N in static test 2. The increase can be due to better compaction of the sand. The break in static test 1 at of 400 N also makes the load at a $3/^c irc$ rotation questionable.

Plotting the rotation of the static test 2 with the cyclic test, cf. Figure A.2 (b), the curves of the static test 2 and the first load cycle of the cyclic test follow each other well.. This is despite the fact that the compaction of the sand in the static test, $D_r = 0.81$, is larger than the one in the cyclic test, $D_r = 0.77$.

Unfortunately, an error was detected in measurements while the test was run. Looking at the displacement measurements the displacement follow each other with increase in distance and give peak values at the same time, Figure A.3. However, the initial displacements are incorrect, cf. Figure A.3 to the right. The first displacements are negative for H_2 and H_3. Also, a disturbance in the displacement for H_1 is shown.

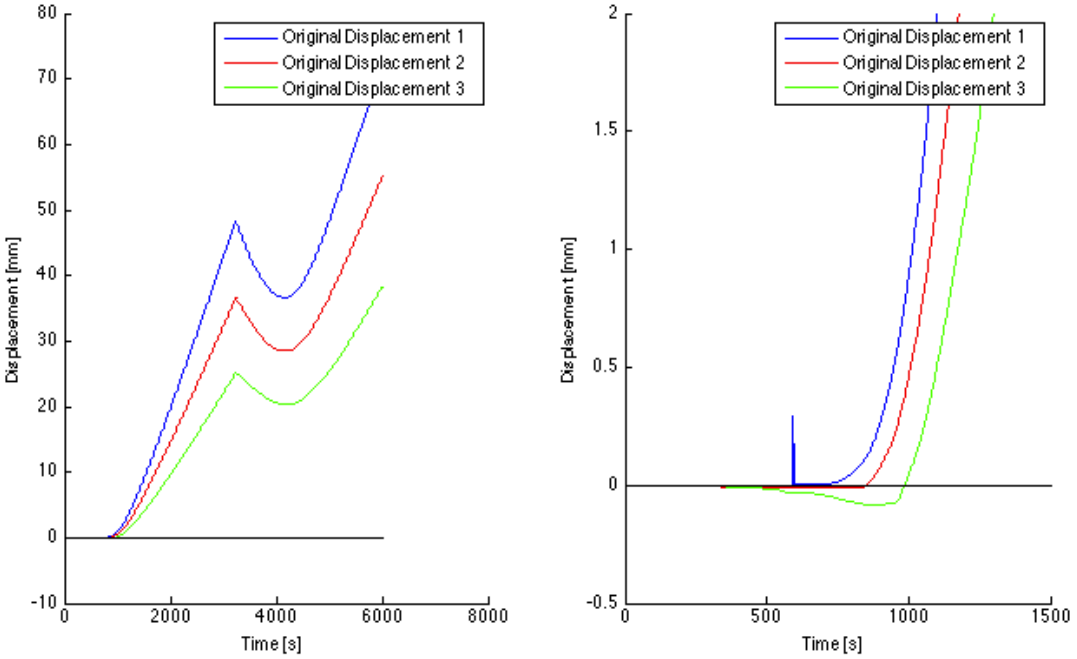

Figure A.3: The three displacement measurements. To the right, a zoom on the initial displacement measurements.

When comparing the static and cyclic effects on the pile first measurements are of great importance important. Due to the disturbances is the displacement measures in static test 2 this test is not fit for comparison.

Electric Noise

The test setup is place in the laboratory amongst several other experimental setups. A great deal of electric noise due to these surroundings is detected when testing newly purchased load transducers for the cyclic tests. When the motor for the cyclic test was turned on the load transducers experienced overflow. Several attempts to detect the source of the noise was done. All unnecessary equipment was removed from the surroundings and all cables were rearranged and separated from the load transducers. Also, 4.5 m earth rod was installed to lead the disturbance away. Noise was reduced but not enough to avoid the overflow. Finally, the load transducers are replaced with a different pair from the static tests.

Cyclic Test 1

A complication due to the test setup appeared when cyclic test 1 was running. The wire connecting the pile to the cyclic system is round through a pulley connected to a cantilever beam. The beam is mounted to the loading frame. A too thin material thickness is used causing the beam to bend up and down when the cyclic motion is started. The beam is reinforced to avoid the problem. Unfortunately, the test cannot proceed. The pile most be un-installed, the soil most be vibrated, CPT tests most be done and the pile most be installed again.

Cyclic Test 2

During preparation static test 2 is run another complication is detected. Two programmes are used when the test are run: A programme that reads the measurements (A PC-based data acquisition HBM spider records the measurements and transfers them to the computer) and a programme that controls the motor that makes the cyclic motion. The two programme had difficulties working together. Especially, the program controlling the motor was extremely sensitive. When first the motor is started not even another window on the computer can be touched without shutdown of the motor. Cyclic test 2 is started and runs for approximately 12 hours. The motor stops at 5

a.m. in the morning. The source of the stop is unknown but may be due to an update of another computer program. The test is started again the next day. After approximately three hours the measuring program stop. The test cannot be started yet again as the motor has kept running and the pile is affected hereby.

Static Test 3

The pile is finally pulled to failure. Due to the above mentioned technical complications the displacement of the pile cannot be determined.

Appendix B

Calibration of Mini-CPT Cone

Before testing, the mini CPT is calibrated. This is done by installing the set-up shown in Figure B.1. The CPT cone is placed upside-down with a rig balancing on the cone tip. The output from the CPT is zeroed, whereafter a series of 10 load plates are placed on the rig, one after one. The weight plates weigh 10 kg each. During the loading and following unloading, a continuous

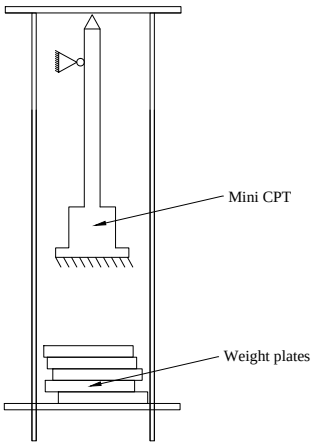

Figure B.1: Set-up for CPT calibration.

measurement from the CPT is made. The sampling rate is 1 Hz. Disturbance during application causes the set-up to oscillate. The measurements are not deemed valid until this oscillation stops. The measurements and the chosen data is shown in Figure B.2. The measured load decreases during damping of the oscillations during the loading phase. During the unloading phase, the opposite behaviour is observed. However, the measurements do not seem to stabilize during the unloading. Even after 10 minutes the measurements still increase. This behaviour results in different measurements during the loading and unloading phases respectively. The measurements during the loading phase are deemed the most reliable, as these stabilize at a considerably faster rate. Also, it is this behaviour of the CPT that is used in the measurements in soils.

The chosen points are fitted to points representing the exact weight applied to the CPT. This is seen in Figure B.3. The measured data is also shown. The fit computes a new calibration factor for use in the data acquisition program used in the laboratory. The original and the new calibration factors are also shown in Figure B.3.

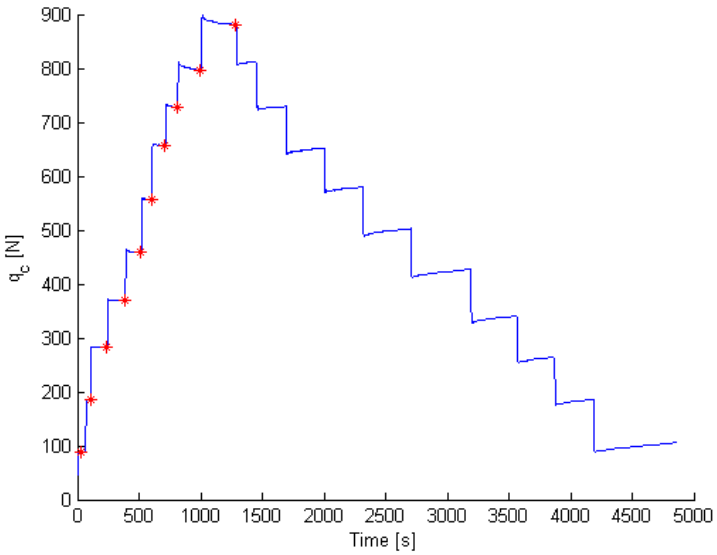

Figure B.2: Measured and chosen data from calibration test.

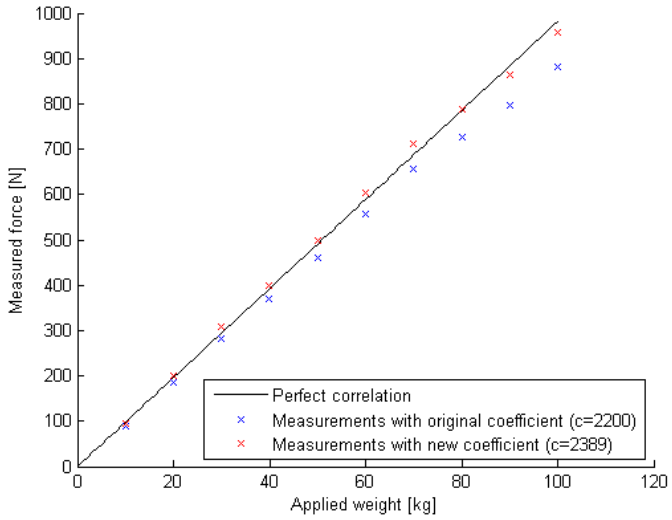

	Calibration factor [-]	Root mean squared error [-]
Old	2200	50.46
New	2389	15.58

Figure B.3: Correlated values of data points to applied weight.

Appendix C

Modelling Laboratory Pile in *Plaxis 3D 2011*

In order to verify the output of the numerical models, and thereby verifying the resulting p-y curves, attempts have been made to model the laboratory setup in *Plaxis 3D 2011*. With the controlled environment of the laboratory, it should be possible to produce a FEM model that agrees well with the results from the tests. However, the attempts have not been fruitful. In the following the procedure for producing a solid model will be described. It should be noted that the geometry is modelled in the exact same way as with the pile used in Chapter 2. Also the soil parameters are extracted in a manner very similar to the other model. All the parameters are gained from mini-CPT testing, as described in Chapter 4.

From the laboratory tests, it is known that the pile will be at failure (defined as a rotation of 3°) at a load of approximately 660 N, attacking at height of 600 mm above the mudline. This behaviour is sought reproduced in the FE model.

Mohr-Coulomb Modelling

At first an attempt is made to model the sand using a Mohr-Coulomb material model. This is done since this material model computes faster than the more advanced models used later in the process. The effective cohesion, c', is set to 0 kPa, as the soil is assumed to be cohesionless.

The model is created using the standard model units. Hence the input is in kN and m. The calculations stopped at a force of 0.08 kN due to soil collapse. After a discussion with the supervisor, it is decided to implement another set of input units. Using N and mm should improve the behaviour of very small models. However, this change does not lead to better results.

Hardening Soil Modelling

Implementing the hardening soil material model should also provide a more stable model at small scale. Therefore this material model is used in the following. The assumption of cohesionless soil is withheld. Using the parameters of Chapter 4 leads to soil collapse at similar loading to the Mohr-Coulomb attempt. Experience from previous models tells that adding cohesion will make the model more stable. Therefore the cohesions of Table C.1 are implemented. None of them produce better results. It should be noted that changing any of the parameters of Table C.1 leads to a new set of moduli, as the moduli are functions of c, ϕ, σ_1,and m. Besides not being able to create a model that withstands the full amount of added force, an other issue is occurring. The pile-soil system behaves much stiffer than the system in the laboratory. This particularly evident when plotting the force versus the displacement of the pile at mudline. This plot is also produced in the laboratory test. Hence the FE model and the system it seeks to describe can be compared directly. This is seen in Figure C.1. It is noted how the deformations of the FE model pile are significantly less than that of the laboratory pile. In order to change the stiffness of the FE model, two approaches can be made: Decreasing the moduli will lead to bigger values of horizontal displace-

c [kPa]	m [-]	ϕ [°]	ψ [°]
0.0	1.0	51.9	17.2
0.1	0.9	40.0	10.0
0.2	0.5		

Table C.1: Adjusted parameters in the FEM model.

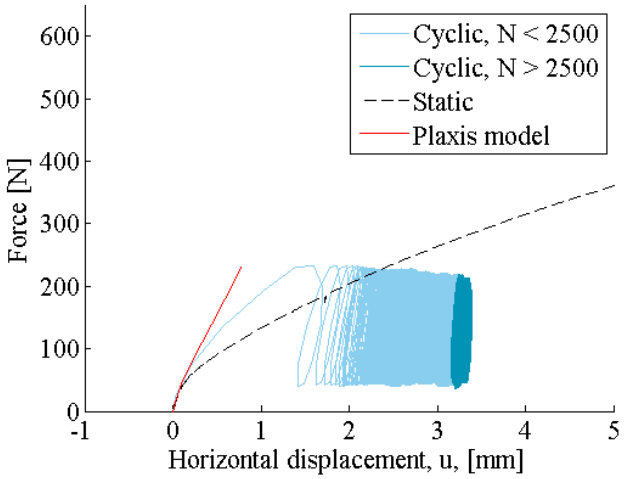

Figure C.1: Response of pile to applied force.

ment for the same load. Decreasing the friction angle decreases the curve asymptote, cf. Figure C.1.

According to the CPT results, the measured moduli increase rather drastically with depth. The power m used to describe the development of moduli is in Chapter 4 set to 1. This leads to the best fit of the computed moduli to the measurements. However, Janbu (1963) recommends a value of 0.5 for sands. The values of Table C.1 are implemented. The value of 0.9 is tried, as this reduces the stiffness without compromising significantly with the measured stiffness parameters. None of these adjusted m-values lead to better results.

The friction angle, ϕ, is reduced according to Table C.1. With this adjustment, the dilation angle ψ is also reduced, using the relationship of $\psi = \phi - 30°$. This does not help either.

As a final attempt to reaching a more realistic stiffness of the FEM system, the moduli are adjusted according to a Light Weight Deflectometer test. The test has not been made in the rig used in Chapter 4, but in an other set-up in the laboratory at Aalborg University. The tests are made on Aalborg University Sand No. 1 at similar d_s though. It is therefore assumed that the test results can be taken directly onto the current set-up. The tests have shown that E_0 is approximately 40 kPa. According to the manufacturer of the equipment, Technology (2012), the impact depth is 60-90 cm. The fall height in the tests is limited, and the impact depth is therefore expected to be around 50-60 cm. The reference pressure used in the input in *Plaxis 3D 2011* is assumed to be the pressure at half the impact depth. Furthermore, it is assumed that $E_0 = E_{ur}$. Adjusting the moduli according to this test does not improve the response in the FE model.

The phases have also been adjusted in search for a solution. Both applied load and forced displacement have been implemented. The size of the steps between phases has been changed as well. Both when loading and unloading. Neither with pleasing results.

The default solver in *Plaxis 3D 2011*, *PICOS*, is an iterative procedure. This is the default since it is the fastest solver. However, there is an alternative procedure inherent in the program. The solver *PARDISO* is a direct solver. It is more robust, but has higher memory consumption. This

solver has been implemented in the model in an attempt to accommodate the problems with the model. This lead to no improvements.

The tolerance, that controls the maximum allowed global equilibrium error, has been adjusted. Allowing for larger errors did not improve the model behaviour.

Throughout the process of modelling in *Plaxis 3D 2011*, it has been noted that the used computers behaved erratically. The problem seems to be due to the fact that the suggested computing power is not met. *Plaxis 3D 2011* recommends 4 GB of RAM and a multi core processor for computing advanced models. By not meeting these recommendations, the computations occasionally stopped in the midst of calculations.

It is a known fact that most material models behave rather unpredictably at very small stresses. Despite the numerous adjustments to the model described above, a working model was never created. In order to successfully model a scaled laboratory setup, one of the following two solutions should be implemented. An overburden pressure could be applied to the set-up. Hereby the stresses move to the more reliable part of the stress-strain curve, and the material models should work properly. Otherwise a more advanced model that behaves well at very small stresses could be adopted. As it is desired to recreate the results from the laboratory test in a FEM model, further attempts at modelling the setup numerically should desirably be made in future studies.

When scrutinising the foot of the pile, it is noted that stress concentrations are apparent. In an attempt to improve the behaviour of the model in this area, the mesh has been refined locally. This has no effect to the failure of the pile. Therefore, in the following section, in which the mesh is refined according to a convergence criteria, this local mesh refinement is not elaborated.

Convergence Test

The mesh handling in *Plaxis 3D 2011* is very limited. There is no way to directly specify the number of elements or node points for geometric entities in the model. A number of general parameters can be set with which the mesh is generated. When these parameters are given the meshing is handled implicitly in the program. The target element dimension (or average element size), I_e, is defined according to a relative element size and the model boundary coordinates, cf. (C.1).

$$I_e = \frac{r_e}{20} \sqrt{(x_{max} - x_{min})^2 + (y_{max} - y_{min})^2 + (z_{max} - z_{min})^2} \tag{C.1}$$

In addition to a target element size, restriction can be made regarding the polyline and surface angle tolerances in the model. This restriction will automatically reduce element sizes around circular or complex objects to maintain angles within the specified tolerances. The parameters can be defined by choosing from six default mesh settings. Alternatively, expert settings can be chosen in order to manually specify the mesh parameters. The default mesh settings for the laboratory model can be seen in Table Table C.2.

Settings		Very coarse	Coarse	Medium	Fine	Very fine
Relative element size, r_e	[-]	2	1.5	1	0.7	0.5
Element dimension, I_e	[mm]	340.7	255.6	170.4	119.3	85.18
Polyline angle tolerance	[°]	30	30	30	30	30
Surface angle tolerance	[°]	15	15	15	15	15

Table C.2: Mesh settings for the element distributions in *Plaxis 3D 2011*.

It is clear to see from Table Table C.2 that only choosing a default mesh setting would lead to very coarse elements in comparison with the pile diameter. Even a very fine mesh has element sizes in the same range as the pile diameter itself. In addition to the global mesh settings, local fineness can be adjusted for each individual geometric entity in the model. By default the local fineness factor is set to 1.0 for most geometry entities whereas the value is 0.5 for structures and loads,

which would reduce the element size to half the target element size. In order to achieve a satisfying mesh density in and near the pile, a volume geometry is defined around the embedded pile within which the local fineness is defined. The volume has no physical influence in the calculations and the soil is automatically assigned the correct parameters. The volume is extended 20 cm vertically underneath the pile corresponding to 2 times the pile diameter, see Figure C.2.

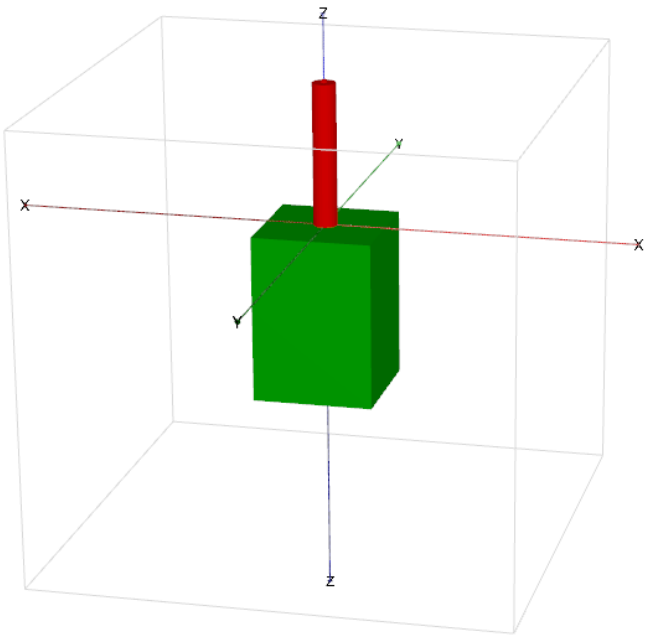

Figure C.2: The volume geometry and pile for which the fineness factor is adjusted.

In order to validate the mesh convergence the fineness factor of the volume geometry and pile is decreased until convergence is achieved. The convergence parameter is chosen as the maximum lateral deflection, u_x, of the pile at a horizontally applied load of 50 N. A mesh of medium fineness is chosen. The model is refined as shown in Table Table C.3.

Fineness factor	0.45	0.35	0.33	0.32	0.305	0.3
Number of nodes	30357	41525	46224	48956	52785	56211
Number of elements	20556	28687	32104	34104	36893	39451
Minimum quality	0.18	0.27	0.26	0.23	0.33	0.22
Maximum deflection	0.1325	0.1336	0.1328	0.1331	0.1338	0.1329

Fineness factor	0.25	0.245	0.24	0.2	0.15*
Number of nodes	78578	84591	84399	133155	259534
Number of elements	55857	60306	60154	95262	188301
Minimum quality	0.37	0.41	0.41	0.31	0.36
Maximum deflection	0.1336	0.1334	0.1338	0.1338	0.1334

Table C.3: Pile deflection at different fineness factors. *fineness factor of 0.8 for rest of soil.

In Table Table C.3 it is noticeable that a decrease in fineness factor does not consistently increase the number of elements in the model. This may be due to the small geometry near the pile toe and the way the mesh is built in the program so that the target element dimension at some degree of fineness forces certain elements to fit the geometry. Consequently, it is seen that the minimum quality of the mesh is not increasing in a predictable manner. The quality of an element is given as the inner sphere divided by the outer sphere of the element where an idealised

tetrahedral element is normalised as 1. This unpredictable behaviour is emphasised in Figure Figure C.3 where it is seen that the mesh does not converge by increasing the fineness factor (and thereby the number of nodes).

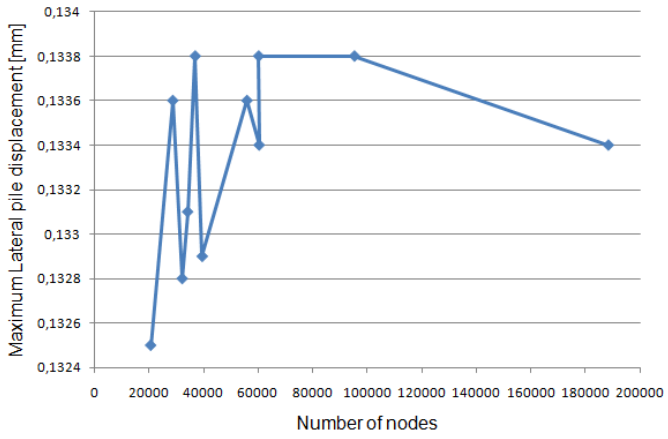

Figure C.3: The maximum horizontal pile displacement as function of number of nodes in the model.

Another approach is to look at the minimum quality as a measure of the convergence. As mentioned the minimum quality of the mesh is difficult to control and does not rely, to a certain extent, on the refinement of the mesh. The influence of the mesh quality can be seen in Figure Figure C.4.

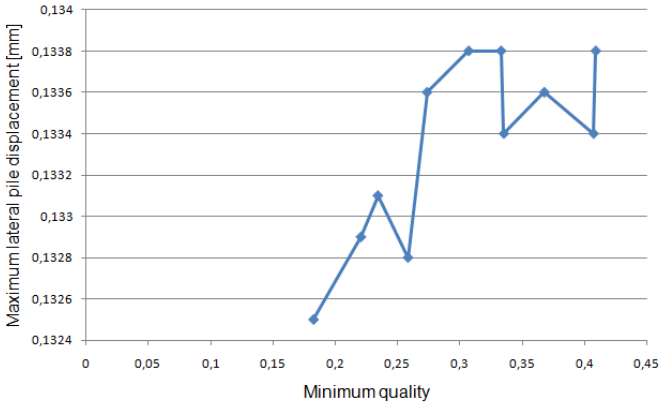

Figure C.4: The maximum horizontal pile displacement as function of the minimum quality.

Based upon judgement of Figure C.3 and C.4 the mesh with a fineness factor of 0.24 is chosen as appropriate. Finer meshes do not yield better results and the number of elements increases significantly which would produce long calculation times.

Appendix D

Guide to *Plaxis 3D 2011 p-y* Extraction Program

When using the $p-y$ extraction routine written in *Matlab*, a specific set of *Plaxis* output files must be implemented. The following is a short presentation of how to extract the data files from *Plaxis*, and how to load them in to the *Matlab* program.

A model of a monopile must be created using *Plaxis 3D Input*. It is of great importance to include interfaces such as described in 2. The phases must be created using either an applied load at the pile top or a forced displacment of the entire pile. The phases should follow the following pattern for applied load:

1. K_0 step
2. Implementation of pile (plate- and interface elements)
3. Nill-step
4. Small load applied
    (a) Load deactivated
5. larger load applied
    (a) Load deactivated
6. etc.

The unloading steps are computed independently of the other steps. Hence, the step 4 continues in direct extension of step 3. For a model incorporating forced displacement, the load steps are simply exchanged with displacement steps. In the following only the case with applied load will be described. If modelling with forced displacement, the loading/unloading is simply exchanged with displacing/letting go.

After successfully finishing the computation of a monopile in *Plaxis 3D Input*, the output is opened in *Plaxis 3D Output*. Here the *Report Generator* function is launched. Under *Export type* the box with *Separate data files* is ticked. An appropriate file path is chosen. Hereafter all the steps with applied load are chosen. In the *Model* window (reached by pressing *next*) the box with *Stresses -¿ Cartesian Effective Stresses -¿ Table* is ticked. Hereafter *Next -¿ Export* is pressed.

Once report is generated, the *Report Generator* is opened again. The same procedure is executed, however with ticks in the unloading steps, and with *Plate -¿ Deformations -¿ Table* checked in the *Structures* window.

Report generator cannot be used for extracting the stresses in the interface, as it does not differentiate between negative and positive interface (which share coordinates). Therefore the outer interface must be marked and shown separately in the main window. After doing so, a table of the interface stresses in can be opened by pressing *Interface stresses -¿ Table of stress point values.*

With this table open, the first load step is chosen in the drop-down menu. All the data is marked (ctrl+A), and the *Export to file* button is pressed. By doing so a separate data file for this load step is saved. This must be done for all the load steps.

Once all the data files are created, they must be loaded in to the *Matlab* program. It is recommended to move the files in to the respective folders in the Matlab program folder, named respectively *Interface Stress Files*, *Plate Displacement Files*, and *Report Generator*.

Firstly, the *InputFunction.m* file is opened. In here the geometry of the pile is stated. Furthermore the desired data plot depths and the desired integration division is determined. Finally the circumference for obtaining stress points in the soil is determined. The meaning of this dimension is explained in 2. Similarly dimensions for obtaining datapoints within and below the pile are determined. These should be left at the default values. It should be noted, that if the integration divisions are so small that a division will occur with no stress points, an error message will occur in the *Command Window* when running the progam.

The file *main.m* is opened and excecuted. A window pops up asking for a *Plate Displacement File*. The first displacement file is chosen (the phase after the first load phase). Herafter the two stress files must be loaded. After doing so, the program will plot the stress distribution over the circumference of the pile, the pile displacement over the depth, the subgrade reaction over the depth, and the resulting point on the $p - y$ curves. A prompt asks for confirmation if the loaded data is correct. If it is accepted, the point of the curve will be saved in the *pydata.txt* file. This procedure is repeated until all data files are loaded into the program.

It should be noted that the p-values determined by the program correspond to the force acting over the entire integration height determined in *InputFile.m*, measured in kN. For the conventional units of kN/m the p-values should be divided by the integration heights.

Appendix E

p-y Curves

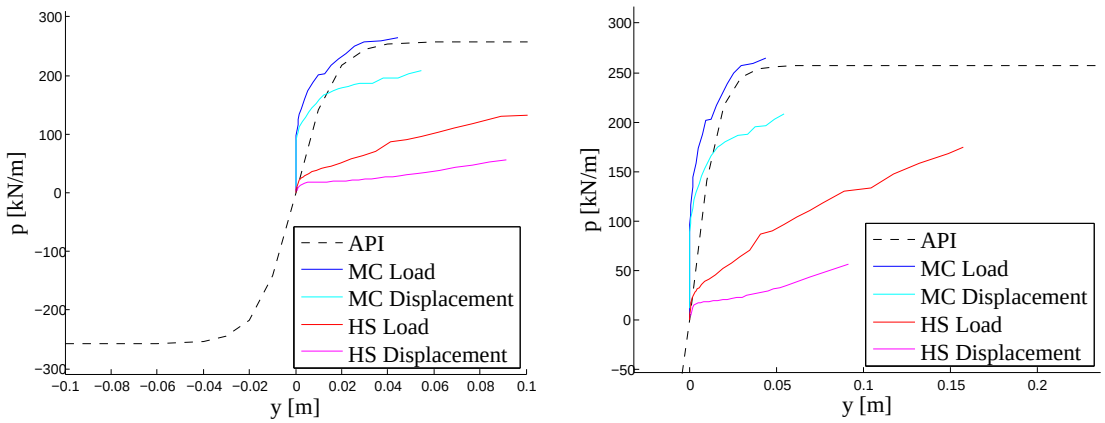

Figure E.1: d = 0.4 m.

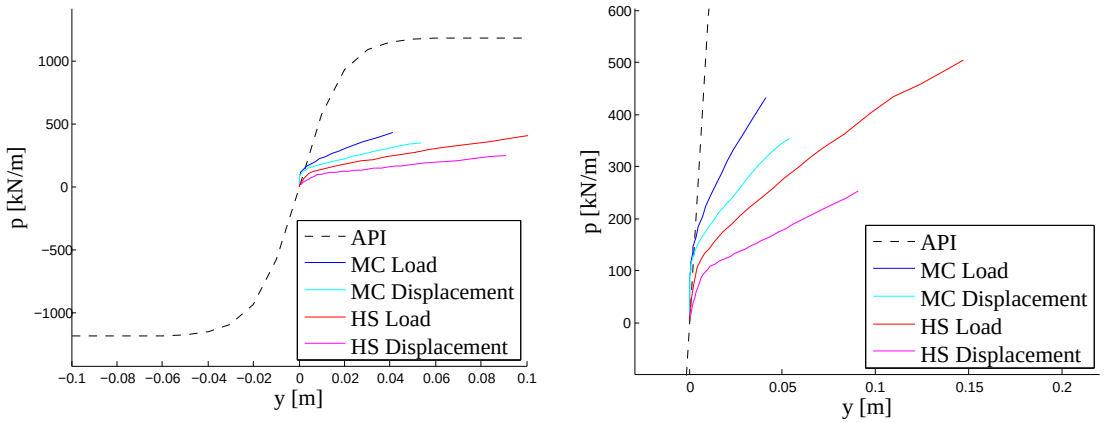

Figure E.2: d = 1.5 m.

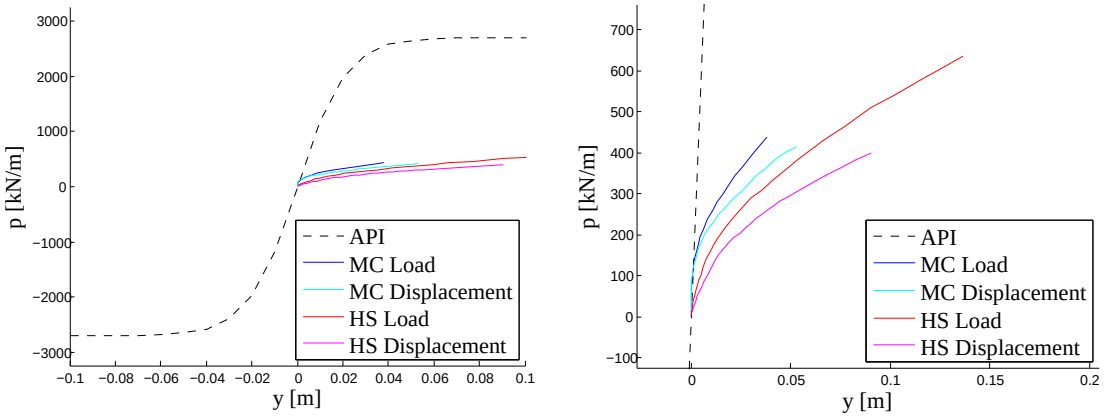

Figure E.3: d = 3.1 m.

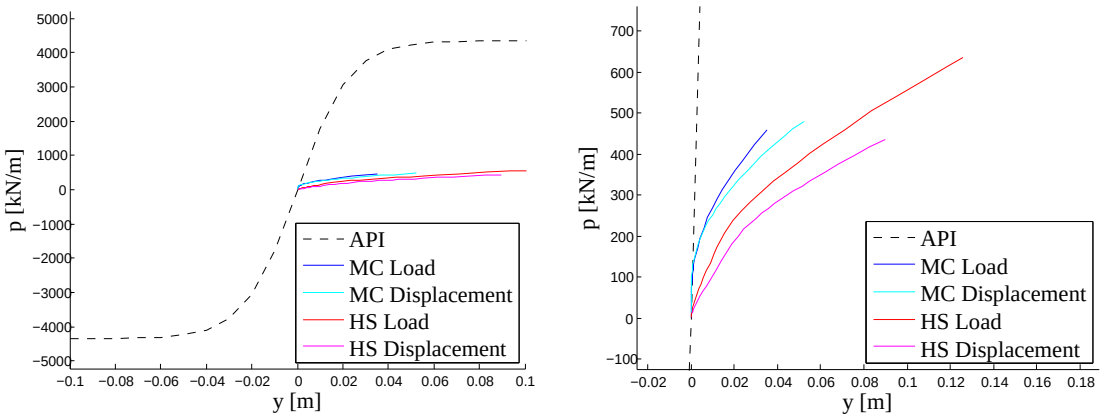

Figure E.4: d = 4.6 m.

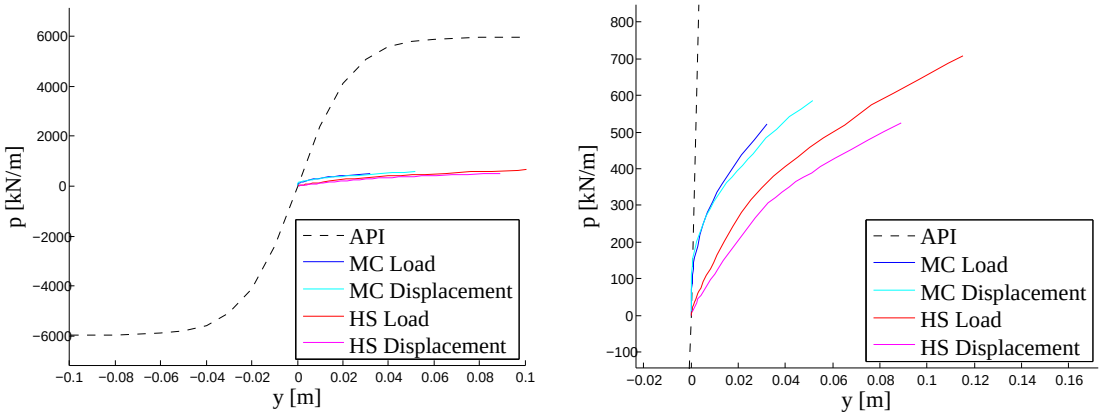

Figure E.5: d = 6.2 m.

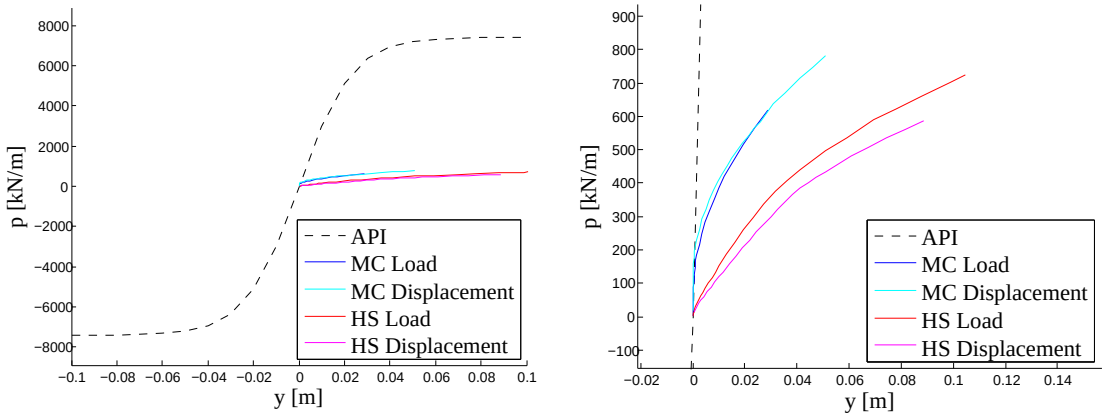

Figure E.6: d = 7.7 m.

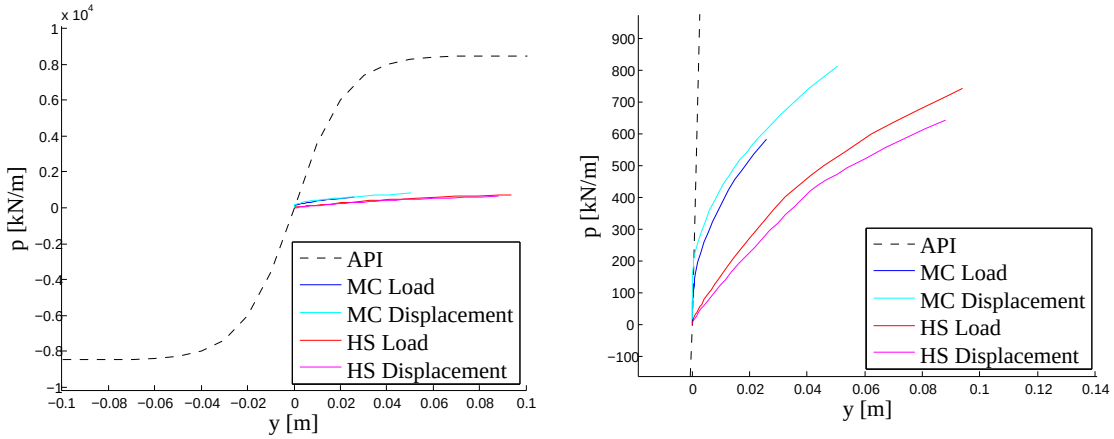

Figure E.7: d = 9.3 m.

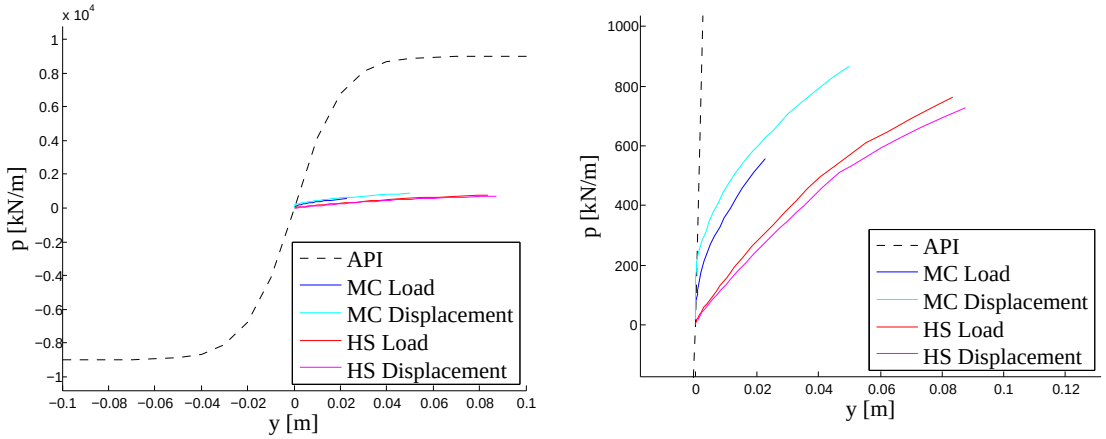

Figure E.8: d = 10.8 m.

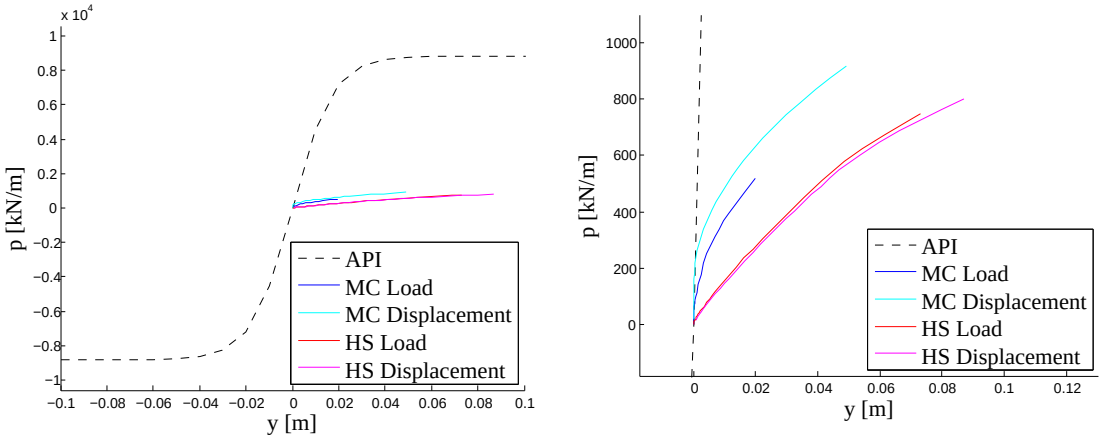

Figure E.9: d = 12.4 m.

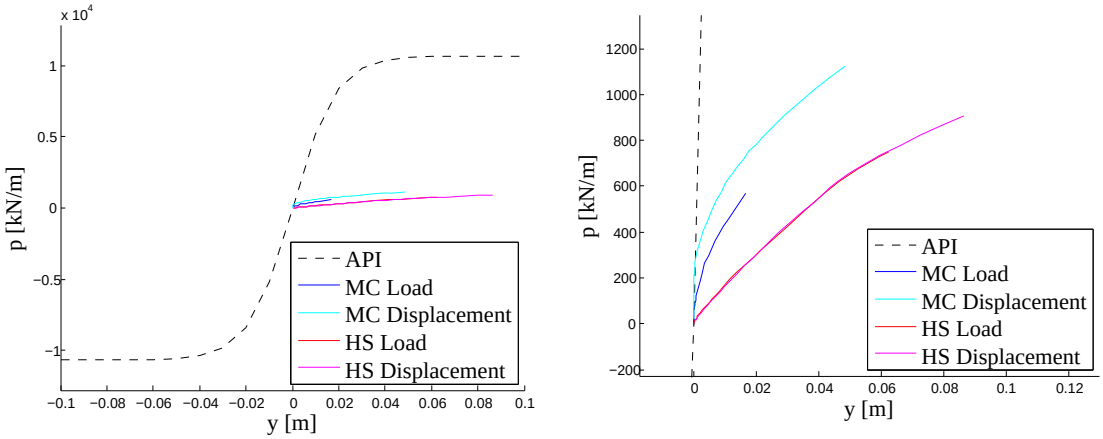

Figure E.10: d = 13.9 m.

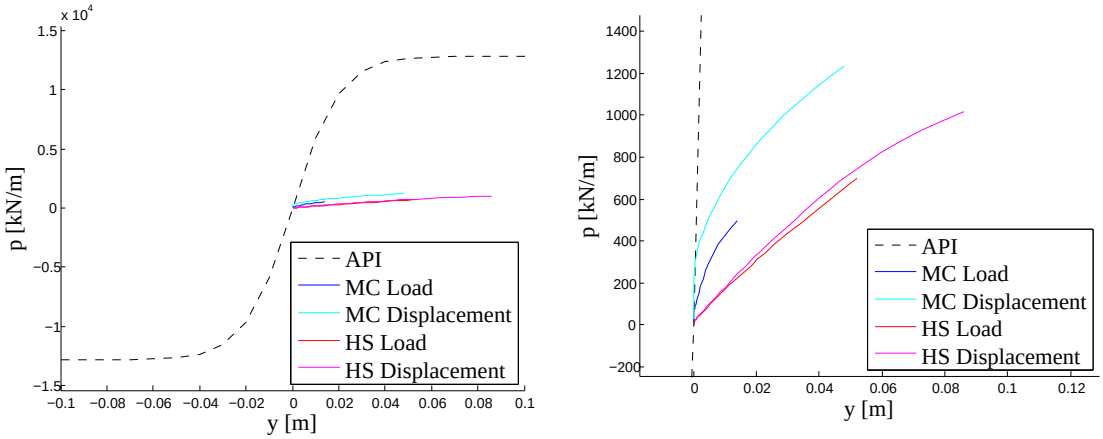

Figure E.11: d = 15.5 m.

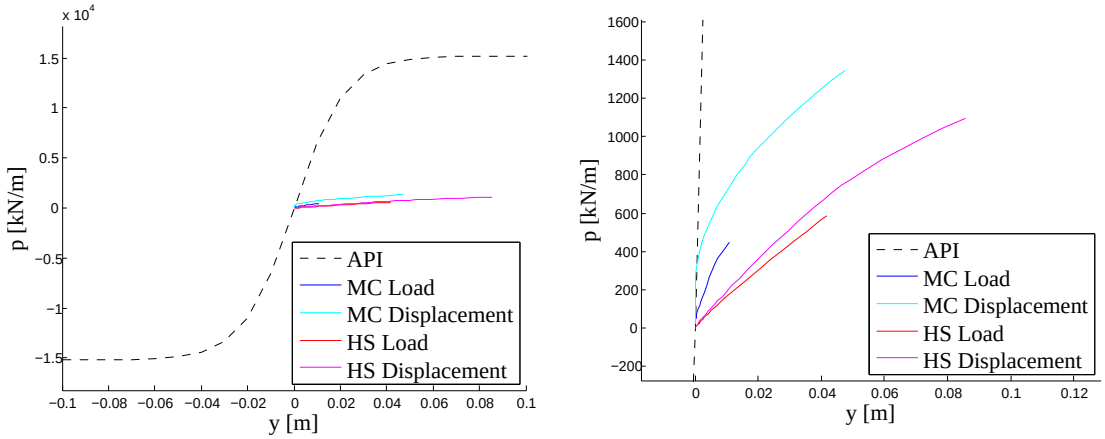

Figure E.12: d = 17.0 m.

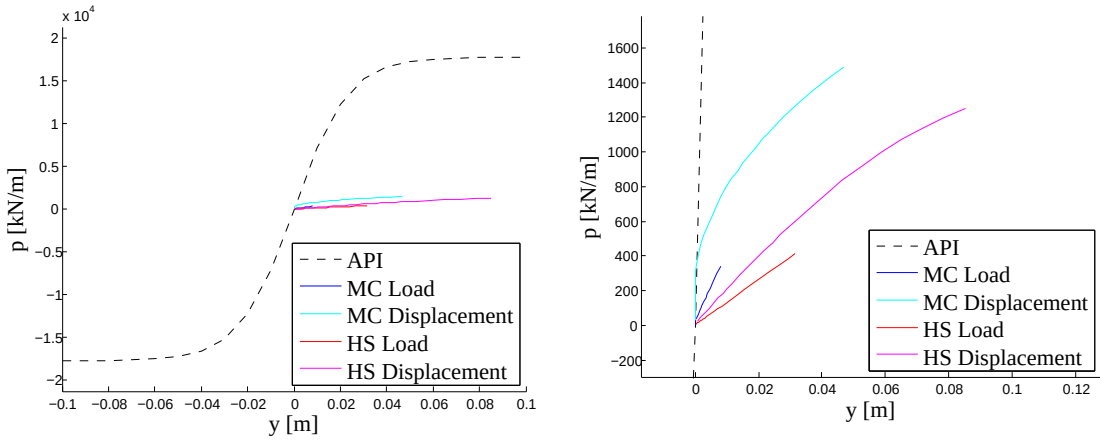

Figure E.13: d = 18.6 m.

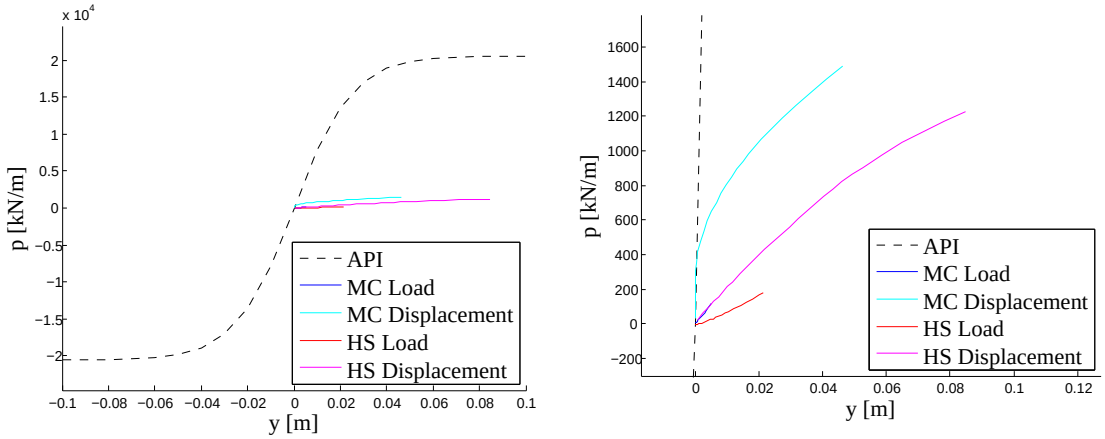

Figure E.14: d = 20.1 m.

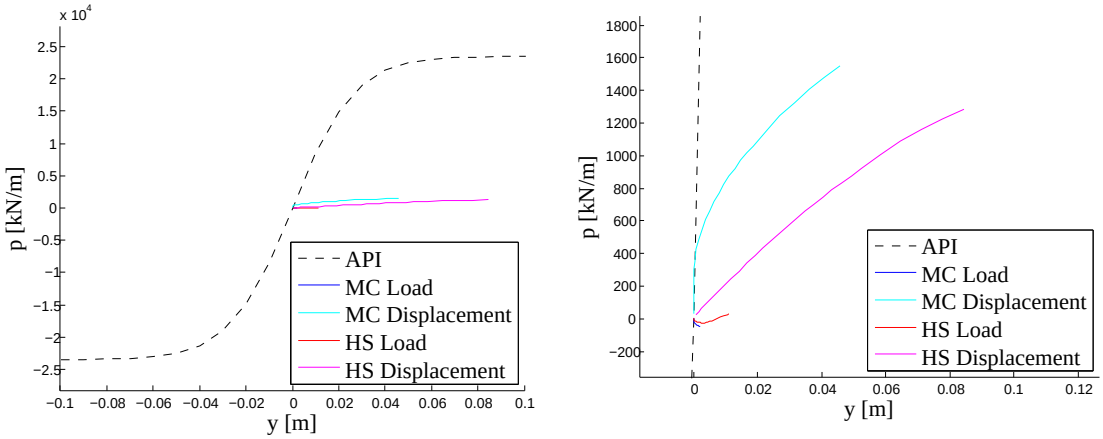

Figure E.15: d = 21.7 m.

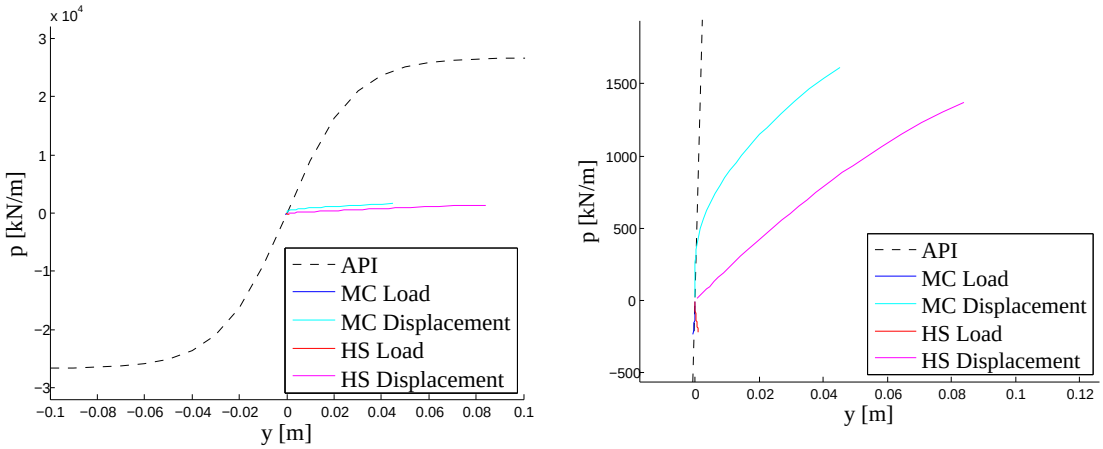

Figure E.16: d = 23.2 m.

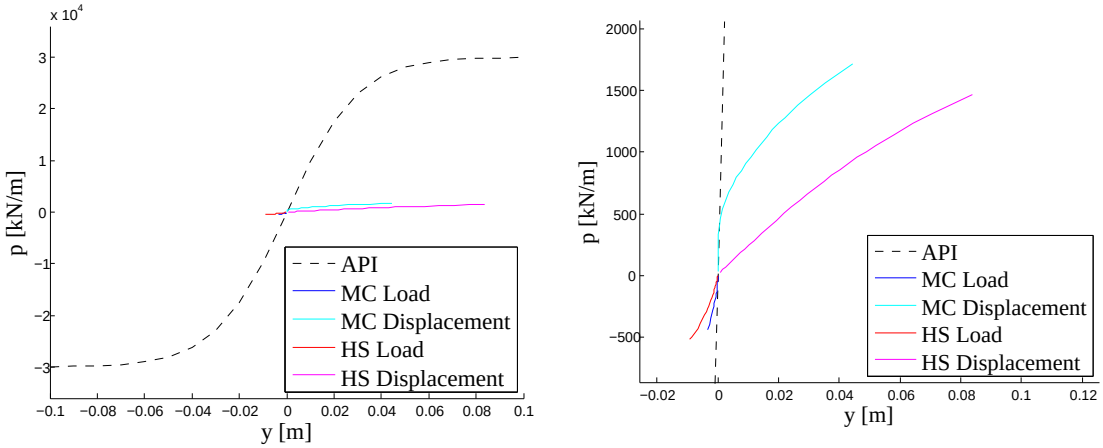

Figure E.17: d = 24.8 m.

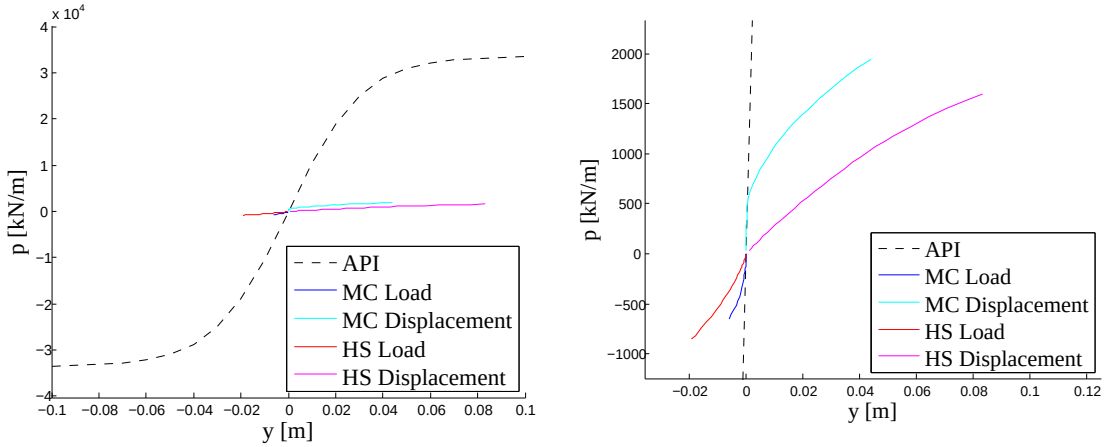

Figure E.18: d = 26.3 m.

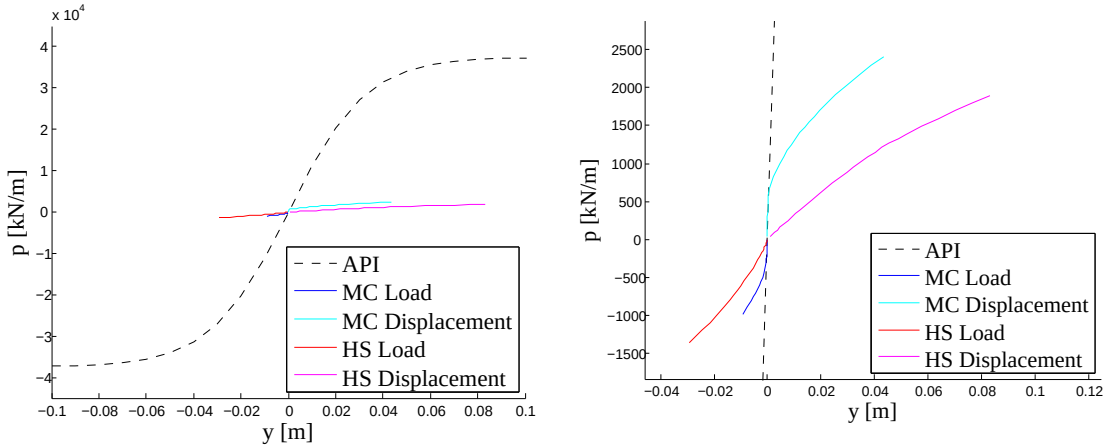

Figure E.19: d = 27.9 m.

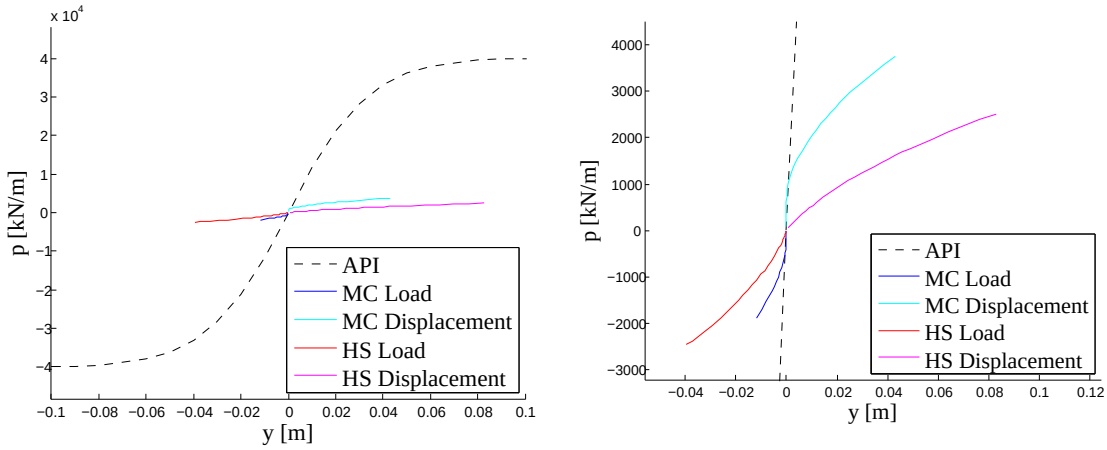

Figure E.20: d = 29.0 m.